UNIVERSIDADE DE LISBOA
FACULDADE DE CIÊNCIAS
DEPARTAMENTO DE FÍSICA

Search for a light vector dark matter particle in the tt final state at the LHC

João Lopes Rodrigues Carreira

Mestrado em Física
Especialização em Física Nuclear e de Partículas

Dissertação orientada por:
Professor Doutor Rui Alberto Serra Ribeiro dos Santos
Professor Doutor António Joaquim Onofre Abreu Ribeiro Gonçalves

2024

Acknowledgements

First, I want to thank my supervisors, Prof. Rui Santos and Prof. António Onofre, for all the guidance, advice and for the opportunity of making a project with them. I appreciate a lot their effort to explain me several experimental and theoretical physics concepts that were necessary for the understanding of the work in this dissertation, and their patience when answering my questions, which were sometimes repeated more than once.

I am very thankful for the time spent by my colleagues João Martins, Rodrigo Capucha, Pedro Chaves and Rui Silva, who had previously worked in projects similar to mine, at helping me solve many software issues that I faced, and explaining me how to perform several software-based procedures required in this work. Without them and specially my colleague Gonçalo Freitas, who was working at the same project as this one but for an axial-vector DM mediator, the problem solving would have been a very hard and lonely task.

Thank you to my parents for their patience and always trusting me during my academic journey. Without their financial and emotional support throughout these years, this dissertation wouldn't exist.

I want to express gratitude to my close friends for the crucial emotional support and for trying to calm me down when I was too stressed in the last months spent at writing this dissertation.

Lastly, thank you Bea for having such a patience when I was too stressed to have a normal conversation with you, for always being by my side and for giving me strength when I had so few left. You were a huge help. Thank you for all your love.

Resumo

Atualmente, o Modelo Padrão da Física de Partículas é a teoria mais aceite para descever as partículas fundamentais na natureza e três das quatro interações fundamentais conhecidas. Desde a sua criação que o Modelo Padrão tem estado de acordo com muitos testes experimentais e previsto fenómenos que não tinham sido descobertos, sendo considerada uma das mais bem sucedidas teorias em Física. Contudo, esta teoria ainda tem alguns problemas de índole teórica ou experimental. Uma das grandes limitações do Modelo Padrão é a ausência de uma ou mais partículas que sejam candidatas viáveis a matéria escura.

Ao longo do século passado e presente, várias evidências experimentais astronómicas e cosmológicas têm favorecido a existência de matéria escura, que por sua vez é não-luminosa e interage fracamente entre si e com as partículas descritas pelo Modelo Padrão. Com os atuais dados, esta matéria compõe 26.4% da total energia-matéria do universo. Candidatos a descreverem matéria escura têm sido propostos desde a sua descoberta. Os físicos de partículas criaram uma grande classe de candidatos com o intuito de descreverem a matéria escura através de partículas. Inicialmente, propôs-se que os neutrinos fossem possíveis candidatos a matéria escura, mas o facto de esta partícula ser relativista na epóque de formação de estrutura impossiblita os neutrinos e qualquer partícula com esta propriedade de comporem uma grande fração de matéria escura de modo a acordar com dados experimentais. Sendo que o Modelo Padrão não descreve nenhuma partícula que seja não-relativista nesta epóque, eletricamente neutra, estável, e entre outras propriedades derivadas de observações experimentais que uma partícula candidata a matéria escura deve possuir, os físicos de partículas têm teorizado modelos de matéria escura nos quais incluem setores escuros com novas partículas candidatas a matéria escura.

Diferentes procuras por assinaturas de matéria escura em aceleradores de partículas foram realizadas no passado, focando-se em eventos mono-, tais como mono-jato e mono-Higgs. Algumas procuras baseavam-se na produção de um par $t\bar{t}$ ou um único quark top juntamente com partículas de matéria escura no estado final, maioritariamente recorrendo à variável missing transverse energy ($\not{E}_T$) como um discriminador, sem reconstruírem a cinemática dos quarks top. O trabalho desenvolvido nesta dissertação é motivado pela procura da produção de pares $t\bar{t}$ juntamente com um mediador de matéria escura no LHC e pelas seguintes questões: um sinal com estado final composto por um mediador invisível de matéria escura muito leve e um par $t\bar{t}$ teria diferenças substanciais nas distribuições de observáveis escolhidos em comparação com o sinal de estado final $t\bar{t}$ esperado no Modelo Padrão no LHC? E, se não encontrarmos diferenças substanciais, a reconstrução do par $t\bar{t}$ poderá ser usada para estabelecer limites de exclusão nos valores da constante de acomplamento do mediador de matéria escura aos quarks top?

De modo a responder às nossas questões, no presente trabalho consideramos um modelo simplificado de matéria escura (DMsimp model) que introduz um mediador vetorial de matéria escura, Y_{1^+}, ao Modelo Padrão e estudamos o seu acoplamento aos quarks top. Os eventos de sinal com $t\bar{t}Y_{1^+}$ como estado final produzidos a partir de colisões protão-protão com uma energia de centro-de-massa de 13 TeV foram gerados no gerador de Monte Carlo MADGRAPH5_AMC@NLO para valores da massa de Y_{1^+} iguais a 0.1, 1, 10, 100 e 125 GeV e valor da constante de acoplamento de Y_{1^+} com os quarks top

de $g^V_{u33} = g_{SM} = 0.25$. Estes eventos foram gerados apenas para o canal dileptónico do decaimento do par $t\bar{t}$ ($t\bar{t} \rightarrow W^+bW^-\bar{b} \rightarrow l^+\nu_l b l'^-\overline{\nu}_{l'}\bar{b}$) e Y_{1^+} foi considerado estável. As packages MADSPIN e PYTHIA6 foram utilizadas para preservar os efeitos de correlação de spin durante o decaimento de partículas pesadas, e para simular o chuveiro de partões e a hadronização, respetivamente.

Depois de gerados, procedeu-se à simulação rápida da resposta do detetor ATLAS do LHC a estes eventos através da package DELPHES. Para além dos eventos de sinal, eventos de processos de background do Modelo Padrão que podem originar estados finais com topologias similares aos eventos de sinal foram também gerados e as suas respostas no detetor ATLAS simuladas, usando o mesmo software e packages.

De seguida, partiu-se para a análise destes eventos usando o MADANALYSIS5. Tanto na análise como na geração e simulação de eventos, cortes de seleção de eventos foram realizados com o principal propósito de aumentar o rácio entre sinal e background. A associação de objetos simulados pelo DELPHES às respetivas partículas a nível partónico procedeu-se de dois modos distintos: um com Thruth-Match (TM), no qual a associação tem acesso à informação das partículas a nível partónico, e o outro sem TM, no qual a associação apenas tem acesso à informação simulada do detetor, tal como na experiência real em ATLAS. A associação com TM foi realizada para avaliar num primeiro instante a reconstrução cinemática efetuada neste trabalho e mudá-la de modo a aumentar a percentagem de eventos simulados em ATLAS que são corretamente associados ao nível partónico. Na associação sem TM, utilizando o TMVA que faz uso de distribuições de variáveis cinemáticas a partir de informação do gerador, escolheu-se o método de estatística multivariável BDTG para ajudar na discriminação entre associações corretas e incorretas de jatos aos quarks b e $\bar{b}$ do decaimento do par $t\bar{t}$. Na reconstrução do $t\bar{t}$, foi assumido que a $\not{E}_T$ total advém dos neutrinos, ignorando a contribuição do Y_{1^+} para esta variável cinemática. Eventos que não tenham uma solução que reconstrua todas as partículas envolvidas no decaimento dileptónico de $t\bar{t}$ são descartados, sendo requerido, no final, que todos os eventos tenham dois jatos identificados como b-jatos e pelos menos dois leptões carregados isolados de cargas opostas.

Observou-se uma boa correlacão entre os valores de p_T dos objetos reconstruídas sem TM e das partículas ao nível do gerador nos eventos do sinal $t\bar{t}Y_{1^+}$ para a massa mais baixa considerada de Y_{1^+}, que é a massa na qual temos mais interesse neste trabalho, dando-nos confiança na estratégia do método de análise aplicado. Quanto maior é o valor desta massa, pior é a correlação, indicando que a suposição de que o p_T de Y_{1^+} contribui negligivelmente para o valor total de $\not{E}_T$ não é válida para massas maiores.

Após a análise sobre os eventos de sinal e de background, e normalizando-os a uma luminosidade integrada (L) de 100 fb^{-1}, os eventos $t\bar{t}$ de background do Modelo Padrão são de longe os que têm a maior contribuição esperada no LHC. Da literatura e de um projeto anterior do grupo no qual este trabalho se insere, escolheram-se dois observáveis da cinemática dalgumas partículas reconstruídas sem TM nesta análise, $\Delta\phi_{l^+l^-}$ e $b_4 = \frac{(p^z_{\bar{t}}.p^z_t)}{(|\vec{p}_t|.|\vec{p}_{\bar{t}}|)}$, que são sensíveis à presença de um mediador vetorial de matéria escura no background do Modelo Padrão. As distribuições de sinal e background destes observáveis foram usadas para avaliar limites de exclusão no multiplicador $\kappa = \frac{g^V_{u33}}{g_{SM}}$ da constante de acoplamento no cenário em que o Modelo Padrão é assumido como hipótese nula e o Modelo Padrão mais um mediador vetorial de matéria escura com acoplamentos aos quarks top é a hipótese alternativa. As distribuições do observável b_4 resultaram em limites de exclusão sensivelmente mais restritos, e, para $m_{Y_{1^+}} = 0.1$, 1, 10 e 100 GeV e $L = 3000$ fb^{-1}, as distribuições de ambos os observáveis considerados providenciaram limites de exclusão com 95% de grau de confiança em valores de $\frac{g^V_{u33}}{g_{SM}}$ que estão abaixo de 1.

Motivados por um trabalho realizado no passado no nosso grupo, no qual o sinal era muito similar ao que é estudado no trabalho apresentado nesta dissertação, considerando o mediador de matéria es-

cura como um escalar (Y_{0^+}), um pseudo-escalar (Y_{0^-}) ou uma mistura de ambos [1], ao invés de um vetor, proposemos mais dois cenários, nos quais o Modelo Padrão + Y_{1^+} é a hipótese nula e o Modelo Padrão + Y_{0^+} ou Y_{0^-} são as hipóteses alternativas. Estes cenários foram apenas estudados para a massa do mediador de 1 GeV e g^V_{u33} fixo a $g_{SM} = 0.25$. A avaliação dos limites de exclusão nestes cenários, utilizando as distribuições dos mesmos dois observáveis, permitiu-nos concluir que, se um sinal muito similar ao do $t\bar{t}Y_{1^+}$ for descoberto no futuro no LHC e assumirmos o Modelo Padrão + Y_{1^+} como a hipótese nula, então conseguimos excluir as hipóteses em que o mediador de matéria escura é um escalar ou um pseudo-escalar associado à produção de pares $t\bar{t}$ para todos os valores das contantes de acoplamento destes dois mediadores de spin 0 com os quarks top e $L = 3000$ fb^{-1}.

Palavras-chave: Matéria Escura, Modelo Padrão, LHC, Partículas Invisíveis, Spin 1.

Abstract

The dark matter (DM) problem can be addressed by the addition of a dark sector composed of viable DM particle candidates to the Standard Model (SM), requiring a DM boson to mediate the interactions between the dark and SM sectors. Employing a simplified DM model - the DMsimp model - in the work of this dissertation, we present a phenomenological study where we successfully perform the kinematic reconstruction of the system $t\bar{t}$ in the presence of a pure vector DM mediator, Y_{1^+}, described by the DMsimp model, that only couples to the top quarks of the SM. Events involving the dileptonic channel of this final state, $t\bar{t}Y_{1^+}$, were generated for the Large Hadron Collider using the Monte Carlo generator MADGRAPH5_AMC@NLO for different DM mediator mass scales, from the low-mass region ($\sim$ 0 GeV) to the Higgs boson mass (125 GeV), and their response at the ATLAS detector were simulated. The reconstruction of the $t\bar{t}$ system is done with a kinematic fit for the dileptonic final state of the $t\bar{t}$ system, without reconstructing the mediator. All relevant SM backgrounds for the dileptonic $t\bar{t}$ channel search at the LHC are considered. Lastly, exclusion confidence level limits are set on the pure vector DM mediator couplings with the top quarks for all generated mediator masses using angular observables to probe how well they discern the $t\bar{t}Y_{1^+}$ signal from the SM background. Exclusion confidence level limits are also set on the pure scalar and pure pseudo-scalar DM mediator couplings with the top quarks to assess the exclusion of spin 0 DM mediators with well-defined CP quantum numbers when the SM plus a pure vector DM mediator is assumed as the null hypothesis.

Keywords: Dark Matter, Standard Model, Large Hadron Collider, Invisible Particles, Spin 1.

Contents

List of Tables

List of Figures

List of Abbreviations

BBN Big Bang Nucleosynthesis

BDTG Boosted Decision Tree with Gradient

BSM Beyond the Standard Model

CKM Cabibbo-Kobayashi-Maskawa

CL Confidence Level

CMB Cosmic Microwave Background

DM Dark Matter

ECAL Electromagnetic Calorimeter

EW Electroweak

EXP Reconstruction without truth-match

GEN Information from generated Monte Carlo events

HCAL Hadronic Calorimeters

LAB Laboratory frame

LHC Large Hadron Collider

LO Leading Order

MACHO Massive Compact Halo Object

MOND Modified Newtonian Dynamics

NLO Next-to-Leading order

NNLL Next-to-Next-to-Leading-Log

NNLO Next-to-Next-to Leading Order

NNLO Next-to-Next-to-Leading Order

PMNS Pontecorvo-Maki-Nakagawa-Sakata

QCD Quantum Chromodynamics

QED Quantum Electrodynamics

QFT Quantum Field Theory

REC Reconstruction with truth-match

ROC Receiving Operating Characteristic

SI International System of Units

SM Standard Model of particle physics

SSB Spontaneous Symmetry Breaking

SUSY Supersymmetry

VEV Vacuum Expectation Value

WIMP Weakly-Interacting Massive Particle

Chapter 1

Introduction

In the last and the current centuries, multiple astrophysical and cosmological observations have been pointing toward the existence of a type of matter that physicists did not account for before, requiring the inclusion of its mass in our calculations such that those observations make sense. This matter was dubbed Dark Matter (DM) due to its invisible nature and because, up until now, we do not know exactly what it is made of. A large amount of candidates have been proposed to explain the nature of DM. These candidates are essentially divided into two categories: modified theories of gravity and theories that hypothesize the DM being composed of objects, whether they are astrophysical objects or particles. If one goes by the hypothesis of DM being composed of particles, then they must interact very weakly with the Standard Model (SM), which is currently the most accepted particle physics theory to explain the fundamental nature of the ordinary matter in our universe. From cosmological constraints, the neutrinos, the most likely particles in the SM to fit the requirements of DM particles, were mostly ruled out as DM candidates. Being out of possible DM candidates in the SM that could match the inferred properties of DM from observations, theoretical particle physicists have been building models that introduce new particles that could be viable DM particle candidates. DM models are those that extend the SM with the addition of a dark sector composed of DM particles beyond the SM that interact very weakly with the SM particles via one or more DM mediators, thus coupling the dark sector with the well-studied SM sector. The Large Hadron Collider (LHC) can probe a large spectrum of some parameters related to dark sectors and achieve the highest ever center-of-mass energies for proton-proton collisions, making it more probable to produce any particle if they indeed exist. At the moment, no particular hypothesis that postulates new DM candidates has been favored because no signal from direct, indirect and collider searches was found. Nevertheless, DM searches continue to exclude parameter space in many theoretical frameworks.

Searches for different DM signatures have been performed at colliders, many of them being focused on mono-events, such as mono-jet, mono-Higgs, etc. [2–4]. Some performed DM searches were based on the production of a $t\bar{t}$ pair or single top quark alongside DM particles [5–8] mostly using variables such as the missing transverse energy as a discriminator, with no attempt to reconstruct the kinematics of the top quarks. This dissertation is motivated by the $t\bar{t}$ production alongside a mediator decaying into DM searches at the LHC and by the following questions: would a final state signal composed of a very light mediator produced alongside a $t\bar{t}$ pair substantially alter the distributions of the chosen observables from the SM $t\bar{t}$ final state signal analysis at the LHC? And if no substantial differences are found, could the reconstruction of the $t\bar{t}$ pair be used to set exclusion limits on the couplings of the DM mediator to the SM particles?

Our questions are studied by considering a simplified DM model which introduces a vector DM

mediator, Y_{1^+}, and studying its coupling to the top quarks. We assess the impact of a spin-1 pure vector DM mediator in the production of the final state $t\bar{t}Y_{1^+}$ at the LHC by performing a previous mainstream experimental analysis of $pp \to t\bar{t}$ in the dileptonic channel of the $t\bar{t}$ pair decay, and so by reconstructing the kinematics of all the involved particles except for the DM mediator, instead of only reconstructing the missing energy. The hypotheses of the DM mediator being a scalar or a pseudo-scalar instead of a pure vector is also studied, aiming at computing exclusion limits on those hypotheses assuming the SM plus a pure vector DM mediator with couplings to the top quarks hypothesis.

In this dissertation, we will begin by introducing the principles used in the construction of the SM in Chapter 2 and the history of the discovery of DM and potential particle candidates in Chapter 3, where we also present the simplified DM model that we used in our work. Next, in Chapter 4, we present a short description of the ATLAS detector at the LHC, since in the performed simulations in our work we consider that the proton-proton collisions occur at the ATLAS detector. An also brief presentation of the current top quark physics and why this quark is important for the search of new physics is done in Chapter 5. The main work for this dissertation is presented in Chapter 6 by starting to describe how the generation and the kinematic reconstruction of the dileptonic $t\bar{t}Y_{1^+}$ signal events at a simulated ATLAS environment were performed. In this same chapter, we also present the results of our analysis and the computed exclusion limits, and their respective discussion. Finally, in Chapter 7 we present a summary of our conclusions regarding our results.

Chapter 2

The Standard Model

The Standard Model (SM) of particle physics is currently the theory that describes the known elementary particles and three (electromagnetic, strong, and weak interactions) of the four (the one not described by the SM is the gravitational interaction) known fundamental interactions with the most consensus among the particle physics community. The development of the SM as we know it today took part in the latter half of the 20th century through the work of many particle physicists, and it has been ascertained to explain and predict plenty of experimental results and phenomena, being one of the most well-tested physics theory in history, making use of Quantum Field Theory (QFT) as a mathematical framework to fundamentally describe the particles and the interactions between them. In this theory, each fundamental particle type has its own field and the corresponding particles are excitations of their fields.

At a low-energy scale, one may think that matter (excluding the photons and the remaining bosons, for now) is only made of electrons, electron neutrinos, protons, and neutrons, the latter two being compounds of the nuclei of the atoms. The electrons orbit the nuclei via the electrostatic attraction that they feel from the nuclei, the protons and neutrons are bound together via the strong nuclear force, and the nuclear β-decays and nuclear fusion are explained at this scale by the production of the electron neutrino in these processes. The gravity interaction is too weak to have importance in singular particle interactions, but it must be taken into account when one studies physics at very large mass scales by making use of the General Theory of Relativity, and so no longer in the particle physics realm. This simplicity is appealing, however, at higher energy scales, experimental observations showed that there is more structure in matter than it was previously thought: the protons and neutrons are actually bound states of quarks which the particle physicists believe to be some of the fundamental particles in Nature. Through the use of particle colliders, the proton was observed to be composed of two up-quarks and one down-quark, while the neutron of one up-quark and two down-quarks. So at this point, we would have the electron, the electron neutrino, the up-quark, and the down-quark. Once again, particle physicists discovered that these four particles are not alone. At an even higher energy scale more particles were discovered and an interesting pattern in particle physics appeared: the latter four particles make up what is called the first generation of fundamental particles and two more very identical generations to the first one were discovered over time. They seem to be exact copies, only differing in the mass of the corresponding particles of different generations. These particles, divided into three generations, are the fermions (spin $\frac{1}{2}$ particles) and their dynamics are described by the relativistic Dirac equation. Being Dirac fermions, for each one of these particles there is a corresponding anti-particle with the same mass but opposite charge.

All the fermions of the SM interact via weak interaction; the ones that possess electric charge can interact via electromagnetic interaction (the neutrinos are the only fermions that do not have electric

charge); only the ones that possess colour charge can interact via strong interaction (the fermions that possess colour charge are called quarks, while the remaining fermions are the leptons). In Table 2.1 and Table 2.2 the six leptons and the six quarks of the SM are listed along with their respective charges and masses, and organized by generations. These leptons and quarks, and their corresponding anti-particles, make up the fundamental fermions of the SM. The neutrinos are massless in the SM by construction, but we have strong experimental evidence that they have mass, however, we only have upper limits on their masses, as the Table 2.1 shows.

Table 2.1: Leptons in the SM organized by generations and their corresponding flavour (note that the flavour of each lepton has the same name as the corresponding lepton), electric charge, and mass. The values were taken from [9] where the uncertainties of the mass values can be found.

Leptons (Spin = 1/2)			
Generation	Flavour	Charge (e)	Mass
1^{st}	Electron (e)	-1	0.511 MeV
	Electron Neutrino (ν_e)	0	< 1.1 eV
2^{nd}	Muon (μ)	-1	105.658 MeV
	Muon Neutrino (ν_μ)	0	< 0.19 eV
3^{rd}	Tau (τ)	-1	1.777 GeV
	Tau Neutrino (ν_τ)	0	< 18.2 eV

Table 2.2: Quarks in the SM organized by generations and their corresponding flavour (note that the flavour of each quark has the same name as the corresponding quark), electric charge and mass. The values were taken from [9] where the uncertainties of the mass values can be found.

Quarks (Spin = 1/2)			
Generation	Flavour	Charge (e)	Mass
1^{st}	Up (u)	2/3	2.16 MeV
	Down (d)	-1/3	4.67 MeV
2^{nd}	Charm (c)	2/3	1.27 GeV
	Strange (s)	-1/3	93.4 MeV
3^{rd}	Top (t)	2/3	172.69 GeV
	Bottom (b)	-1/3	4.18 GeV

The aforementioned electrostatic interaction between the electrons and the nuclei, the strong nuclear force, and the nuclear β-decays and nuclear fusion, are all respectively low-energy manifestations of the fundamental quantum field theories of electromagnetic, strong, and weak interactions, that the SM describes. A consequence of QFT is that the interactions are mediated by a specific species of particles called gauge bosons (also named vector bosons), which are spin 1 particles, and the concept of an "action at a distance" between particles no longer persists. The electromagnetic interaction is mediated by the photon, γ; the strong interaction is mediated by the gluon, g; the weak interaction is mediated by the W^+ and W^- bosons, and the Z boson. In Table 2.3 the gauge bosons are listed along with their electric charges and masses.

The final piece of the SM is the Higgs Boson, H, which is a scalar boson, meaning that it has spin 0, and it is the only fundamental scalar boson discovered up until now. This boson is special since it provides a mechanism - the Higgs mechanism (see 2.5.1) - through which all the massive fundamental particles within the SM acquire mass. In Table 2.4 the Higgs boson is listed along with its

Table 2.3: Vector/Gauge bosons in the SM and their corresponding electric charge and mass. The values were taken from [9] where the uncertainties of the mass values can be found.

Vector Bosons (Spin = 1)		
Boson	Charge (e)	Mass
Photon (γ)	0	0 MeV
Gluon (g)	0	0 MeV
W bosons ($W^{\pm}$)	± 1	80.377 GeV
Z boson (Z)	0	91.1876 GeV

electric charge and mass.

Table 2.4: Fundamental scalar boson (there is only one in the SM: the Higgs boson) in the SM and its corresponding electric charge and mass. The mass value was taken from [9] where the uncertainties of the mass values can be found.

Scalar Boson (Spin = 0)		
Boson	Charge (e)	Mass
Higgs Boson (H)	0	125.25 GeV

Note that the masses of the fundamental particles of the SM in Tables 2.1, 2.2, 2.3 and 2.4 are presented in natural units which were used throughout this dissertation.

2.1 Symmetries and gauge principle

QFT makes use of the Lagrangian formalism, wherein the relativistic[1] dynamics are encoded in the action:

$$S = \int d^4x \, \mathcal{L}[\phi_i(x), \partial_\mu \phi_i(x)], \tag{2.1}$$

where $\mathcal{L}$ is the Lagrangian density[2] which is a Lorentz-invariant functional of the quantum fields, ϕ_i, and their space-time derivatives, $\partial_\mu \phi_i$, in order to get the dynamics of a system. The principle of stationary action leads to the Euler-Lagrange equations (also called equations of motion) of the fields that describe their dynamics[3]:

$$\frac{\partial \mathcal{L}}{\partial \phi_i} - \partial^\mu \left(\frac{\partial \mathcal{L}}{\partial(\partial^\mu \phi_i)} \right) = 0. \tag{2.2}$$

The construction of a Lagrangian that should describe the dynamics of the considered system or model must follow the requirement that the Lagrangian should preserve the global symmetries of the system under consideration. Thus, if the Lagrangian is subjected to a transformation under those symmetries it should not be modified, leading to the same physics. In the construction of the Lagrangian we will consider that it does not have interaction terms between the different fields at the start. This is called the free Lagrangian. The free Lagrangian is invariant under transformations of postulated global continuous symmetries, but that is not generally true when the same continuous symmetries are taken to be local (by local it means that the symmetry transformation depends on the space-time coordinates). Demanding that the Lagrangian (and so the model/physics of the system) is also symmetric with respect to those

[1] The SM employs the Special Theory of Relativity to describe the dynamics of the quantum fields.

[2] From now on, the Lagrangian density will be referred to as Lagrangian.

[3] In the following equation and throughout this dissertation, unless a summation symbol, $\sum$, explicitly appears, we use the Einstein summation notation.

local continuous symmetries requires the addition of new fields with appropriate kinetic and interaction terms in the Lagrangian: we are demanding local gauge invariance. This procedure is called the gauge principle. These local symmetries (called gauge symmetries) are defined by Lie groups (for more information about Lie groups and Group Theory, see appendix A), and for each symmetry group generator a massless vector field (called gauge field) is added in a specific way to the free Lagrangian, which leads to the appearance of interaction terms with the fields of the free Lagrangian (called matter fields). The Lagrangian got extended and the theory that the extended Lagrangian describes is called a gauge theory. The SM is a gauge theory with the local SU(3)×SU(2)×U(1) gauge group symmetry. The way that the gauge principle is applied differs from one gauge theory to another. We will first show how it is applied to get a general gauge field theory in 2.1.1. Next, we show how it is specifically applied to get QED in 2.2, which is an Abelian gauge theory[4], since it is symmetric under U(1) transformations. The same will be done for the non-Abelian gauge theories of the SM: QCD in 2.3 and the electroweak theory in 2.4, which are symmetric under SU(3) and SU(2)×U(1) transformations, respectively.

Moreover the SM has the property that its whole Lagrangian is renormalizable. In a quantum field theory, infinities generally arise at higher orders of perturbation theory, and if that quantum field theory is a renormalizable one that means that those infinities can be absorbed at all orders of perturbation theory by redefining a finite number of parameters such as the masses and the coupling constants. The advantage of these theories is that we are able to calculate the physical observables at any order and at high energies, turning the SM into a theory whose accuracy can be tested beyond the lowest order with precise enough experimental data. The counterpart is that those redefined parameters must be determined by comparison to experimental data.

The Lagrangian of the SM is then the most general one whose terms are gauge invariant under the considered gauge group local symmetries and renormalizable.

2.1.1 Construction of a Gauge Field Theory

A free Lagrangian in QFT is invariant under global transformations of some specific symmetry group, G, however, that is not necessarily true under the corresponding local gauge transformations, $U = e^{-ig_a\alpha^a(x)T^a}\mathbb{1}$[5], since $\partial_\mu\phi \to \partial_\mu(U\phi) = (\partial_\mu U)\phi + U(\partial_\mu\phi)$, where ϕ is any type of matter field and $\partial_\mu\phi$ is part of the kinetic term of the ϕ field. The gauge principle tells us that, to turn the Lagrangian into an invariant Lagrangian under local gauge transformations of a specific gauge group, the partial derivative should be replaced by the covariant derivative relative to that gauge group. The covariant derivative of a general gauge group is defined as:

$$D_\mu = \partial_\mu + ig_a A^a_\mu(x)T^a, \tag{2.3}$$

where $a = 1, 2, ...d_G$[6], g_a[7] the coupling constants (which determine the strength of the force exerted in an interaction) of the gauge symmetry, A^a_μ are the added gauge fields, and T^a the generators of the gauge

[4] An Abelian (non-Abelian) gauge theory is symmetric under an Abelian (non-Abelian) gauge group transformation. More details in appendix A.

[5] This definition of a local gauge transformation comes from A.3, and in that appendix, A, more detailed information about group theory and specifically Lie groups is presented.

[6] d_G is the dimension of the gauge group, which is equal to the number of generators within that gauge group.

[7] $g = g_a$ (and so universal) if the symmetry group is simple. $g_a = g_b$ if and only if T^a and T^b belong to the same simple symmetry group.

group. The goal is to get $D_\mu\phi$ to transform as:

$$D_\mu\phi \to UD_\mu\phi \tag{2.4}$$

and so keeping the Lagrangian invariant under this transformation, since a general Lagrangian for a scalar field multiplet is $\mathcal{L} = (D_\mu\phi)^\dagger(D^\mu\phi) - V(\phi,\phi^\dagger)$ and for a Dirac field it is $\mathcal{L} = \overline{\psi}(i\gamma^\mu D_\mu)\psi - V(\psi,\overline{\psi})$, with the potentials $V(\phi,\phi^\dagger)$ and $V(\psi,\overline{\psi})$ defined such that they are invariant under gauge transformations. To achieve this goal, the gauge fields $A^a_\mu(x)$ have to transform under the gauge symmetry group by a specific transformation law. Instead of determining for $A^a_\mu(x)$, it is easier to determine the transform law for the term $g_a A^a_\mu(x)T^a$, and this one should be:

$$g_a A^a_\mu(x)T^a \to U\left(g_a A^a_\mu(x)T^a\right)U^{-1} - iU\left(\partial_\mu U^{-1}\right). \tag{2.5}$$

Having the transformation laws for the matter and the gauge fields, $D_\mu\phi = \partial_\mu + ig_a A^a_\mu(x)T^a$ transforms under the gauge transformation as:

$$\begin{aligned}
D_\mu\phi \to& \left[\partial_\mu + U\left(ig_a A^a_\mu(x)T^a\right)U^{-1} + U\left(\partial_\mu U^{-1}\right)\right]U\phi \\
=&(\partial_\mu U)\phi + U(\partial_\mu\phi) + U\left(ig_a A^a_\mu(x)T^a\right)\phi + U\left(\partial_\mu U^{-1}\right)U\phi \\
=&UD_\mu\phi + \left[\partial_\mu U + U(\partial_\mu U^{-1})U\right]\phi \\
=&UD_\mu\phi + \left[(\partial_\mu U)U^{-1} + U(\partial_\mu U^{-1})\right]U\phi \\
=&UD_\mu\phi + \left[\partial_\mu(UU^{-1})\right]U\phi \\
=&UD_\mu\phi,
\end{aligned} \tag{2.6}$$

given that $UU^{-1} = \mathbb{1}$. The transformation law in 2.5 led to the wanted local gauge transformation of the covariant derivative: the covariant derivative transforms now as the matter fields.

The infinitesimal version of the transformation law U is $U \simeq \mathbb{1} - ig_a\alpha^a(x)T^a$, allowing us to write the transformation law for $A^a_\mu(x)$ as $A^a_\mu(x) \to A^a_\mu(x) + \delta A^a_\mu(x)$. Using the infinitesimal version of U on 2.5 and skipping the calculations that make use of the information in appendix A, we get:

$$\delta A^a_\mu(x) = g_a f^{abc}\alpha^b(x)A^c_\mu(x) + \partial_\mu\alpha^a(x), \tag{2.7}$$

where f^{abc} are the structure constants (see appendix A) of the considered symmetry group. They are null in Abelian gauge field theories, while the same is not true for non-Abelian gauge field theories.

Finally, the gauge field theory is complete with the introduction of kinetic terms for the gauge fields. In general, they are defined as the following gauge invariant term (for the proof of the gauge invariance of this term, see [10]):

$$\mathcal{L}^{\text{gauge}}_{kin} = -\frac{1}{4}F^a_{\mu\nu}F^{\mu\nu\,a}, \tag{2.8}$$

where $F^a_{\mu\nu}$ is the gauge field strength tensor and it comes from the relation $ig_a F^a_{\mu\nu}T^a \equiv [D_\mu, D_\nu]$. Using the commutation rules of the Lie group generators (see appendix A), the calculation of the commutator $[D^\mu, D^\nu]$ leads to the following definition of the gauge field strength tensor:

$$F^a_{\mu\nu} = \partial_\mu A^a_\nu - \partial_\nu A^a_\mu - g_a f^{abc}A^b_\mu A^c_\nu. \tag{2.9}$$

Thus, explicitly replacing the right part of 2.9 on 2.8, we conclude that for non-Abelian gauge theories gauge field kinetic term give rise to 3- and 4-point self-interactions between the gauge fields, which does

not occur in Abelian gauge theories.

The general Lagrangian with the gauge field kinetic terms is now gauge invariant under G local transformations and the corresponding gauge fields are massless. We do not include mass terms for the gauge fields (such as $\frac{1}{2}m^2 A^a_\mu A^{\mu\, a}$ for real vector fields) since they would violate the local gauge invariance with respect to the G symmetry group.

2.2 QED

The Lagrangian for a free Dirac field ψ with mass m such that its equation of motion is the Dirac equation, $i(\gamma^\mu \partial_\mu - m)\psi = 0$, is:

$$\mathcal{L} = \frac{i}{2}\left[\overline{\psi}\gamma^\mu(\partial_\mu\psi) - (\partial_\mu\overline{\psi})\gamma^\mu\psi\right] - m\overline{\psi}\psi, \tag{2.10}$$

where $\overline{\psi} = \psi^\dagger\gamma^0$ is the adjoint field and $\partial_\mu = \frac{\partial}{\partial x^\mu}$ is the partial derivative with respect to the μ component of the 4 space-time coordinates, x^μ. ψ is a 4×1 column field called spinor field, and γ^μ is the μ Dirac matrix. The terms inside the brackets in 2.10 are the kinetic terms, and the last term is the mass term. The Dirac matrices are defined as:

$$\gamma^0 = \begin{bmatrix} \mathbb{1}_2 & 0 \\ 0 & -\mathbb{1}_2 \end{bmatrix};\ \gamma^i = \begin{bmatrix} 0 & \tau^i \\ -\tau^i & 0 \end{bmatrix},\ i = \{1,2,3\}, \tag{2.11}$$

where τ^i is the i Pauli matrix (the definition of the Pauli matrices is provided in appendix A), and they have the following properties:

$$\{\gamma^\mu, \gamma^\nu\} = \gamma^\mu\gamma^\nu + \gamma^\nu\gamma^\mu = 2g^{\mu\nu}\mathbb{1}_4, \tag{2.12}$$

$$(\gamma^0)^\dagger = \gamma^0 \text{ (and so } \gamma^0 \text{ is hermitian)},\ \gamma^0\gamma^\mu\gamma^0 = (\gamma^\mu)^\dagger, \tag{2.13}$$

where $g^{\mu\nu}$ is the Minkowski space-time metric with signature $(+---)$[8]

Given that ∂_μ and m have dimension $[M]$, ψ and $\overline{\psi}$ must have dimension $[M]^{3/2}$, as every term in a Lagrangian must have dimension $[M]^4$.

In order to apply the gauge principle, one has to first choose the continuous symmetry that the QED Langrangian is symmetric under. From classical electromagnetism, we know that charge is conserved, so it is natural to suppose that this continuous symmetry must lead to the conservation of charge. From this supposition, one can make use of the U(1) symmetry group to get the conservation of charge. Under a global U(1) transformation, the Dirac fields transform as:

$$\psi \to e^{-ie\alpha Q}\psi, \overline{\psi} \to e^{ie\alpha Q}\overline{\psi}, \tag{2.14}$$

where e is the electric charge of the proton (or equivalently, the symmetric electric charge of the electron) and also the coupling constant of QED, Q is the generator of the U(1) symmetry group and also, in this case, the electric-charge operator, and α is an arbitrary constant independent on the space-time coordinates (that is why the transformation is a global one). One can easily see that the Lagrangian in 2.10 is invariant under the transformation in 2.14. But to apply the gauge principle, the QED Lagrangian must

[8]This signature is the convention used for the Minkowski space-time metric in this dissertation.

be invariant under a local U(1) transformation ($\alpha = \alpha(x^\mu)$):

$$\psi \to e^{-ie\alpha(x^\mu)Q}\psi, \overline{\psi} \to e^{ie\alpha(x^\mu)Q}\overline{\psi}. \tag{2.15}$$

Under this U(1) local transformation the kinetic term of the Lagrangian in 2.10 transforms as:

$$\frac{i}{2}\left[\overline{\psi}\gamma^\mu(\partial_\mu\psi) - (\partial_\mu\overline{\psi})\gamma^\mu\psi\right] \to \frac{i}{2}\left[\overline{\psi}\gamma^\mu(\partial_\mu\psi) - (\partial_\mu\overline{\psi})\gamma^\mu\psi\right] + eQ(\partial_\mu\alpha)\overline{\psi}\gamma^\mu\psi, \tag{2.16}$$

meaning that this Lagrangian is locally non-invariant under a U(1) transformation. The gauge principle tells us that, in order to restore the gauge invariance, we need to add one or more new fields with appropriate U(1) transformation laws. For the quantum electromagnetism case, we introduce a real vector field A^μ which resembles the classical electromagnetic potential. This introduced field is postulated to transform under a U(1) local gauge transformation as:

$$A^\mu \to A^\mu + \partial^\mu\alpha, \tag{2.17}$$

and we add the following interaction term to the free Lagrangian:

$$-eQ\overline{\psi}\gamma^\mu\psi A_\mu, \tag{2.18}$$

which is equivalent to saying that the partial derivatives operating on the ψ and $\overline{\psi}$ fields transform as:

$$\partial_\mu \to \partial_\mu + ieQA_\mu \text{ and } \partial_\mu \to \partial_\mu - ieQA_\mu, \text{ respectively.} \tag{2.19}$$

Then the gauge invariant Lagrangian is:

$$\begin{aligned}\mathcal{L}' =& \frac{i}{2}\left[\overline{\psi}\gamma^\mu(\partial_\mu\psi) - (\partial_\mu\overline{\psi})\gamma^\mu\psi\right] - m\overline{\psi}\psi - eQ\overline{\psi}\gamma^\mu\psi A_\mu \\ =& \frac{i}{2}\left[\overline{\psi}\gamma^\mu(\partial_\mu + ieQA_\mu)\psi - \left((\partial_\mu - ieQA_\mu)\overline{\psi}\right)\gamma^\mu\psi\right] - m\overline{\psi}\psi,\end{aligned} \tag{2.20}$$

which can be written in the following more compact form:

$$\mathcal{L}' = \overline{\psi}(i\gamma^\mu\partial_\mu - eQ\gamma^\mu A_\mu - m)\psi. \tag{2.21}$$

The final step is to add an appropriate kinetic-energy term ($\frac{1}{4}F_{\mu\nu}F^{\mu\nu}$) for the introduced A_μ gauge field in order to make this field and the QED Lagrangian physically accurate:

$$\begin{aligned}\mathcal{L}^{\text{QED}} =& \overline{\psi}(i\gamma^\mu\partial_\mu - eQ\gamma^\mu A_\mu - m)\psi - \frac{1}{4}F_{\mu\nu}F^{\mu\nu} \\ =& \overline{\psi}(i\gamma^\mu D_\mu - m)\psi - \frac{1}{4}F_{\mu\nu}F^{\mu\nu},\end{aligned} \tag{2.22}$$

where $F_{\mu\nu} = \partial_\mu A_\nu - \partial_\nu A_\mu$ is the field strength tensor of A_μ (note the absence of the term with structure constants in 2.9 since U(1) is an Abelian symmetry group) which is a U(1) gauge invariant term, and $D_\mu = \partial_\mu + ieQA_\mu$ is called the covariant derivative. The A_μ represents the photon field and we now have the full QED Lagrangian, which was derived from the gauge principle. It describes the electromagnetic interaction between charged fermions and photons, and the dynamics of these two types of particles.

2.3 QCD

The strong interaction is described by the non-Abelian gauge theory with gauge group SU(3) termed Quantum Chromodynamics (QCD). This interaction occurs between particles with a relevant quantum number for this interaction: colour; all the other interactions in the SM are blind to this quantum number. Quarks and gluons are the only particles with colour and so the SU(3) gauge group is also represented as $SU(3)_c$ where the c stands for colour meaning only fields with the colour quantum number in the SM transform under the SU(3) gauge group. Quarks (anti-quarks) have one of 3 distinct colours (anti-colours) while gluons carry one of 8 distinct linear combinations of colours and anti-colours. The latter particles are the gauge bosons of the strong interaction. Flavour is another quantum number which distinguishes quarks in the strong interaction. As shown before, there are six types of quark flavours in the SM: up, down, charm, strange, top, and bottom.

The QCD Lagrangian is:

$$\mathcal{L}^{\text{QCD}} = \sum_{q=\{u,d,s,c,b,t\}} \sum_{j,k=1}^{3} \bar{q}_j i\gamma^\mu (D_\mu)_{jk} q_k - \frac{1}{4} \sum_{a=1}^{8} G^a_{\mu\nu} G^{\mu\nu}_a, \tag{2.23}$$

with the covariant derivative as:

$$(D_\mu)_{jk} = \partial_\mu \delta_{jk} + i g_s \sum_{a=1}^{8} G^a_\mu \left(\frac{\lambda_a}{2} \right)_{jk}, \tag{2.24}$$

and the gluon field strength tensor as:

$$G^a_{\mu\nu} = \partial_\mu G^a_\nu - \partial_\nu G^a_\mu - g_s \sum_{b,c=1}^{8} f^{abc} G^b_\mu G^c_\nu. \tag{2.25}$$

In 2.23, 2.24 and 2.25, q_k is the quark field with flavour $q = u, d, s, c, b, t$[9] and colour $k = 1, 2, 3$ and so the first summation is on the quark flavours and the second one is on the three quark colours, $\delta_{jk} = 1$ if $j = k$ and $\delta_{jk} = 0$ if $j \neq k$, g_s is the strong coupling constant, G^a_μ are the gluons fields with a representing one of the eight gluon linear combinations of colours and anti-colours, and λ_a are the Gell-Mann matrices, A.9, from the definition of generators of the SU(3) symmetry group in A.8, and f^{abc} are the structure constants of SU(3), A.10. The quark field is composed of a part that acts on the Dirac space and another one that acts on the colour space: that is why there is a 4×4 matrix - γ^μ which acts on the Dirac space - and a 3×3 matrix - λ_a which acts on the colour space - in the Lagrangian of QCD.

As expected from the fact that SU(3) is a non-Abelian symmetry group, the term $g_s \sum_{b,c=1}^{8} f_{abc} G^b_\mu G^b_\nu$ in the gluon field strength tensor, 2.25, gives rise to the appearance of self-interaction terms for the gluons (three and four gluon interactions).

2.3.1 Hadronization and Jets

Colour charged particles (gluons and quarks, treated altogether as partons in hard scattering processes such as the ones within proton-proton collisions at hadron colliders) suffer from a phenomenon called colour confinement. This phenomenon reveals itself by no free quark and gluon having been directly

[9] These are the first letters of each quark flavour name.

observed which is understood as being impossible to isolate a single colour charged particle, whether it is a parton or a composite state of partons [9].

A free parton with sufficient energy (those can be, for example, the partons originated from the hard scattering proton-proton collisions at the LHC) undergoes fragmentation, breaking into many further collimated partons, and the set of partons originating from the initial parton is called a parton shower. The partons produced in a parton shower are successively lower in energy and when the scale energy of the constituents of the parton shower is around the order 1 GeV[10], they hadronize into colourless bound states composed of quarks and gluons called hadrons, such as the mesons (consisting of a valence[11] quark and a valence anti-quark) and the baryons (consisting of 3 valence quarks or 3 valence anti-quarks in the case of anti-baryons). Unlike the free partons, we can directly detect hadrons and their decay products. In hard interactions, after the parton shower and the hadronization, the final-state partons and hadrons appear in approximately narrow cones called jets. By identifying and measuring the jets produced at collider detectors, we can reconstruct the kinematics of the high-energy QCD processes that originated them.

2.4 Electroweak Theory

The electromagnetic and the weak interactions are unified in the SM through the electroweak gauge theory, whose gauge group is the direct product of the SU(2) symmetry group with the $\mathrm{U}(1)_Y$ symmetry group: $\mathrm{SU}(2)\times\mathrm{U}(1)_Y$. The SU(2) gauge group has g as coupling constant, and $T^1 = \frac{\tau^1}{2}$, $T^2 = \frac{\tau^2}{2}$ and $T^3 = \frac{\tau^3}{2}$ as generators (see A.5), where τ^1, τ^2 and τ^3 are the Pauli matrices, explicitly presented in A.6. This group is called the group of weak isospin (T) whose 3rd component, $T^3 = \frac{\tau^3}{2}$, leads to an important quantum number with the same name. On the other hand $\mathrm{U}(1)_Y$ has g' as the coupling constant and has only one generator, the hypercharge, Y, playing the same role as Q in QED. From now on, the $\mathrm{U}(1)_Q$ and $\mathrm{U}(1)_Y$ symmetry groups will refer to the U(1) gauge group of QED and of the electroweak theory, respectively. Thus, from 2.3, the covariant derivative of the electroweak interaction is:

$$D^\mu = \partial^\mu + ig(W_1^\mu T_1 + W_2^\mu T_2 + W_3^\mu T_3) + ig' B^\mu Y. \tag{2.26}$$

For the SU(2) gauge group, $W_i^\mu (i = 1, 2, 3)$ are the gauge fields, while B^μ is the gauge field of the $\mathrm{U}(1)_Y$ gauge group. However, none of these fields are the physical ones. The physical fields of the electroweak theory ($W^{+\mu}, W^{-\mu}, Z^\mu, A^\mu$) are defined from the gauge eigenstates:

$$W^{\pm\mu} = \frac{W_1^\mu \mp iW_2^\mu}{\sqrt{2}}, \tag{2.27}$$

$$\begin{bmatrix} A^\mu \\ Z^\mu \end{bmatrix} = \begin{bmatrix} \cos\theta_w & \sin\theta_w \\ -\sin\theta_w & \cos\theta_w \end{bmatrix} \begin{bmatrix} B^\mu \\ W_3^\mu \end{bmatrix}, \tag{2.28}$$

[10] QCD enters its non-perturbative regime when the energy scale is bellow the order $\Lambda_{\mathrm{QCD}} \sim 200$ MeV (Λ_{QCD} is the Landau pole of QCD). This is due to QCD's running coupling constant getting stronger as the distance (momentum transfer) between the partons gets larger (smaller). For energy scales bellow Λ_{QCD}, the QCD's running coupling constant is so strong that the partons get tightly bound in colourless bound states described by non-perturbative QCD.

[11] Valence (anti-)quarks are the (anti-)quarks that determine the quantum numbers of the hadron that they constitute. Apart from the valence quarks, there are plenty of virtual sea quarks, antiquarks, and gluons within the hadron that are constantly being created and annihilated. Even though the 3 latter particles do not contribute to the quantum numbers of the hadron, they make up the bigger fraction of its mass.

where we made use of the weak mixing angle (also called Weinberg angle), θ_w, to rotate B^μ and W_3^μ into the physical SU(2)×U(1)$_Y$ neutral gauge fields, A^μ and Z^μ.

Rotating the W_3^μ and B^μ fields into the physical fields transforms their respective terms in 2.26 into:

$$igW_3^\mu + ig'B^\mu = i(g\sin\theta_w T_3 + g'\cos\theta_w Y)A^\mu + i(g\cos\theta_w T_3 - g'\sin\theta_w Y)Z^\mu. \tag{2.29}$$

In the electroweak theory, we should recover the QED covariant derivative within the EW covariant derivative, thus the term $i(g\sin\theta_w T_3 + g'\cos\theta_w Y)A^\mu$ must be equal to $ieQA^\mu$. We start to define $Q \equiv T_3 + Y$[12] such that the Q operator explicitly appears in the EW Lagrangian:

$$\begin{aligned} igW_3^\mu + ig'B^\mu = i\left((g\sin\theta_w - g'\cos\theta_w)T_3 + g'\cos\theta_w Q\right)A^\mu \\ + i\left((g\cos\theta_w + g'\sin\theta_w)T_3 - g'\sin\theta_w Q\right)Z^\mu. \end{aligned} \tag{2.30}$$

Next, in order to recover the $ieQA^\mu$ term in the EW Lagrangian, the coefficient of the T_3 generator in the first line of 2.29 must be equal to zero, providing a relation between the g and g' coupling constants in function of the Weinberg angle, $g\sin\theta_w = g'\cos\theta_w$, and the coefficient of the Q generator in this term must be equal to e and so we get $e = g'\cos\theta_w$. We can now write both the g and the g' coupling constants as functions of the QED coupling constant and the Weinberg angle:

$$\begin{aligned} g' &= \frac{e}{\cos\theta_w}, \\ g &= \frac{e}{\sin\theta_w}, \end{aligned} \tag{2.31}$$

and so we end up with:

$$igW_3^\mu + ig'B^\mu = ieQA^\mu + i\frac{g}{\cos\theta_w}(T_3 - Q\sin^2\theta_w)Z^\mu. \tag{2.32}$$

Making use of the of the ladder operators of SU(2):

$$T_\pm = \frac{T_1 \pm T_2}{\sqrt{2}}, \tag{2.33}$$

and the transformation 2.27 into the physical $W^{\pm\mu}$ fields, we can finally write down the full SU(2)×U(1)$_Y$ covariant derivative in such a way that the physical gauge fields explicitly appear:

$$D^\mu = \partial^\mu + ieQA^\mu + i\frac{g}{\cos\theta_w}(T_3 - Q\sin^2\theta_w)Z^\mu + ig(W^{+\mu}T_+ + W^{-\mu}T_-) \tag{2.34}$$

Here we can clearly distinguish the QED term from the terms of the weak interaction.

2.4.1 Fermion interaction terms

In the SM, the fermions are described by Dirac spinor fields. A Dirac spinor field, ψ, can always be divided into two parts: the left-handed part, ψ_L, and the right-handed part, ψ_R, such that $\psi = \psi_L + \psi_R$. There is a 4×4 matrix whose eigenvalues distinguish the left-handed part from the right-handed of the

[12] This definition is justified in 2.5.1. $Q \equiv T_3 + Y$ is the only linear combination of the SU(2)×U(1) generators that keeps the $\langle\phi\rangle_0$ doublet invariant. Moreover, defining Q as being the electric charge operator, means that $\langle\phi^0\rangle_0$ is electric neutral. $\langle\phi\rangle_0$ and $\langle\phi^0\rangle_0$ are introduced in 2.5.1.

Dirac field that this matrix operates on. This matrix is termed γ_5 and it is defined as $\gamma_5 = i\gamma^0\gamma^1\gamma^2\gamma^3$. Its eigenvalues are ± 1 and are called chirality. Right-handed Dirac fields have chirality $+1$, while the left-handed ones have chirality -1[13]. One can obtain the left- and right-handed components of a Dirac field using the projection operators which make use of the γ_5 matrix. The left- and right-handed projection operators are, respectively:

$$P_L = \frac{\mathbb{1}_4 - \gamma_5}{2},\ P_R = \frac{\mathbb{1}_4 + \gamma_5}{2}, \tag{2.35}$$

which operate on a Dirac field as:

$$P_L\psi = \psi_L,\ P_R\psi = \psi_R. \tag{2.36}$$

Being projection operators, they obey the usual projection operators relations:

$$P_R + P_L = \mathbb{1}_4,\ (P_R)^2 = P_R,\ (P_L)^2 = P_L,\ P_RP_L = P_LP_R = 0. \tag{2.37}$$

By making use of the first relation we obtain again $\psi = \psi_L + \psi_R = (P_L + P_R)\psi$. The Dirac adjoint fields transform under these projection operators as:

$$\begin{aligned} \overline{\psi}P_L =& \psi^\dagger\gamma^0P_L = \psi^\dagger P_R\gamma^0 = (P_R\psi)^\dagger\gamma^0 = \overline{P_R\psi} = \overline{\psi}_R, \\ \overline{\psi}P_R =& \psi^\dagger\gamma^0P_R = \psi^\dagger P_L\gamma^0 = (P_L\psi)^\dagger\gamma^0 = \overline{P_L\psi} = \overline{\psi}_L. \end{aligned} \tag{2.38}$$

where we made use of the anti-commutation relation $\{\gamma_5, \gamma^\mu\} = 0$ to get $\gamma^0P_{L/R} = P_{R/L}\gamma^0$.

The reasoning behind the introduction of the concept "chirality" in this section is the experimental observation that, in the weak interaction, Dirac fields with distinct chiralities interact differently, and so we call the weak interaction a chiral interaction. The first experimental observation of this property of the weak interaction was when Chien Shiung Wu observed that the weak interaction within β decay violates Parity[14] in an experiment performed by her in 1957 [11].

The $W^\pm$ bosons do not interact with right-handed fermions, while the Z bosons do but with a different strength than with the left-handed fermion. To translate this experimental observation onto the theoretical framework of the weak interaction, SU(2) is defined as a chiral symmetry of the SM by only operating on left-handed fermion fields and because of this the SU(2) symmetry of the SM is referred to as SU(2)$_L$. That the SU(2)$_L$ symmetry in the SM only applies to left-handed fermions is because it was defined that the left-handed Dirac fields form SU(2)$_L$ doublets while the right-handed ones form SU(2)$_L$ singlets.

The left-handed lepton SU(2)$_L$ doublets are separated by generation ($i = e, \mu, \tau$) and are defined as:

$$L_L^i = \begin{bmatrix} \nu_{eL} \\ e_L \end{bmatrix},\ \begin{bmatrix} \nu_{\nu L} \\ \nu_L \end{bmatrix},\ \begin{bmatrix} \nu_{\tau L} \\ \tau_L \end{bmatrix}. \tag{2.39}$$

Since they are SU(2)$_L$ doublets, the top components of these doublets have $T_3 = +\frac{1}{2}$, while the bottom components have $T_3 = -\frac{1}{2}$[15]. The top components are the neutrino fields, and so they have $Q = 0$; the bottom ones are the charged leptons, and so they have $Q = -1$. Thus, from the $Q = T_3 + Y$ relation,

[13] In the limit that the Dirac field is massless, the chirality and helicity $\left(\frac{\vec{S}\cdot\vec{p}}{|\vec{p}|}\right)$ of the fermion described by the Dirac field have the same eigenspinors and eigenvalues; this is the reasoning beyond the naming of left- and right-handed. $\vec{S}$ is the spin vector and $\vec{p}$ is the linear momentum of the spinor particle.

[14] See 2.6 for more information about the Parity symmetry.

[15] It is trivial to check this by applying the generator T_3 defined in A.5 on a SU(2)$_L$ doublet.

these doublets have $Y = -\frac{1}{2}$. The right-handed lepton SU(2)$_L$ singlets are:

$$l_R^i = \{e_R,\ \mu_R,\ \tau_R\}. \tag{2.40}$$

Since they are singlets, their weak isospins T are equal to 0. These are charged fields with $Q = -1$, therefore their hypercharges are $Y = -1$. There are no right-handed neutrinos in the SM, since neutrino oscillations were not known at the time of the construction of the EW gauge theory, and therefore they were thought to be massless [12]. The absence of right-handed neutrinos in the SM turn these particles theoretically massless via the Higgs mechanism, described in 2.5.

The left-handed quark SU(2)$_L$ doublets are similarly grouped by generations:

$$Q_L^i = \begin{bmatrix} u_L \\ d_L \end{bmatrix},\ \begin{bmatrix} c_L \\ s_L \end{bmatrix},\ \begin{bmatrix} t_L \\ b_L \end{bmatrix}. \tag{2.41}$$

The top components are the left-handed up-type quark fields and have $T = +\frac{1}{2}$ and $Q = +\frac{2}{3}$, while the bottom components are the left-handed down-type field with $T = +\frac{1}{2}$ and $Q = -\frac{1}{3}$. Therefore, the left-handed quark SU(2)$_L$ doublets have $Y = +\frac{1}{6}$. The right-handed quark SU(2) singlets are:

$$\begin{aligned} u_R^i &= \{u_R,\ d_R,\ c_R\}, \\ d_R^i &= \{s_R,\ t_R,\ b_R\}, \end{aligned} \tag{2.42}$$

with $T_3 = 0$ since they are singlets, and so, because of their charges (they are the same as the ones of the corresponding left-handed quark fields), the right-handed up-type quark SU(2)$_L$ singlets have $Y = +\frac{2}{3}$ and the down-type ones have $Y = -\frac{1}{3}$. Essentially, since SU(2)$_L$ singlets have $T_3 = 0$ then their charge, Q, is equal to their hypercharge, Y. In 2.41 and 2.42, $i = \{1, 2, 3\}$ represents the i^{th} quark generation with the 1$^{\text{st}}$, 2$^{\text{nd}}$ and 3$^{\text{rd}}$ generations corresponding to the up-, charm- and top-generations, respectively. In 2.42, u_R^i (d_R^i) is the right-handed up-type (down-type) quark field of the i^{th} generation.

Making use of the SU(2)$_L$ fermion doublets[16] and singlets, we can now construct the Lagrangian that connects the Dirac fields to the SU(2)$_L$×U(1)$_Y$ gauge fields. Applying the SU(2)$_L$×U(1)$_Y$ covariant

[16]Note that if there were only singlets in our Lagrangian, no field would "interact" with the weak isospin matrices in the covariant derivative of SU(2)$_L$×U(1)$_Y$.

derivative on the lepton sector, we get:

$$
\begin{aligned}
&\mathcal{L}^{\text{EW}}_{\text{Leptons}} = \sum_{j=\{e,\mu,\tau\}} \left(\overline{L}^j_L i\gamma^\mu D_\mu L^j_L + \overline{l}^j_R i\gamma_\mu D^\mu l^j_R \right) \\
&= \sum_{l=\{e,\mu,\tau\}} \left(\overline{L}^j_L i\gamma_\mu (\partial^\mu + igW^\mu_a T_a + ig' B^\mu Y) L^j_L + \overline{l}^j_R i\gamma_\mu (\partial^\mu + ig' B^\mu Y) l^j_R \right) \\
&= \sum_{l=\{e,\mu,\tau\}} \left(\overline{L}^j_L i\gamma_\mu \left[\partial^\mu + ieQA^\mu + i\frac{g}{2} \left(\tau^+ W^{+\mu} + \tau^- W^{-\mu} \right) + i\frac{g}{\cos\theta_w} \left(\frac{\tau_3}{2} - Q\sin^2\theta_w \right) Z^\mu \right] L^j_L \right. \\
&\quad \left. + \overline{l}^j_R i\gamma_\mu \left[\partial^\mu + ieQA^\mu + i\frac{g}{\cos\theta_w} \left(-Q\sin^2\theta_w \right) Z^\mu \right] l^j_R \right) \\
&= \sum_{l=\{e,\mu,\tau\}} \left(\overline{L}^j_L i\gamma_\mu \left[\partial^\mu + ieQA^\mu + i\frac{g}{\sqrt{2}} \begin{bmatrix} 0 & W^{+\mu} \\ W^{-\mu} & 0 \end{bmatrix} + i\frac{g}{c_w} \begin{bmatrix} \frac{1}{2} - Qs^2_W & 0 \\ 0 & -\frac{1}{2} - Qs^2_W \end{bmatrix} Z^\mu \right] L^j_L \right. \\
&\quad \left. + \overline{l}^j_R i\gamma_\mu \left[\partial^\mu + ieQA^\mu + i\frac{g}{\cos\theta_w} \left(-Q\sin^2\theta_w \right) Z^\mu \right] l^j_R \right) \\
&= \sum_{l=\{e,\mu,\tau\}} \left(\overline{L}^j_L i\gamma_\mu \left[\partial^\mu + ie \begin{bmatrix} 0 & 0 \\ 0 & -1 \end{bmatrix} A^\mu + i\frac{g}{\sqrt{2}} \begin{bmatrix} 0 & W^{+\mu} \\ W^{-\mu} & 0 \end{bmatrix} + i\frac{g}{c_w} \begin{bmatrix} \frac{1}{2} & 0 \\ 0 & -\frac{1}{2} + s^2_W \end{bmatrix} Z^\mu \right] L^j_L \right. \\
&\quad \left. + \overline{l}^j_R i\gamma_\mu \left[\partial^\mu - ieA^\mu + ig\frac{\sin^2\theta_w}{\cos\theta_w} Z^\mu \right] l^j_R \right).
\end{aligned}
\tag{2.43}
$$

Similarly, we apply the $\text{SU}(2)_L \times \text{U}(1)_Y$ covariant derivative on the quark sector:

$$
\begin{aligned}
&\mathcal{L}^{\text{EW}}_{\text{Quarks}} = \sum_{j=1}^{3} \left(\overline{Q}^j_L i\gamma_\mu D^\mu Q^j_L + \overline{u}^j_R i\gamma_\mu D^\mu u^j_R + \overline{d}^j_R i\gamma_\mu D^\mu d^j_R \right) \\
&= \sum_{j=1}^{3} \left(\overline{Q}^j_L i\gamma_\mu \left[\partial^\mu + ie \begin{bmatrix} \frac{2}{3} & 0 \\ 0 & -\frac{1}{3} \end{bmatrix} A^\mu + i\frac{g}{\sqrt{2}} \begin{bmatrix} 0 & W^{+\mu} \\ W^{-\mu} & 0 \end{bmatrix} + i\frac{g}{c_W} \begin{bmatrix} \frac{1}{2} - \frac{2s^2_W}{3} & 0 \\ 0 & \frac{s^2_W}{3} - \frac{1}{2} \end{bmatrix} Z^\mu \right] Q^j_L \right. \\
&\quad + \overline{u}^j_R i\gamma_\mu \left[\partial^\mu + ie\frac{2}{3} A^\mu - ig\frac{2}{3}\frac{\sin^2\theta_w}{\cos\theta_w} Z^\mu \right] u^j_R \\
&\quad \left. + \overline{d}^j_R i\gamma_\mu \left[\partial^\mu - ie\frac{1}{3} A^\mu + ig\frac{1}{3}\frac{\sin^2\theta_w}{\cos\theta_w} Z^\mu \right] d^j_R \right),
\end{aligned}
\tag{2.44}
$$

where $s_w = \sin\theta_w$ and $c_w = \cos\theta_w$.

From the Lagrangians in 2.43 and 2.44, we see that the matrix with the $W^\pm$ bosons fields leads to interaction terms that not only couple fields with different charges but also with different flavours: in the lepton sector it leads to the interaction between a neutrino flavoured lepton with a charged flavoured lepton of the same generation; in the quark sector it leads to the interaction between an up-type flavoured quark and a down-type flavoured quark of the same generation[17]. For this reason, the interactions of the $W^\pm$ bosons fields with the fermion Dirac fields are named Flavour Changing Charged Currents (FCCCs). Furthermore, the $W^\pm$ bosons only interact with left-handed fermions and right-handed anti-fermions. On the other hand, the matrices and terms involving the A^μ and Z^μ boson fields are diagonal so they couple to fermion fields of equal flavour, thus there are no Flavour Changing Neutral Currents (FCNCs) at tree

[17]Here we take the generations of the quarks as being the ones used in the weak basis, where the fields are unphysical. In 2.5.2 we introduce the generations in the mass basis, where the fields are the physical ones and interactions between up-type and down-type quarks from different families can occur via $W^\pm$ mediation.

level in this sector. These neutral gauge bosons couple to both left- and right-handed Dirac fields. For the A^μ boson they couple equally to them, but for the Z^μ the interaction terms differ, since there is the absence of the τ_3 matrix of the SU(2)$_L$ group in the right-handed part of these Lagrangians.

Also from 2.43 and 2.44 and using the projection operators definitions and properties (2.35, 2.36, 2.37, 2.38), we can rearrange the coupling terms in the following way:

$$\textbf{Couplings between fermions and } \boldsymbol{A^\mu}\textbf{:} - eQ_{f^i}\overline{\psi}^i\gamma_\mu\psi^i A^\mu; \tag{2.45}$$

$$\textbf{Couplings between fermions and } \boldsymbol{W^{\pm\mu}}\textbf{:} - \frac{g}{\sqrt{2}}\overline{\psi}^i\gamma_\mu P_L\psi^j W^{\pm\mu} = -\frac{g}{2\sqrt{2}}\overline{\psi}^i\gamma_\mu(1-\gamma_5)\psi^j W^{\pm\mu}; \tag{2.46}$$

$$\textbf{Couplings between fermions and } \boldsymbol{Z}\textbf{:} - \frac{g}{2\cos\theta_w}\overline{\psi}^i\gamma_\mu(g_V^i - g_A^i\gamma_5)\psi^i Z_\mu; \tag{2.47}$$

where ψ^i and ψ^j are fermion fields with i and j flavours of the same generation, respectively, and $g_V^i = (T_3^i - 2Q^i\sin\theta_w)$ and $g_A^i = T_3^i$ are the vector (V) and axial (A) couplings of the Z boson to the fermions with flavour i. Thus, the electromagnetic interaction is a vector one since it contains $\overline{\psi}\gamma_\mu\psi$, while the weak interaction is a vector minus axial interaction given that it contains $\overline{\psi}(c_V\gamma_\mu - c_A\gamma_\mu\gamma_5)\psi$, where the coefficients c_V and c_A are equal to 1 for the interaction with the $W^\pm$ boson and different from 1 and from each other for the interaction with the Z boson.

An important remark is the absence of mass terms for the fermion fields in the Lagrangians 2.43 and 2.44 due to their gauge breaking of the SU(2)$_L\times$U(1)$_Y$ symmetry invariance. A general fermion field mass term can be decomposed on the left- and right-handed fermion fields in the following way:

$$\begin{aligned} m\overline{\psi}\psi =& m\overline{\psi}(P_L+P_R)\psi \\ =& m\overline{\psi}(P_L^2+P_R^2)\psi \\ =& m(\overline{\psi}_R\psi_L + \overline{\psi}_L\psi_R). \end{aligned} \tag{2.48}$$

With ψ_R as a SU(2)$_L$ singlet and ψ_L as a SU(2)$_L$ doublet component in the SM, these fields transform differently under SU(2)$_L\times$U(1)$_Y$, thus a mass term like 2.48 would break the SU(2)$_L\times$U(1)$_Y$ symmetry of the SM, and so the gauge invariance of the SM Lagrangian. At this point the SM should be incomplete since we do not include mass terms for the particles of charged lepton fields and quark fields, whose particles we know are massive. To justify the appearance of mass terms for the fermions, the SM makes use of one mechanism which spontaneously breaks the SU(2)$_L\times$U(1)$_Y$ symmetry into the $U(1)_Q$ symmetry, in order to preserve the electric charge conservation: the Higgs Mechanism, 2.5.1. The fermion masses arise from the Yukawa interactions (see 2.5.2) with the ϕ SU(2)$_L$ doublet introduced in 2.5.

2.4.2 Electroweak gauge sector

Next, we must include kinetic terms for the gauge fields of the weak interaction. In EW the gauge group is SU(2)$_L\times$U(1)$_Y$, where SU(2)$_L$ is a non-Abelian gauge group and so its gauge field strength tensor is $F_a^{\mu\nu} = \partial^\mu W_a^\mu - \partial^\nu W_a^\nu - g\sum_{b,c=1}^3 \epsilon_{abc}W_b^\mu W_c^\nu$, where ϵ^{abc} are structure constants of the SU(2) group (A.7), and U(1)$_Y$ is an Abelian gauge group, thus its gauge field strength tensor is $F_Y^{\mu\nu} = \partial^\mu B^\mu - \partial^\nu B^\nu$. Both these gauge field strength tensors are constructed from 2.9. From 2.8,

the Lagrangian for the kinetic terms of the $SU(2)_L \times U(1)_Y$ gauge fields is:

$$\mathcal{L}^{\text{EW}}_{\text{Gauge}} = -\frac{1}{4} F_Y^{\mu\nu} F_{\mu\nu\, Y} - \frac{1}{4} \sum_{a=1}^{3} F_a^{\mu\nu} F_{\mu\nu\, a}. \tag{2.49}$$

Then we transform the unphysical gauge fields into the physical ones and the resulting Lagrangian has terms quadratic, cubic, and quartic on the physical gauge fields. The quadratic terms are the kinetic energy terms of the physical $SU(2)_L \times U(1)$ gauge fields, while the cubic and quartic terms are the ones describing interactions between three and four of the corresponding gauge bosons, respectively. The quadratic terms of 2.49, with the physical gauge fields explicitly appearing, are:

$$\begin{aligned} \mathcal{L}^{\text{EW}\,(2)}_{\text{Gauge}} = &-\frac{1}{2}(\partial^\mu A^\nu)(\partial_\mu A_\nu) + \frac{1}{2}(\partial^\mu A^\nu)(\partial_\nu A_\mu) \\ &-\frac{1}{2}(\partial^\mu Z^\nu)(\partial_\mu Z_\nu) + \frac{1}{2}(\partial^\mu Z^\nu)(\partial_\nu Z_\mu) \\ &-(\partial^\mu W^{+\nu})(\partial_\mu W^-_\nu) + (\partial^\mu W^{+\nu})(\partial_\nu W^-_\mu). \end{aligned} \tag{2.50}$$

As stated in 2.1.1, we should not include mass terms for the $SU(2)_L \times U(1)_Y$ gauge bosons in the electroweak Lagrangian, since they will not be gauge invariant under transformations of that symmetry group. We know, however, that the $W^\pm$ and Z bosons are the only massive gauge bosons in the SM. The Higgs mechanism, 2.5.1, will provide the appearance of mass terms for the gauge fields of these massive bosons.

2.5 The Higgs sector

The Lagrangians in QFT are invariant under specific symmetries. For several reasons, one may want to purposely break a symmetry of the considered Lagrangian or of specific states of the physical system. There are two types of symmetry breaking:

- **Explicit Symmetry Breaking:** It occurs when one adds extra terms to the Lagrangian, turning the whole Lagrangian non-invariant under the transformations of the initial symmetry group;
- **Spontaneous Symmetry Breaking:** It occurs when the ground state (also called vacuum state) of the theory described by the Lagrangian is not invariant under the transformations of symmetry group of the Lagrangian. However, the Lagrangian itself continues to be invariant under transformations of that symmetry group.

In the SM, the fermions and the massive gauge bosons get mass terms through the inclusion of a whole sector in the SM: the Higgs sector. Those mass terms arise from Spontaneous Symmetry Breaking in the vacuum state of one of the fields of the Higgs sector. The arising of the mass terms for the massive gauge bosons and for the fermions is described in 2.5.1 and 2.5.2, respectively.

2.5.1 Higgs Mechanism

As stated before, the inclusion of mass terms for the massive gauge bosons in the Lagrangian of the SM breaks their gauge symmetry invariance by explicit symmetry breaking. We need a workaround in order to include these mass terms and still keep the gauge invariance of the SM Lagrangian.

In the SM, the workaround is the Higgs mechanism [13]. The Higgs mechanism generates mass terms by adding a scalar field with a non-zero vacuum expectation value (VEV) to the SM, causing the

Spontaneous Symmetry Breaking (SSB) of the SU(2)$_L$×U(1)$_Y$ gauge symmetry into the U(1)$_Q$ gauge symmetry in the vacuum. For the breaking of the SU(2)$_L$×U(1)$_Y$ gauge symmetry, the scalar field cannot be a SU(2)$_L$ singlet since it could not break that gauge symmetry, and it must be electric neutral, preventing the U(1)$_Q$ symmetry of being broken and the photon of getting mass. There are several ways of introducing a scalar field that fulfills the requirements above. The simplest way and the one that is currently used in the SM is by embedding that scalar field on a single SU(2)$_L$ doublet, and this solution is termed the minimal Higgs structure [14] and it is explained below.

The SU(2)$_L$ doublet scalar field, ϕ, is usually defined as:

$$\phi = \begin{bmatrix} \phi^+ \\ \phi^0 \end{bmatrix} = \frac{1}{\sqrt{2}} \begin{bmatrix} \phi_1 + i\phi_2 \\ \phi_3 + i\phi_4 \end{bmatrix}, \tag{2.51}$$

where the $+$ and 0 superscripts on the ϕ^+ and ϕ^0 complex scalar fields indicate that those fields have $Q = 1$ and $Q = 0$, respectively, by assuming beforehand that this doublet has $Y = \frac{1}{2}$, which leads to the $Q = T_3 + Y$ relation as we will show bellow.

We want to write a potential for ϕ and so it must follow some requirements: the terms in the potential must be invariant under SU(2)$_L$×U(1)$_Y$ and with dimension $[M]^4$ at most. Given that ϕ transforms as $\phi \to U\phi$ under a SU(2)$_L$ transformation, where U is a SU(2)$_L$ unitary matrix, i.e, $U^\dagger U = \mathbb{1}$, then the term $\phi^\dagger\phi$ transforms as $\phi^\dagger\phi \to (U\phi)^\dagger U\phi = \phi^\dagger U^\dagger U\phi = \phi^\dagger\phi$, and so this and every term which is the $n \in \mathbb{N}$ power of the latter term are invariant terms under SU(2)$_L$. These terms are also trivially invariant under U(1)$_Y$ symmetry transformations. Given also that the doublet scalar field has dimension $[M]$ then we can write the following simple potential for ϕ:

$$V = \mu^2\phi^\dagger\phi + \lambda(\phi^\dagger\phi)^2, \tag{2.52}$$

with μ^2 having dimension $[M]^2$ and λ being dimensionless. We can check that every term in this potential has dimension $[M]^4$. The ground state of the doublet scalar field corresponds to its value when the scalar potential is on its minimum. This minimum occurs at $\phi^\dagger\phi = -\frac{\mu^2}{2\lambda} = \frac{v^2}{2}$ with $\lambda > 0$ to guarantee that the potential has indeed a minimum, meaning that it is bounded from below, and $\mu^2 < 0$ since $\phi^\dagger\phi > 0$.

We aim to set a VEV to the ϕ doublet such that $\langle\phi\rangle_0$[18] leads to the minimum condition $\langle\phi^\dagger\phi\rangle_0 = \frac{v}{\sqrt{2}}$ of the potential 2.52. Since $\phi^\dagger\phi = \frac{1}{2}(\phi_1^2 + \phi_2^2 + \phi_3^2 + \phi_4^2)$ is invariant under SU(2)$_L$×U(1)$_Y$ symmetry transformations, there is an infinite number of degenerate VEV of ϕ that fulfill the minimum condition. Any choice of a VEV of the ϕ doublet is equivalent in the sense that under a SU(2)$_L$×U(1)$_Y$ symmetry transformation the chosen VEV value transforms into another VEV belonging to the infinite set of degenerate $\langle\phi\rangle_0$ doublets that minimize the potential in 2.52, keeping the SU(2)$_L$×U(1)$_Y$ and physics invariance of the considered system. However, the VEV, and therefore the ground state, of ϕ is not invariant under the SU(2)$_L$×U(1)$_Y$ symmetry. Thus, by definition, we get a spontaneous SU(2)$_L$×U(1)$_Y$ symmetry breaking of the system [15].

In general, we can attribute a non-zero VEV to both ϕ^+ and ϕ^0 fields of the ϕ doublet. A non-zero VEV for the ϕ^+ field would break the charge conservation of the SM giving rise to an electric charged vacuum, but with a specific SU(2)$_L$ transformation in the ϕ doublet we can always rotate away the VEV of the ϕ^+ field so that the vacuum remains invariant under U(1)$_Q$. A convenient choice is to set $\langle\phi_1\rangle_0 = \langle\phi_2\rangle_0 = \langle\phi_4\rangle_0 = 0$, requiring that $\langle\phi_3\rangle_0 = v$. This choice allows us to redefine the real neutral

[18] $\langle\phi\rangle_0 = \langle 0|\phi|0\rangle$ is the vacuum expectation value of the ϕ doublet. $|0\rangle$ is the vacuum/ground state in the Fock space.

component of the ϕ doublet, $\frac{\phi_3}{\sqrt{2}}$, as a field that fluctuates around its VEV:

$$\phi^0 = \frac{1}{\sqrt{2}}(\phi_3 + i\phi_4) = \frac{1}{\sqrt{2}}[(v + H) + i\chi], \tag{2.53}$$

and so we get:

$$\phi = \begin{bmatrix} \phi^+ \\ \frac{1}{\sqrt{2}}[(v + H) + i\chi] \end{bmatrix}; \ \langle\phi\rangle_0 = \frac{1}{\sqrt{2}} \begin{bmatrix} 0 \\ v \end{bmatrix}. \tag{2.54}$$

H and $\chi = \phi_4$ are real scalar fields whose VEVs are equal to zero. Now, one can easily check that $\langle\phi\rangle_0$ is not invariant under SU(2)$_L$×U(1)$_Y$: under a non-trivial SU(2)$_L$×U(1)$_Y$ transformation, $e^{-i(g'\alpha'(x)Y + g\alpha^a(x)T^a)}$, the invariance requirement for $\langle\phi\rangle_0$ is that the application of any SU(2)$_L$×U(1)$_Y$ generator on $\langle\phi\rangle_0$ must be equal to zero such that $\delta\langle\phi\rangle_0 = 0$ in $\langle\phi\rangle_0 \to \langle\phi\rangle_0 + \delta\langle\phi\rangle_0$; Y, T_1, T_2 and T_3 give non-zero values when applied to $\langle\phi\rangle_0$, thus the ground state is non-invariant under SU(2)$_L$×U(1)$_Y$ transformations and these generators are called broken generators. However, the linear combination $Q \equiv T_3 + Y$ leads to $Q\langle\phi\rangle_0 = 0$, thus, as expected, the ground state is invariant under U(1)$_Q$ transformations. The convenient choice for the VEV of the ϕ doublet, 2.54, was made in order to preserve the invariance of the ground state under U(1)$_Q$ transformations when the ϕ doublet is assumed to have $Y = \frac{1}{2}$. Thus, the electric charge operator must be defined as $Q \equiv T_3 + Y$.

Replacing ϕ in the form shown in 2.54 on the scalar potential expression 2.52 and replacing λ with $-\frac{\mu^2}{v^2}$, we get the potential written in the following way in which we can distinguish different types of terms and explicitly see all the real fields within the ϕ and $\phi^\dagger$ doublets:

$$\begin{aligned} V = {} & \mu^2\frac{v^2}{4} - \mu^2 H^2 - \frac{\mu^2}{v}(H^3 + H\chi^2 + 2H\phi^-\phi^+) \\ & - \frac{\mu^2}{v^2}\left[\frac{H^4}{4} + \frac{\chi^4}{4} + \frac{H^2\chi^2}{2} + \phi^-\phi^+H^2 + \phi^-\phi^+\chi^2 + (\phi^-\phi^+)^2\right] \end{aligned} \tag{2.55}$$

In 2.55 there are no mass terms for the χ, ϕ^+, and ϕ^- fields. They are the fields of the Goldstone bosons, and they are predicted by the Goldstone theorem [16, 17] which states that one massless field, corresponding to a Goldstone boson, appears in the Lagrangian for each generator of a continuous global symmetry that is spontaneously broken. They are unphysical because they can be set to 0 by an appropriate gauge transformation. In the spontaneous breaking of the SU(2)$_L$×U(1)$_Y$ symmetry of the SM, the 4 group generators are broken but a linear combination of two of them is not, as aforementioned, thus we get 3 Goldstone bosons. On the other hand, the H boson is massive, since 2.55 contains the term $-\mu^2H^2$ which means that $m_H = \sqrt{-2\mu^2} = \sqrt{2\lambda v^2}$. Excluding the first term (which is simply a constant) and the mass term, the remaining terms in the scalar potential 2.55 are interaction terms.

This scalar potential is part of the Lagrangian of the ϕ doublet. Being a SU(2)$_L$×U(1)$_Y$ doublet, the kinetic-energy terms of its Lagrangian, $\mathcal{L}_{kin} = (D_\mu\phi)^\dagger(D^\mu\phi)$, have D^μ as the EW covariant derivative,

2.34. Applying the EW covariant derivative to the ϕ doublet, we get:

$$\begin{aligned} D^\mu\phi &= \left[\partial^\mu + ieQA^\mu + i\frac{g}{2}\left(\tau^+W^{+\mu} + \tau^-W^{-\mu}\right) + i\frac{g}{\cos\theta_w}\left(\frac{\tau_3}{2} - Q\sin^2\theta_w\right)Z^\mu\right]\phi \\ &= \left[\partial^\mu + i\frac{g}{\sqrt{2}}\left(\begin{bmatrix}0 & 1\\ 0 & 0\end{bmatrix}W^{+\mu} + \begin{bmatrix}0 & 0\\ 1 & 0\end{bmatrix}W^{-\mu}\right) + i\frac{g}{\cos\theta_w}\frac{1}{2}\begin{bmatrix}1 & 0\\ 0 & -1\end{bmatrix}Z^\mu \right. \\ &\quad \left. + \left(ieA^\mu - ig\frac{\sin^2\theta_w}{\cos\theta_w}Z^\mu\right)\begin{bmatrix}\frac{1}{2}+Y & 0\\ 0 & -\frac{1}{2}+Y\end{bmatrix}\right]\phi \\ &= \left[\partial^\mu\phi + i\frac{g}{\sqrt{2}}\begin{bmatrix}W^{+\mu}\phi^0\\ W^{-\mu}\phi^+\end{bmatrix} + i\frac{g}{\cos\theta_w}\frac{1}{2}\begin{bmatrix}\phi^+\\ -\phi^0\end{bmatrix}Z^\mu + \left(ieA^\mu - ig\frac{\sin^2\theta_w}{\cos\theta_w}Z^\mu\right)\begin{bmatrix}\phi^+\\ 0\end{bmatrix}\right]. \end{aligned} \tag{2.56}$$

Then, from $\mathcal{L}_{kin} = (D_\mu\phi)^\dagger(D^\mu\phi)$, we get the following quadratic terms:

$$\begin{aligned} \mathcal{L}^{(2)}_{kin} =& (\partial_\mu\phi^-)(\partial^\mu\phi^+) + \frac{1}{2}[(\partial_\mu H)(\partial^\mu H) + (\partial_\mu\chi)(\partial^\mu\chi)] \\ &+ \frac{g^2v^2}{4}W^-_\mu W^{+\mu} + \frac{g^2v^2}{8\cos^2\theta_w}Z_\mu Z^\mu \\ &+ i\frac{gv}{2}(W^{+\mu}\partial_\mu\phi^- - W^-_\mu\partial^\mu\phi^+) - \frac{gv}{2\cos\theta_w}Z_\mu\partial^\mu\chi. \end{aligned} \tag{2.57}$$

The mass term of a general C^μ spin 1 massive field (also called Proca field) has the form $\eta_C m_C^2 C_\mu C^\mu$, with $\eta_C = \frac{1}{2}$ if C^μ is a real field and $\eta_C = 1$ if C^μ is a complex field, and so, by inspecting 2.57 we observe the existence of those mass terms for the $W^{\pm\mu}$ and Z^μ fields. Thus, the Higgs mechanism provides mass terms for the massive bosons of the weak interaction, with the following masses:

$$m_{W^\pm} = \frac{gv}{2} \text{ and } m_Z = \frac{gv}{2\cos\theta_w}, \tag{2.58}$$

which are related by:

$$m_W = m_Z\cos\theta_w. \tag{2.59}$$

From [9], $\sin^2\theta_w = 0.22339$, using the on-shell scheme, and $v = 246.22$ GeV.

The last line of 2.57 contains terms where an EW gauge boson field gets multiplied to the derivative of a Goldstone scalar field, which in turn complicates the definition of their propagators. To deal with this problem, the simpler way is by choosing to use the unitary gauge (this choice of gauge is used in [18], for example), which removes the Goldstone bosons from the Lagrangian by performing an appropriate SU(2)$_L$ transformation of ϕ, thus explicitly proving that the Goldstone bosons are not physical degrees of freedom. We will make use of the unitary gauge from now on.

With the inclusion of the Higgs Mechanism, the SM Lagrangian keeps its SU(2)$_L\times$U(1)$_Y$ gauge invariance, while the vacuum does not.

2.5.2 Yukawa sector

Experimentally we know that quarks and the charged leptons have mass, and we need an alternative way of giving mass to these fermions, in opposition to the not allowed inclusion of Dirac mass terms to the initial Lagrangian since these terms break the precious gauge invariance of the SM as we have seen before. The ϕ doublet will once again provide an alternative way of adding mass terms to these fermions. This is possible by introducing interaction terms between the ϕ doublet and the fermions fields into the SM Lagrangian. Those terms compose the Yukawa Lagrangian (it is called Yukawa because it

gives interaction terms between a scalar field and two fermion fields).

The Yukawa Lagrangian of the SM for the leptons is:

$$\mathcal{L}^{\text{Yukawa}}_{\text{Leptons}} = \sum_{i=\{e,\mu,\tau\}} \left\{ -y_i \begin{bmatrix} \overline{\nu}^i_L & \overline{l}^i_L \end{bmatrix} \begin{bmatrix} \phi^+ \\ \phi^0 \end{bmatrix} l^i_R - y^*_i \overline{l}^i_R \begin{bmatrix} \phi^- & \phi^{0*} \end{bmatrix} \begin{bmatrix} \nu^i_L \\ l^i_L, \end{bmatrix} \right\}, \tag{2.60}$$

y_i being a complex coupling constant and the second term inside the summation is the hermitian conjugate of the first one. The lepton SU(2)$_L$ doublets and singlets are the same ones from 2.39 and 2.40, respectively. This Lagrangian is invariant under SU(2)$_L$×U(1)$_Y$ transformations, unlike the fermion mass terms that we saw before that did not make use of the Higgs field, and it is renormalizable since the fermion Dirac fields have dimension $[M]^{\frac{3}{2}}$ and the scalar fields have dimension $[M]$. Moreover, we have assumed that the leptons do not interact with leptons from other families in this Lagrangian, and so there is no mixing within the Lepton Yukawa sector. Substituting the definition of the ϕ doublet, 2.54, in the unitary gauge[19] into 2.60, we get:

$$\begin{aligned} \mathcal{L}^{\text{Yukawa}}_{\text{Leptons}} &= \sum_{i=\{e,\mu,\tau\}} \left\{ -y_i \overline{l}^i_L l^i_R \phi^0 - y^*_i \overline{l}^i_R l^i_L \phi^0 \right\} \\ &= \sum_{i=\{e,\mu,\tau\}} \left\{ -\frac{y_i v}{\sqrt{2}} \overline{l}^i_L l^i_R - \frac{y_i}{\sqrt{2}} \overline{l}^i_L l^i_R H - \frac{y^*_i v}{\sqrt{2}} \overline{l}^i_R l^i_L - \frac{y^*_i}{\sqrt{2}} \overline{l}^i_R l^i_L H \right\} \\ &= \sum_{i=\{e,\mu,\tau\}} \left\{ -\frac{y_i v}{\sqrt{2}} \overline{l}^i l^i - \frac{y_i}{\sqrt{2}} \overline{l}^i l^i H \right\}. \end{aligned} \tag{2.61}$$

In the last line of 2.61 the l^i_R was rephased in order to make the y_i real and positive. The general mass term for a Dirac fermion, ψ, within a Lagrangian is $-m\overline{\psi}\psi$ and so, from the Yukawa Lagrangian for the leptons, 2.61, the mass of the l^i charged lepton is $m_i = \frac{y_i v}{\sqrt{2}}$. There is no mass term for the neutrinos, since we have assumed in our Lagrangian that these particles cannot be right-handed. To account for their mass, we should have introduced in 2.60 terms with ν_R and $\overline{\nu}_R$ singlets.

As opposed to the leptons, there is a right-handed quark for each left-quark (in the lepton sector there are no right-handed neutrinos) and we experimentally know that there are $W^\pm$ currents with flavour changing between different generations within the quark sector (the first signs of the existence of these $W^\pm$ currents come from the experimental discovery of CP[20] violation in kaon decays in 1964 [19]; in 1973, Makoto Kobayashi and Toshihide Maskawa showed that the CP violation within the quark sector could be explained by demanding the existence of at least 3 generations of quarks [20]) and so we cannot assume that the quarks do not interact with other quarks from different generations in the Yukawa sector. In order to find a mass term for the up-quarks, one must use the $\tilde{\phi} = i\tau_2\phi^*$ doublet since in this doublet the upper-component is the one that has the v constant, unlike the ϕ doublet, which has v in the down-component, and it also transforms as a SU(2)$_L$ doublet. Now, we can write the following Yukawa Lagrangian for the quarks:

$$\mathcal{L}^{\text{Yukawa}}_{\text{Quarks}} = -\sum_{j,k=1}^{3} \left\{ Y^d_{jk} \overline{Q}^j_L d^k_R \begin{bmatrix} \phi^+ \\ \phi^0 \end{bmatrix} + Y^u_{jk} \overline{Q}^j_L u^k_R \begin{bmatrix} \phi^{0*} \\ -\phi^- \end{bmatrix} \right\} + h.c., \tag{2.62}$$

where Y^d_{jk} and Y^u_{jk} are entries of 3×3 complex and arbitrary matrices with the Yukawa couplings of

[19] Since we use the unitary gauge, $\phi_0 = \phi^*_0$.

[20] See 2.6 for more information about the CP symmetry.

the down- and up-type quarks, respectively, and the Q_L^j doublet and u_R^k and d_R^k singlets are the same as the ones from 2.41 and 2.42, respectively. These matrices are not both diagonal[21], and so the quark fields we have used so far are unphysical states - weak eigenstates - given that diagonal matrices would mean that we would immediatly get the mass terms of the physical states - mass eigenstates. For the diagonalization of these matrices and for the mass eigenstates of the quarks to explicitly appear, we have to perform a basis transformation on the weak eigenstates. The basis transformation from the unphysical fields to the physical fields is:

$$\begin{aligned} U_L \equiv \begin{bmatrix} \hat{u}_L \\ \hat{c}_L \\ \hat{t}_L \end{bmatrix} = V_L^{u\dagger} \begin{bmatrix} u_L \\ c_L \\ t_L \end{bmatrix}, \; U_R \equiv \begin{bmatrix} \hat{u}_R \\ \hat{c}_R \\ \hat{t}_R \end{bmatrix} = V_R^{u\dagger} \begin{bmatrix} u_R \\ c_R \\ t_R \end{bmatrix}, \\ D_L \equiv \begin{bmatrix} \hat{d}_L \\ \hat{s}_L \\ \hat{b}_L \end{bmatrix} = V_L^{d\dagger} \begin{bmatrix} d_L \\ s_L \\ b_L \end{bmatrix}, \; D_R \equiv \begin{bmatrix} \hat{d}_R \\ \hat{s}_R \\ \hat{b}_R \end{bmatrix} = V_R^{d\dagger} \begin{bmatrix} d_R \\ s_R \\ b_R \end{bmatrix}, \end{aligned} \tag{2.63}$$

where $V_{L,R}^{u,d}$ are 3×3 unitary (the Lagrangian is invariant under unitary transformations) matrices and $\hat{q}_{L,R}$ are the physical q flavoured quark fields. The mass matrices of the unphysical quark fields are defined as $M_u = \frac{v}{\sqrt{2}} Y^u$ and $M_d = \frac{v}{\sqrt{2}} Y^d$. We aim to diagonalize these mass matrices in such a way that the resulting diagonal matrix has real and non-negative diagonal matrix elements. Using the theorem that states that any square matrix M can be bi-diagonalized by two unitary matrices U and U' as $U^\dagger M U' = D$ such that D is a diagonal matrix with real and non-negative diagonal matrix elements [21], we can now transform the M_u and M_d matrices by multiplying them with the appropriate unitary matrices (those are the $V_{L,R}^{u,d}$ matrices), in order to get the mass matrices of the physical quark fields:

$$\begin{aligned} V_L^{u\dagger} M_u V_R^u = \hat{M}_u \equiv \begin{bmatrix} m_u & 0 & 0 \\ 0 & m_c & 0 \\ 0 & 0 & m_t \end{bmatrix}, \\ V_L^{d\dagger} M_d V_R^d = \hat{M}_d \equiv \begin{bmatrix} m_d & 0 & 0 \\ 0 & m_s & 0 \\ 0 & 0 & m_b \end{bmatrix}. \end{aligned} \tag{2.64}$$

Rotating the left- and right-handed unphysical quark fields into the physical ones in 2.62 we get:

$$\begin{aligned} \mathcal{L}_{\text{Quarks}}^{\text{Yukawa}} &= -\left\{ \begin{bmatrix} \overline{U}_L V_L^{u\dagger} & \overline{D}_L V_L^{d\dagger} \end{bmatrix} Y^d V_R^d D_R \begin{bmatrix} \phi^+ \\ \phi^0 \end{bmatrix} + \begin{bmatrix} \overline{U}_L V_L^{u\dagger} & \overline{D}_L V_L^{d\dagger} \end{bmatrix} Y^u V_R^u U_R \begin{bmatrix} \phi^{0*} \\ -\phi^- \end{bmatrix} + h.c. \right\} \\ &= -\left\{ \overline{D}_L V_L^{d\dagger} M^d V_R^d D_R \left(1 + \frac{H}{v}\right) + \overline{U}_L V_L^{u\dagger} M^u V_R^u U_R \left(1 + \frac{H}{v}\right) + h.c. \right\} \\ &= -\left\{ \overline{D}_L \hat{M}^d D_R \left(1 + \frac{H}{v}\right) + \overline{U}_L \hat{M}^u U_R \left(1 + \frac{H}{v}\right) + h.c. \right\}. \end{aligned} \tag{2.65}$$

[21] At least one of these matrices must be non-diagonal, such that the unitary CKM matrix, which will be later presented, is non-diagonal and we can describe the $W^\pm$ flavour changing currents between different generations within the quark sector (see the rest of this section, section 2.6 and appendix B for more information about this topic). Usually, Y^d is set to be the only non-diagonal one, such that the mixing in the SM quark sector occurs only in the down-type quark fields. The physics regarding the quark sector stays the same, whether we set one or both Yukawa matrices in the weak basis as being non-diagonal.

Using $U = U_L + U_R$ and $D = D_L + D_R$:

$$\mathcal{L}^{\text{Yukawa}}_{\text{Quarks}} = -\left\{\overline{D}\hat{M}_d D + \frac{1}{v}\overline{D}\hat{M}_d D H + \overline{U}\hat{M}_u U + \frac{1}{v}\overline{U}\hat{M}_u U H\right\} \tag{2.66}$$

We can check that, as for the case of the charged leptons, we get quark mass terms like $m_q\overline{q}q$ from the $\overline{D}\hat{M}_d D$ and $\overline{U}\hat{M}_u U$ terms.

With the addition of the ϕ doublet, the Higgs Mechanism, and the Yukawa interactions to the SM, we got a way to provide mass terms in the SM for all the particles that experimentally have mass without spoiling the gauge invariance of the SM Lagrangian. We got a new physical particle, the Higgs boson, and interactions with itself, with the charged fermions and with the massive gauge bosons. Additionally, the Yukawa interactions of the ϕ doublet with the quarks give rise to the mixing of the physical quark fields in the SM.

In 2.44, the left- and right-handed quark fields are in the weak basis. In order to describe the flavour changing charged currents associated with the $W^{\pm\mu}$ fields, we need to transform those unphysical quark fields into the physical ones as in 2.63. The only terms in 2.44 that do not remain unchanged by the transformation in 2.63 (and so the only terms where two quark fields from different generations couple to each other) are the ones associated with the $W^{\pm\mu}$ fields. For example, the terms associated with the W^+_μ field can be rewritten as:

$$\begin{aligned}
&-\frac{g}{\sqrt{2}}\begin{bmatrix}\overline{u}_L & \overline{c}_L & \overline{t}_L\end{bmatrix}\gamma^\mu\begin{bmatrix}d_L\\ s_L\\ d_L\end{bmatrix}W^+_\mu \\
&= -\frac{g}{\sqrt{2}}\overline{U}_L V_L^{u\dagger}\gamma^u V_L^d D_L W^+_\mu \\
&= -\frac{g}{\sqrt{2}}\overline{U}_L V_{CKM}\gamma^u D_L W^+_\mu \\
&= -\frac{g}{\sqrt{2}}\overline{U} V_{CKM}\gamma^u P_L D W^+_\mu \\
&= -\frac{g}{2\sqrt{2}}\overline{U} V_{CKM}\gamma^u(1-\gamma_5) D W^+_\mu,
\end{aligned} \tag{2.67}$$

where $V_{CKM} = V_L^{u\dagger}V_L^d$ is the Cabibbo-Kobayashi-Maskawa (CKM) matrix (see appendix B).

2.6 CP Symmetry

The gauge symmetries are continuous symmetries, but there are also discrete symmetries in the SM, or at least for some parts of its Lagrangian, such as the CP symmetry which transformation is defined as the product of two consecutive transformations of the parity (P) and charge conjugation (C) symmetries.

The parity transformation changes the sign of the spatial coordinates: $x^\mu \to x_\mu, \partial^\mu \to \partial_\mu$. With $\phi(t,\vec{r})$, $V^\mu(t,\vec{r})$, and $\psi(t,\vec{r})$ as a generic scalar field, four-vector field, and fermion Dirac field, we

transform them under Parity transformation as:

$$\begin{aligned}
\mathcal{P}\phi(t,\vec{r})\mathcal{P}^\dagger &= e^{i\alpha_p}\phi(t,-\vec{r}) \\
\mathcal{P}\phi^*(t,\vec{r})\mathcal{P}^\dagger &= e^{-i\alpha_p}\phi^*(t,-\vec{r}) \\
\mathcal{P}V^\mu(t,\vec{r})\mathcal{P}^\dagger &= e^{i\gamma_p}V_\mu(t,-\vec{r}) \\
\mathcal{P}V^{\mu\dagger}(t,\vec{r})\mathcal{P}^\dagger &= e^{-i\gamma_p}V_\mu^\dagger(t,-\vec{r}) \\
\mathcal{P}\psi(t,\vec{r})\mathcal{P}^\dagger &= e^{i\beta_p}\gamma^0\psi(t,-\vec{r}) \\
\mathcal{P}\overline{\psi}(t,\vec{r})\mathcal{P}^\dagger &= e^{-i\beta_p}\overline{\psi}(t,-\vec{r})\gamma^0,
\end{aligned} \tag{2.68}$$

where $\mathcal{P}$ is the parity operator acting on the Fock space of particle states and α_p, γ_p and β_p are arbitrary phases. If $e^{i\alpha_p} = +1$, ϕ is a pure scalar field, and if this phase is equal to -1 then ϕ is a pure pseudo scalar field. If $e^{i\alpha_p} = +1$, V^μ is a pure vector field and if $e^{i\alpha_p} = -1$, V^μ is a pure axial vector field. The photon field is a pure vector field so that the QED Lagrangian 2.10 is invariant under parity using the parity field transformations in 2.68. QCD is also invariant under parity transformation.

Charge conjugation is another discrete symmetry transformation. It transforms a particle into its anti-particle. The generic fields defined above, transform under charge conjugation in the following way:

$$\begin{aligned}
\mathcal{C}\phi\mathcal{C}^\dagger &= e^{i\alpha_c}\phi^* \\
\mathcal{C}\phi^*\mathcal{C}^\dagger &= e^{-i\alpha_c}\phi \\
\mathcal{C}V^\mu\mathcal{C}^\dagger &= e^{i\gamma_c}V^{\mu\dagger} \\
\mathcal{C}V^{\mu\dagger}\mathcal{C}^\dagger &= e^{-i\gamma_c}V^\mu \\
\mathcal{C}\psi\mathcal{C}^\dagger &= e^{i\beta_c}C\overline{\psi}^T \\
\mathcal{C}\overline{\psi}\mathcal{C}^\dagger &= -e^{-i\beta_c}\psi^T C^{-1},
\end{aligned} \tag{2.69}$$

where $C = i\gamma^0\gamma^2$ is an unitary matrix. Both QED and QCD Lagrangians are invariant under charge conjugation transformations. In the weak interaction we got currents of the type $\overline{\psi}\gamma^\mu P_L\psi'$. Now we will check if the weak interaction is invariant under both parity and charge conjugation transformations separately. Under parity this current transforms as:

$$\begin{aligned}
\mathcal{P}\overline{\psi}\gamma^\mu P_L\psi'\mathcal{P}^\dagger =& e^{-i\beta_p}\overline{\psi}(t,-\vec{r})\gamma^0\gamma_\mu\frac{\mathbb{1}-\gamma_5}{2}e^{i\beta'_p}\gamma^0\psi'(t,-\vec{r}) \\
=& e^{i(\beta'_p-\beta_p)}\overline{\psi}(t,-\vec{r})\gamma_\mu\frac{\mathbb{1}+\gamma_5}{2}\psi'(t,-\vec{r}) \\
=& e^{i(\beta'_p-\beta_p)}\overline{\psi}(t,-\vec{r})\gamma_\mu P_R\psi'(t,-\vec{r}),
\end{aligned} \tag{2.70}$$

where we made use of the anti-commutation relations $\{\gamma^\mu,\gamma^\nu\} = 2g^{\mu\nu}\mathbb{1}$ and $\{\gamma_5,\gamma^\mu\} = 0$. Under

charge conjugation, the same current transforms as:

$$\begin{aligned}\mathcal{C}\overline{\psi}\gamma^\mu P_L\psi'\mathcal{C}^\dagger =& - e^{-i\beta_c}\psi^T C^{-1}\gamma^\mu\frac{\mathbb{1}-\gamma_5}{2}e^{i\beta'_c}C\overline{\psi'}^T\\ =& - e^{i(\beta'_c-\beta_c)}\psi^T C^{-1}\gamma^\mu\frac{\mathbb{1}-\gamma_5}{2}C\overline{\psi'}^T\\ =&e^{i(\beta'_c-\beta_c)}\psi^T\gamma^{\mu T}\frac{\mathbb{1}-\gamma_5^T}{2}\overline{\psi'}^T\\ =& - e^{i(\beta'_c-\beta_c)}\overline{\psi'}\frac{\mathbb{1}-\gamma_5}{2}\gamma^\mu\psi\\ =& - e^{i(\beta'_c-\beta_c)}\overline{\psi'}\gamma^\mu\frac{\mathbb{1}+\gamma_5}{2}\psi\\ =& - e^{i(\beta'_c-\beta_c)}\overline{\psi'}\gamma^\mu P_R\psi,\end{aligned} \tag{2.71}$$

where, once again, we made use of the aforementioned anti-commutation relations of the γ^μ matrices, of the relations $C\gamma^\mu C^{-1}=-\gamma^{\mu T}$ and $C\gamma_5 C^{-1}=\gamma_5^T$, and finally of the following relations:

$$\begin{aligned}&\psi^T\overline{\psi'}^T=-\overline{\psi'}\psi\\ &\psi^T\gamma^{\mu T}\overline{\psi'}^T=-\overline{\psi'}\gamma^\mu\psi\\ &\psi^T\gamma^{\mu T}\gamma_5^T\overline{\psi'}^T=-\overline{\psi'}\gamma_5\gamma^\mu\psi,\end{aligned} \tag{2.72}$$

which are obtained from the anticommutation property of the fermion fields: $\{\overline{\psi}_\alpha(t,\vec{x}),\psi_\beta(t,\vec{y})\}\ =\ \delta^{(3)}(\vec{x}-\vec{y})\delta_{\alpha\beta}$, with α and β as spinor indices of the SU(2) doublets.

From 2.70 and 2.71 we observe that parity and charge conjugation transformations change the chirality of the weak interactions, transforming left-handed currents into right-handed currents and vice versa. In the SM, the $W^\pm$ boson fields do not couple to right-handed currents and the Z boson field couples differently to the left- and right-handed currents, so the weak interaction Lagrangian, and therefore the SM, is not invariant under both parity and charge conjugation transformations. From the fact that the combination of a charge conjugation and a parity transformation (CP transformation) also keeps the QED and QCD Lagrangians invariant, one may question if the same is true for the weak interaction Lagrangian since CP conserves the chirality of the left- and right-handed currents. Considering the quark couplings to the $W^\pm$ fields in 2.44, which contains currents of the type $\overline{\psi}\gamma^\mu P_L\psi'$, in the quark mass basis we get:

$$\mathcal{L}^{W^\pm}_{\text{Quarks}}=\sum_{i,j=1}^{3}-\frac{g}{\sqrt{2}}\left[\overline{\hat{u}}_i\gamma_\mu P_L V_{CKM,ij}\hat{d}_j W^{+\mu}+\overline{\hat{d}}_j\gamma_\mu P_L V^*_{CKM,ij}\hat{u}_i W^{-\mu}\right]. \tag{2.73}$$

From 2.70 and 2.71 we obtain the transformation of the current $\overline{\psi}\gamma^\mu P_L\psi'$ under CP:

$$\begin{aligned}(\mathcal{CP})\overline{\psi}\gamma^\mu P_L\psi'(\mathcal{CP})^\dagger =&\mathcal{C}e^{i(\beta'_p-\beta_p)}\overline{\psi}(t,-\vec{r})\gamma_\mu P_R\psi'(t,-\vec{r})\mathcal{C}^\dagger\\ =& - e^{i(\beta'_c+\beta'_p-\beta_c-\beta_p)}\overline{\psi'}(t,-\vec{r})\gamma_\mu P_L\psi(t,-\vec{r}),\end{aligned} \tag{2.74}$$

where we observe that under CP transformations the currents of the type $\overline{\psi}\gamma^\mu P_L\psi'$ keep their chirality. From [21], the $W^\pm$ bosons transform under CP as:

$$\begin{aligned}(\mathcal{CP})W^{+\mu}(t,\vec{r})(\mathcal{CP})^\dagger =& - e^{i\xi}W^-_\mu(t,-\vec{r}),\\ (\mathcal{CP})W^{-\mu}(t,\vec{r})(\mathcal{CP})^\dagger =& - e^{-i\xi}W^+_\mu(t,-\vec{r}),\end{aligned} \tag{2.75}$$

by imposing CP-invariance of all the Lagrangian terms of the weak interaction. We transform now the interaction terms of the quarks with the $W^{\pm}$ bosons, 2.73, under CP using the results from 2.74 and 2.75:

$$(\mathcal{CP})\mathcal{L}^{W^{\pm}}_{\text{Quarks}}(\mathcal{CP})^{\dagger} = \sum_{i,j=1}^{3} -\frac{g}{\sqrt{2}} \Big[e^{i(\beta_j-\beta_i+\xi)} \overline{\hat{d}}_j \gamma_\mu P_L V_{CKM,\,ij} \hat{u}_i W^{-\mu} + \\ + e^{i(\beta_i-\beta_j-\xi)} \overline{\hat{u}}_i \gamma_\mu P_L V^{*}_{CKM,\,ij} \hat{d}_j W^{+\mu} \Big], \tag{2.76}$$

where $e^{i\beta_i}$ and $e^{i\beta_j}$ are the CP-transformation arbitrary phase factors of the i and j quarks. Since these and the $e^{i\xi}$ phase factors are arbitrary, we will equal them to one for the sake of simplicity. Comparing 2.73 with its CP transformation,2.76, we would need that $V_{ij\,CKM} = V^{*}_{ij\,CKM}$ for every i and j index, which means that the CKM matrix should be real, in order for the interaction terms between the quarks and the $W^{\pm}$ bosons to be CP invariant. However, this is not possible for three quark generations: the CKM in this case has a complex phase that cannot be removed. Therefore, the coupling terms of the quarks to the $W^{\pm}$ bosons violate the CP invariance in the weak interaction, and so in the SM.

2.7 SM Flaws

Although SM is a very successful theory concerning its predictive power, there are multiple phenomena, experimental observations, and theoretical problems that this theory does not address. Therefore, particle physicists are currently invested at extending the SM by assuming that the SM is an effective low-energy manifestation of a more general theory or at creating new whole theories aiming at including and solving those problems. Some of the main flaws of the SM are:

- The neutrinos are considered to be massless, even though particle physicists suggest that they have non-zero mass values due to the observation of neutrino oscillations [12];
- The free parameters related to the fermions, which are the Yukawa couplings (or equivalently their masses) and the CKM matrix parameters, get their values from experiments. The SM does not provide an explanation for the existence of 3 generations of quarks and leptons neither the hierarchy of values of these parameters among the different flavours of the fermions. This is called the flavour puzzle;
- In the SM, the Higgs boson mass gets very large corrections from loops, requiring fine-tuning such that these corrections get cancelled out. For many theoretical particle physicists, this fine-tuning seems unnatural, and raises the possibility that there may exist new physics at the TeV energy scale [9]. This is called the hierarchy problem;
- The SM is inconsistent with the most currently accepted theory of cosmology, the ΛCDM model of cosmology, and the astrophysical and cosmological observations that the latter one is based on: the SM cannot explain the large observed amount of dark matter, dark energy, and matter-antimatter asymmetry in our universe (the CP violation within the SM is not sufficient to explain this observed asymmetry).

Chapter 3

Dark Matter

Nowadays, we know that 26.4% [22] of the total energy-matter composition of the universe is dark matter (DM). As the name suggests, we cannot directly see DM and we do not know what is its fundamental nature. However, we do know that this type of matter weakly interacts or does not even interact with the matter described by the SM and that it interacts via gravity. In the last and current century, multiple observations, mostly based on gravitational effects, have been strongly favoring the existence of DM, and the theoretical concept of what it is made of has been evolving a lot.

In the next section, 3.1, we will introduce three of the main types of astrophysical and cosmological observational evidence for the existence of some type of matter (invisible mass) we did not take into account in the past. After that, in 3.2, some possible candidates for DM will be listed, mainly focusing on the candidates from particle physics, and in 3.3, we briefly introduce the current classes of DM models used in particle physics and the specific DM model used in our work.

3.1 Evidence for the existence of DM

3.1.1 Galaxy Clusters

In the 1930s, Fritz Zwicky and Sinclair Smith found a higher mass-per-galaxy value than the Hubble estimate (that was largely based on only luminous material) in the Coma [23] and Virgo [24] clusters, respectively, by looking at the velocity dispersion in these clusters of galaxies and using the virial theorem. They inferred there must exist some type of extra matter that we can't see in order to keep the galaxies together. Fritz Zwicky associates DM with "cold stars, macroscopic and microscopic solid bodies, and gases"[25], and Sinclair Smith associates it with "internebular material, either uniformly distributed or in the form of great clouds of low luminosity surrounding the [galaxies]"[25]. In 1961, the Conference on the Instability of Systems of Galaxies took place in Santa Barbara, California, and there the consensus was that the mass discrepancy in clusters of galaxies may be explained by an "invisible inter-galactic material in the clusters, totaling to 90% to 99% of their mass"[25] or that these clusters may be unstable (and so one cannot use the virial theorem).

3.1.2 Rotation Curves of Spiral Galaxies

It is possible to infer the mass distribution of galaxies from their rotation curves[1]. Using this tool, it was observed that the rotation curves of a large sample of spiral galaxies were flat (constant in r) at

[1] A rotation curve of a galaxy is the circular velocity profile of the stars and gas in a galaxy as a function of their distance from the galactic center.

large radii until the optical extent[2] opposing the previous theoretical estimate that the circular velocity is proportional to $r^{-\frac{1}{2}}$ at large radii if the galaxy is only made of visible mass, which could be explained by large amounts of non-luminous matter (dark matter) at the outer areas of these galaxies. The mass-to-luminosity ratio was also in agreement with this suggestion: this ratio increases with the distance from the galactic center. In 3.1, we can clearly see the discrepancy in the outer areas of the Andromeda Galaxy between experimental data (points) and the theoretical prediction (solid blue line) of its rotation curve.

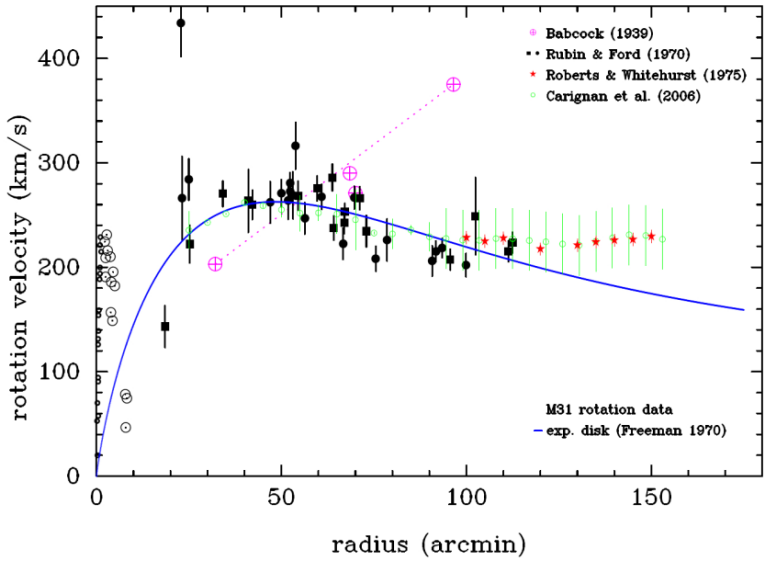

Figure 3.1: Rotation velocity (km/s) data in function of the radius (arcmin) from the center of the M31 (Andromeda) galaxy. Purple, black, red, and green points are data points, while the solid blue line corresponds to the rotation curve of an exponential disc with a scale length according to the value given in [26], that is, if the galaxy was only composed of luminous material in the outer areas. Image from [25].

3.1.3 Weak gravitational lensing: the Bullet Cluster and cosmic shear

More recently, gravitational lensing[3] measurements started to be employed in order to check for the existence and assess the spatial distribution of DM in clusters of galaxies and in larger structures.

In 2006, the phenomenon known as "Bullet Cluster" was first observed [27]. This observation provided further evidence for the existence of DM. The "Bullet Cluster" is a pair of colliding clusters with the catalog name 1E0657-558. The majority of the visible matter in the "Bullet Cluster" is in the form of hot gas that emits X-ray radiation, making it possible to trace the distribution of this hot gas. On the other hand, the distribution of the total mass (visible + DM matter) was independently traced through weak gravitational lensing[4]. It was observed that the distributions of visible matter and total mass matter

[2]Optical extent is the maximal extent of the galaxy that we can see from light only; since dark matter may exist in a large amount at the outer area of the galaxy, the extent of the galaxy may be bigger than the optical extent.

[3]Gravitational lensing is the effect described by the General Theory of Relativity of Albert Einstein wherein objects with huge mass values (called gravitational lens) bend the light rays that pass near them. Gravitational lensing measurements rely on the observation of luminous arcs or closed rings surrounding a foreground gravitational lens, such as galaxy clusters. The photons of those luminous arcs and closed rings photons originate from one or more background sources.

[4]Weak gravitational lensing occurs when the gravitational lens does not produce a sufficiently strong gravitational field to form multiple images or arcs from the source, but rather a generic distortion of the light rays from the background source. On the other hand, strong gravitational lensing occurs when the gravitational lens produces a strong gravitational field and the source is close enough to it, forming clear multiple images of the source. Both lensings can be employed in the measurement of the mass of the gravitational lens. The strong one will give more precise measurements, however, the weak one is more probable to observe [28].

are displaced, and so the visible matter and DM distributions are spatially separated. In Figure 3.2 this displacement is easy to ascertain. One may interpret this observation as if the DM distributions of the two colliding clusters passed through each other during the collision because of negligible collisions of DM with itself and with visible matter, while the visible matter distributions of the clusters interacted between themselves with a much larger strength, creating a collisional shock wave. Hence, cluster collisions may provide information about the probability of a DM-DM particle interaction.

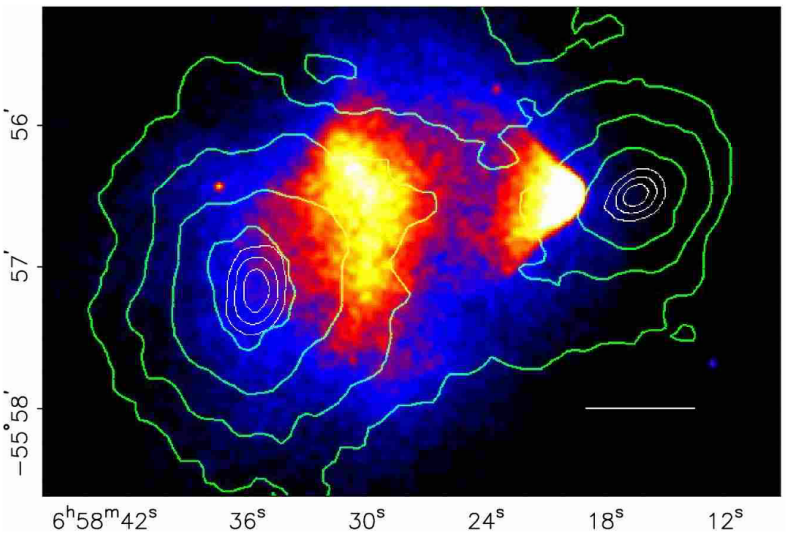

Figure 3.2: Image of the pair of colliding clusters 1E0657-558. The coloured map represents the X-ray image of the hot baryonic gas, obtained in a 500 second exposure with Chandra. The green contours are the weak lensing reconstruction of the total mass of the system. The white bar corresponds to the length of 200 kpc at the location of the system. Image from [27].

In the detection of large and diffuse DM structures in length scales between the galactic/cluster and the cosmic scales, weak gravitational lensing is also employed. The deflection of light from very distant galaxies by the gravitational attraction from these foreground DM structures is called cosmic shear. The measurements of cosmic shear give a better estimate of the portion of DM in the universe.

A similar phenomenon to the weak gravitational lensing from the Bullet Cluster and the cosmic shear is the Cosmic Microwave Background (CMB) lensing [29]. The CMB is a nearly uniform and isotropic microwave radiation that covers the observable universe. The CMB observation is one of the main evidences for the Big Bang theory. Within Big Bang cosmological models, the CMB is explained as being a source of redshifted photons that started to freely stream from the epoch of the universe in which protons and electrons combined to form neutral atoms of mostly hydrogen. This background is the earliest observable light of the Universe to us. Foreground mass concentrations caused distortions on the CMB map, and by studying those distortions, the CMB could potentially probe and study large DM structures at high redshifts [22].

3.2 DM Candidates

Initially, the expression "Dark Matter" was associated with astrophysical objects made of non-luminous matter (baryonic or non-baryonic matter[5]) which were called Massive Astrophysical Compact

[5]In astronomy and cosmology, baryonic matter refers to all objects made of normal atomic matter. Neutrinos are examples of particles that do not count for baryonic matter. Non-baryonic matter, as implied by the name, is any sort of matter that is not primarily composed of baryons. This might include neutrinos and free electrons, dark matter, supersymmetric particles, axions, etc.

Halo Objects (MACHOs) such as planets, brown dwarfs, red dwarfs, white dwarfs, neutron stars, and black holes. However, gravitational microlensing surveys and determinations of the cosmic baryon density conclude that MACHOs purely made of baryonic matter cannot make up a big fraction of the dark matter in our Universe if they were created in the late Universe, which is the most natural expectation. The primordial black holes are however MACHOs that were formed before Big Bang Nucleosynthesis (BBN) and they could still make up a big portion of the dark matter in the whole universe.

Some of the observational evidences for the existence of DM could be simply explained by accepting that the currently used theory of gravity, General Relativity, is not complete and by introducing modified theories of gravity to explain some of those phenomena. However, it is still hard to match all the observational evidence without taking into account some fraction of cold DM [22].

In the last decades, particle physicists became interested in DM and there was a shift towards the questioning of what particles is DM made of. Already known SM particles and unknown non-SM particles were suggested as DM candidates. By the end of the 1970s, the physics community started to argue in favor of SM neutrinos as DM particle candidates. However, the emergence of numerical simulations would let the neutrinos as less probable candidates for DM. These simulations could test if the DM candidates could replicate the large scale structure and other observables we obtained through astrophysical and cosmological observations. A DM particle candidate can be characterized through many characteristics. One of them is if it is relativistic (hot) or non-relativistic (cold) during the epoch of structure formation. SM neutrinos are included in the class of hot DM particle candidates. The numerical simulations showed that the hot DM particles tend to collapse after the Big-Bang, forming very large structures, and fragmenting into smaller structures such as galaxy-sized structures. Cold DM structure formation occurs differently, according to the simulations: first small structures are formed and bigger structures are formed through merging of the previous ones. By comparing the simulation results with observations (namely the CfA galaxies survey [30]), physicists concluded that hot DM particles could not account for most of DM in the Universe. Therefore, the SM neutrinos were rejected as the main DM candidates. Nevertheless, the SM neutrinos led to a more general class of DM particle candidates: the Weakly Interacting Massive Particles (WIMPs), which will be introduced in 3.2.1. It was obvious that DM must be made of still unknown particle(s). In the late 1980s, the non-SM particles gained much more support as being valid DM candidates. DM particle candidates are often embedded in SM extensions that address not only the DM problem but also other problems that the SM cannot solve, as we will see below. From cosmological and astrophysical experimental observations and direct detection experiments' bounds, a DM particle candidate must be cold or at least not too hot, must have a null or very small electric charge, must be weakly interacting with the SM, and must be stable or at least possess a lifetime longer than the Universe's age (see [22] for more details about the reasoning behind these requirements). The allowed range of the mass value of the DM particle candidate depends on the model that describes it and whether it is a boson or a fermion; a priori the DM mass can have any value between 10^{-21} eV[6] and the Planck scale, $M_{Pl} \sim 1.22 \times 10^{28}$ eV [22].

To detect and understand what the DM particles are, we first need to detect their interactions with the SM particles, which have not occurred up until this date. There are three ongoing main classes of DM particle detection experiments:

[6]By requesting that the De Broglie wavelenght of a DM particle must be smaller than the gravitationally bound dwarf galaxies, which are the smallest astrophysical structures known to contain Dark Matter, we get this lower limit. For particles with mass values bellow $\sim$ 1 eV to be DM particle candidates, they must be bosonic. DM composed by these light bosons can be described by a classical field [22].

- **Direct Detection:** These experiments' goal is to detect and measure the recoil of the nuclei and electrons of the detector caused by passing galactic DM particles (they belong to the DM halo that Earth is inside) hitting on those SM particles. These detectors are located deep underground on Earth and are highly shielded to reduce the background;
- **Indirect Detection:** These experiments' goal is to detect DM pair-annihilations or DM decays (in the case where some DM particles are unstable), from or outside the DM halo, into SM particles, by searching for excess in the cosmic rays fluxes measured on Earth or near it;
- **Detection at accelerators:** These experiments aim to detect DM particles that could be produced at high-energy accelerators from the collision of SM particles. The detection of the produced DM particles at the detectors of the colliders would occur via an excess from the SM predictions of missing transverse energy or visible signatures. The search for a DM signature in our work is a collider search at the LHC.

Below, we briefly introduce some of the currently most important DM particle candidates. Note, however, that besides those, there is a huge number of candidates, including composite DM particles made of fundamental SM or DM particles.

3.2.1 WIMPs

In the broader sense, WIMPs are stable and massive particles (their mass is typically taken to be around 100 GeV; it can be some orders lower or higher than this value) that couple to other weak-scale particles such as the Higgs or the top quark in the SM through couplings as weak as those of the weak interaction of the SM (the couplings of the WIMPs to the other particles could be couplings of the SM weak interaction or another interaction not described by the SM). For example, WIMP-like particles are predicted by Supersymmetry (SUSY)[7] theories where these particles would be the lightest supersymmetric particles. In the minimal supersymmetric extension to the SM, this particle is the neutralino which is the mass eigenstate resulting from the mixing of the superpartners of the photon, Z boson, and two neutral scalar Higgs bosons. Theories that introduce WIMP-like particles often address the hierarchy problem of the SM while at the same time explaining the observed DM relic abundance by making use of these particles, turning these theories into attractive new physics theories for providing mechanisms that address more than one of the problems in the SM.

3.2.2 Axions and axion-like particles

Axions are Nambu-Goldstone bosons that appear by introducing a new global U(1) symmetry that is spontaneously broken to solve the strong-CP problem in QCD [31–33]. From experimental constraints, axions must have very low masses and must interact very weakly [25]. If stable, the axions produced in the early Universe would have survived and could make up DM.

3.2.3 Sterile Neutrinos

Sterile neutrinos are right-handed neutrinos that can be inserted in the SM (the left-handed neutrinos in the SM are called the active neutrinos) for the neutrinos in the SM to get mass terms. Besides the possibility of the sterile neutrinos explaining the small neutrino masses inferred from neutrino oscillations

[7] Supersymmetry is a space-time symmetry requiring that for every fermion must exist a boson with the same quantum numbers, and vice versa. The partner of a SM particle in Supersymmetry is the superpartner.

[12], they could also be DM particle candidates in scenarios where DM is made of hot/warm[8] sterile neutrinos and cold massive DM particles [12].

3.2.4 DM particles in Dark Sectors Models

There are several models in which DM is charged under one or more theorized dark forces and not charged under SM gauge symmetries. These models introduce a dark sector made of one or more DM particles and one or more DM mediators of the dark forces. Being no longer limited by the SM interactions, the phenomenology of the DM particles changes substantially with the addition of a dark force. Usually, the interactions between the SM particles and the DM mediator are called portal interactions (its name is due to being the only term that couples the SM sector to the DM sector) and these DM mediators have commonly, but not necessarily, the following names[9] in literature [22]: "dark Higgs" if the mediator is a scalar particle; "axion" or "axion-like pseudoscalar" if it is a pseudo-scalar; "dark photon" or "light Z'" if it is a vector mediator. Moreover, there are models whose dark sectors are composed of gauge singlet fermions denoted "heavy neutral leptons", such as the sterile neutrinos, that interact with the SM lepton via SM Yukawa couplings.

3.3 DM Models

There are plenty of qualitatively different models and theories of physics beyond the SM which include at least one viable DM candidate particle. Those can be divided into 3 different classes [34, 35]:

- **DM Effective Field Theories:** When one is studying interactions between DM and particles of the SM in which the DM mediator is taken to be heavier than the typical momentum exchange in the interaction, one can make use of Effective Field Theories to describe these interactions. In these theories, the interaction between DM and SM particles appears to be a contact interaction by integrating out the DM mediator. This way, we can describe these interactions without fixing a specific mediation mechanism, providing us with the exploration of multiple possibilities for the interaction between DM and SM particles. Usually, they involve one or very few free parameters;

- **Simplified DM Models:** The simplest models that specify the DM-SM mediation mechanics are called "Simplified DM Models". These models only try to describe collider phenomenology, so they do not attempt to describe additional physics to be found at energies higher than the collider energy scales. The dark sector in simplified models must have just a few particles because the purpose of these models is to describe typical leading-order (LO) processes that can occur at distinct larger theories and make the LHC capable of exploring a large spectrum of DM mediator masses and coupling strengths to the SM without specifying a complete DM theory with several constraints;

- **Complete DM Models:** Due to their simplicity, Simplified Models may fail to find important correlations between observables from possible collider signatures which would look like random accidents [35]. By adding more particles (at least one of them must be a viable DM candidate) and introducing new symmetries, the complete DM models could explain those correlations and the full complexity of DM collider signatures. Some SUSY models, such as the Minimal Supersymmetric Standard Model with R-Parity [36][37], are examples of complete DM models. Given

[8] Warm DM is relativistic at the time of freeze-out, but becomes non-relativistic during the radiation dominated epoch.
[9] Some of these names are also used for DM candidates.

their detailed and complex structure in comparison to our very small knowledge about the nature of DM, and their large number of free parameters, complete DM models may be too hard and specific to employ in order to determine and explain some of the DM collider signatures which may be completely unrepresentative of those models.

3.3.1 Vector DM Mediator Model

In this dissertation, we use the spin-1 mediator version of the DMSimp model [38], which is, as its name suggests, a simplified DM model. This model introduces two new particles to the SM: X_D (the massive DM particle) and Y_1 (the mediator between X_D and the SM particles). X_D is a Dirac fermion and Y_1 is a spin-1 DM mediator between the DM particle, X_D, and the SM particles. Throughout our work, we will ignore X_D and we will focus on the Y_1 instead, given that we are interested only in the coupling of the DM mediator with the SM particles. Given that the DMSimp model was created for searches of DM production at the LHC, which is a hadron collider and so quarks, gluons, and jets have special roles in the studying of collider signatures, it is natural to search specifically for interactions between quarks and the DM mediator. Thus, in this simplified model, the only considered SM-DM interactions are those between quarks and the DM mediator.

The Lagrangian of the interaction between Y_1 and the SM is the following:

$$\mathcal{L}_{\text{SM}}^{Y_1} = \sum_{i,j=1}^{3} [\overline{\hat{d}}_i \gamma_\mu (g_{d_{ij}}^V + g_{d_{ij}}^A \gamma_5) \hat{d}_j + \overline{\hat{u}}_i \gamma_\mu (g_{u_{ij}}^V + g_{u_{ij}}^A \gamma_5) \hat{u}_j] Y_1^\mu, \tag{3.1}$$

where $\hat{u}$ and $\hat{d}$ denote up- and down-type quarks, respectively, $i, j = 1, 2, 3$ are the flavour indices, and $g^{V/A}$ are the vector/axial-vector couplings of Y_1 to the SM quarks.

This dissertation will specifically focus on the case where the spin-1 DM mediator is a pure vector mediator and we will refer to it as Y_{1^+}, where the $+$ signal stands for its parity $(+1)$, while $-$ would stand for a pure axial-vector mediator, whose parity is -1, as stated in 2.6.

Since we are studying the pure vector mediator case, then $g_{d_{ij}}^A = g_{u_{ij}}^A = 0$. Furthermore, we assume that flavour off-diagonal couplings are 0 ($g_{d/u_{ij}}^V = 0$ for $i \neq j$) and that Y_{1^+} only interacts with the top quarks since we intend to study only the coupling of a pure vector DM mediator with a top quark. Therefore, the only non-zero coupling constant of the interaction between Y_{1^+} and the SM sector is $g_{u_{33}}^V$. Information about the considered mass and coupling constant values in our work will be presented in 6.

By employing this simplified model in our work, we intend to constrain the parameter space of the interactions between the top quarks and a general pure vector DM mediator at the LHC.

Chapter 4

The Large Hadron Collider

The Large Hadron Collider (LHC) at the European Organization for Nuclear Research (CERN) is the world's largest and highest energy particle collider. The LHC mainly collides proton-proton beams, but it can also accelerate beams of heavy ions to collide them with a proton beam or with another heavy ion beam. The main goal of the LHC is to test the theoretical predictions of the SM and to search for hints and signatures of new physics beyond the SM (BSM).

The LHC is a ring with four crossing points (as shown in the depicted CERN accelerator complex in Figure 4.1) where the beams collide and nine detectors are placed in these crossing points. Each one of these detectors is specified to detect and study different phenomena. The two most important detectors at the LHC are the ones from the ATLAS ("A Toroidal LHC ApparatuS") [39] and CMS ("Compact Muon Solenoid") [40] experiments.

Since the LHC started, it has undergone upgrades in order to increase the center-of-mass energy of the beams ($\sqrt{s}$). The LHC started operation at Run 1 by colliding beams with $\sqrt{s}$ equal to 7 and 8 TeV and 30 fb^{-1} of integrated luminosity. At the moment the LHC is on its Run 3 with $\sqrt{s}$ =13.6 TeV and is expected to deliver an integrated luminosity of 300 fb^{-1}. In the following years, there will be another shutdown for another upgrade of the LHC. This time the LHC will be converted into the High-Luminosity Large Hadron Collider (HL-LHC) in which the accumulated integrated luminosity could reach 3000 fb^{-1} for $\sqrt{s} = 14$ TeV.

At particle physics experiments, the event rate of a specific physics process within a collider is given by:

$$\frac{dN}{dt} = L_{\text{inst}}(t) \times \sigma, \tag{4.1}$$

where σ is the cross-section of that process which depends on the center-of-mass energy of the colliding beams, and $L_{\text{inst}}(t)$ is the instantaneous luminosity of the collider. Integrating 4.1 in an interval of time, Δt, we get the total number of events of the physics process in question over Δt:

$$N = \int_{\Delta t} dt\, L_{\text{inst}}(t) \times \sigma = L \times \sigma, \tag{4.2}$$

where $L = \int_{\Delta t} dt\, L_{\text{inst}}$ is the integrated luminosity[1] over the interval of time Δt and it is a measure of the collected data size over that period of time. We will use picobarn (pb) and the inverse of femtobarn (fb^{-1}) as units for the cross-section and integrated luminosity, respectively. The increase of the $\sqrt{s}$ and integrated luminosity at the LHC over the years is justified by the increasing of the σ of rare physics processes with the increase of $\sqrt{s}$, making it more probable to produce and observe those processes, and

[1] In this dissertation we will sometimes refer to the integrated luminosity as simply luminosity.

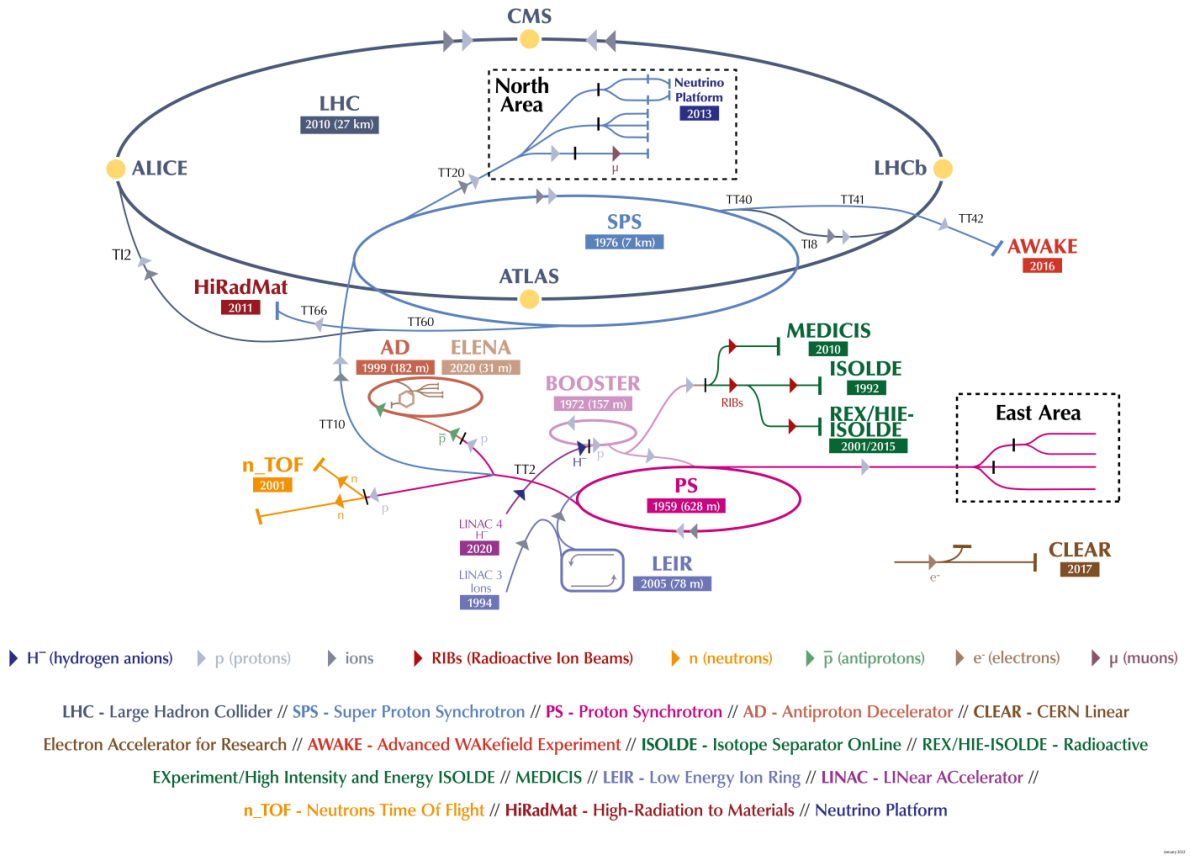

Figure 4.1: The CERN accelerator complex. The dark blue line (which is also the biggest line) is the LHC ring. Image from [41].

by the fact that the increasing of the integrated luminosity leads to a higher number of produced rare events, particularly useful for tests of the SM.

In our work, we search for signs of DM in the ATLAS detector, and so below is a short description of this detector.

4.1 ATLAS detector

4.1.1 Right-handed coordinate system convention

In order to have meaningful experimental observables in a collider, one needs to use a coordinate system convention. The ATLAS collaboration uses a right-handed coordinate system convention, with its origin at the nominal interaction point[2] in the center of the detector, the z-axis along the beampipe[3], the x-axis pointing from the nominal interaction point to the center of the LHC ring (4.1), and the y-axis points upward. The x- and y- axis form the transverse plane and in this plane it is useful to use polar coordinates (r, ϕ), where r is the radial distance from the beampipe and ϕ is the azimuthal angle around the z-axis [42]. The angle between a particle's momentum and the z-axis is the polar angle θ. In collider physics, one often uses the pseudorapidity, η, instead of θ, defined as $\eta = -\ln \tan\left(\frac{\theta}{2}\right)$.

The $\eta - \phi$ space reveals the direction of a particle, and utilizing these angular observables, one can calculate the angular distance between two particles/objects, which is defined as $\Delta R = \sqrt{\Delta\phi^2 + \Delta\eta^2}$.

[2]The nominal interaction point is the point where the particles are supposed to collide. Physically, the interaction point may deviate from the nominal one.

[3]Beampipe is the pipe through which a beam of particles is accelerated in a particle accelerator.

This distance is a Lorentz invariant under a boost along the longitudinal (beam) direction. The smaller ΔR between two particles, the closer are their directions.

4.1.2 ATLAS components

The ATLAS detector is made of the following components of interest to us:

- **Inner Detector:** It is made of trackers immersed in a 2 T magnetic field generated by the central solenoid. The Inner Detector measures the direction, momentum, and charge of electrically-charged particles produced in each proton-proton collision within the range $|\eta| < 2.5$. It also tracks those particles' path. The solenoid deflects the charged particles so that their charges and momenta can be measured.

- **Calorimeter:** There are two types of calorimeters: the Electromagnetic Calorimeters (ECAL), which measure the energy deposited by electrons and photons, and the Hadronic Calorimeters, which measure the energy deposited by hadrons. Calorimeters cannot stop, however, neutrinos and muons. In ATLAS the calorimetry components are the Liquid Argon Calorimeter (LAr) acting as the ECAL and surrounds the solenoid magnet, and the Hadronic Calorimeter (HCAL) which surrounds the LAr in the central part of ATLAS. In the end-caps the LAr is also used as an HCAL calorimeter.

- **Muon Spectrometer:** Located in the outer layer of the ATLAS, this component identifies and measures the momenta and energy of muons. The muon spectrometer was built once the muons, being so much heavier than the electrons, they cross ATLAS with very slight changes in their momenta and energies. They are, however, tracked in the Inner Detector just like the electrons once they are also eletric-charged. In order to bend the muons' trajectories, and so to measure their momenta with precision, ATLAS makes use of toroids that apply a magnetic field on the muons up to 3.5 T close to the muon chambers.

The layout of the ATLAS detector is shown in Figure 4.2.

4.1.3 Event Reconstruction

The goal of measuring deposits of energy and the momentum of the objects detected by the ATLAS experiment is to do an event reconstruction such that the physics process that occurred at the interaction point can be determined and studied. The photon and charged leptons (electrons and muons) are the easiest objects to reconstruct. Taus[4] and jets[5] are, however, more difficult to reconstruct.

The photons and the charged leptons have relatively simple methods and algorithms to reconstruct them, except for the taus. Due to the large mass of the taus, they are unstable particles and decay inside ATLAS via weak interaction. Their decay products include neutrinos and/or hadrons. Its possible decay modes make the reconstruction of the tau leptons a challenging task, given that one needs to reconstruct the missing transverse energy (this observable will be explained below) of the neutrinos and the jets.

Quarks and gluons cannot be directly detected due to confinement. However, they form hadrons that may be detected. After parton shower, the hadronization produces hadrons which can decay into

[4]The reason for the difficulty in reconstructing the taus lies in their decay within the LHC wherein their decay products include neutrinos or/and hadrons. The neutrinos are not detectable, and the hadrons may originate jets.

[5]When one refers to jet reconstruction, one is also referring to the reconstruction of the quark or gluon that originated that jet.

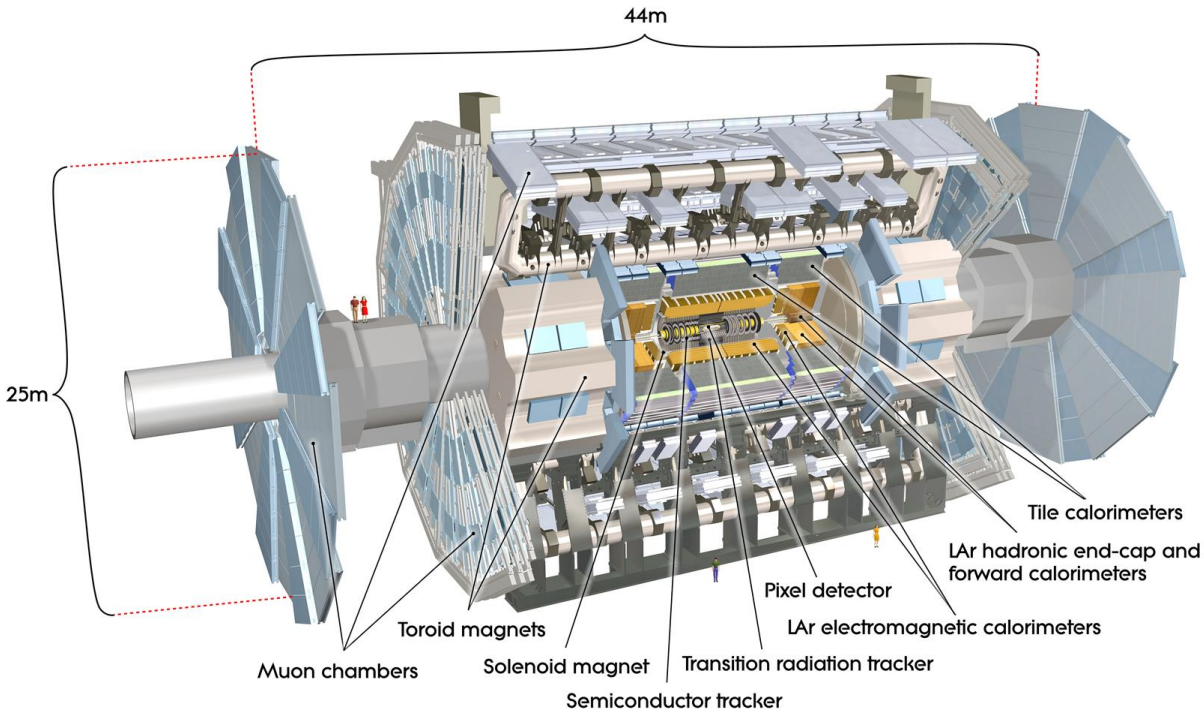

Figure 4.2: The ATLAS detector layout. Image from [43].

other hadrons, leptons and photons. These particles, which may possibly be traced from a single quark or gluon, form collimated sprays called jets. Due to the diverse amount of objects within a jet, all the detectable particles in it must be reconstructed to reconstruct the quark or gluon that originated them. This task requires a jet-clustering algorithm to reconstruct the jet, and it is complex once the measurement of the energy of hadrons involves uncertainties associated to wrongly attributing particles that are not actually originated in that jet (those particles may belong to an underlying event[6]) as well as not including those that belong to it. The most commonly used jet-clustering algorithm is the anti-k_t algorithm [46].

The heavy quarks such as the c- and b-quarks can be identified by their flavour and the identification of their jets is called jet heavy-flavour tagging. This is possible because the c- and b-quarks form hadrons that are relatively long-lived and decay in an observable distance from the interaction point (also called primary vertex). The point where the hadron decays is called the secondary vertex and its decay products form a distinct jet that clearly does not originate near the primary interaction point. For the jet flavour tagging, one needs once again an algorithm.

The proton beams at the LHC collide head-on along a well-defined beam axis. Since they suffer hard scattering, the true colliding particles are not the protons but rather some of the constituents of the protons: the partons. We know the energy of each proton, but the same is not true for the partons. In the interaction between two partons in the proton-proton collision, one parton of a proton may have a higher momentum when compared to the parton of the opposing proton, allowing no access to the exact mag-

[6] Alongside the particles from the hard scattering between two partons within a proton-proton collision, additional semi-hard interactions between the partons of the proton can occur. The detected energy fraction of the particles in the final state of the latter interactions and the proton remnants that did not undergo scattering make up the underlying event [44, 45]. Initial state and final state gluon radiation are also commonly contained in the underlying event. Usually, underlying events are characterized by particles with low p_T values.

nitude of the total momentum of the two partons. However, due to the relativistic nature of the protons along the beam axis, the partons have momenta aligned with this axis, implying their total transverse momentum, $p_T = |\vec{p}_T|$, must be zero. However, in hadron collider detectors, we observe that the p_T of the detected objects do not sum up to 0 GeV. This is because the efficiency of the detector is not 100% but more importantly: some particles are not simply detected by the ATLAS detector due to being very weakly-interacting. These particles can be neutrinos or any other weakly-interacting particle in extensions of the SM and are called invisible particles. The imbalance of the total transverse momentum from 0 is called missing transverse energy ($\not{E}_T$) defined as $\vec{\not{E}}_T = -\sum_i \vec{p}_{T\,i}$ (i is the index for each visible particle). The missing transverse energy is however subject to many uncertainties, once it incorporates all the ones associated to each particle individually. Moreover, cosmic rays, dead and noisy regions, pile-up[7], etc., have the effect of fake increasing the measured missing transverse energy.

[7] At LHC the colliding protons are part of colliding bunches containing many protons. So, when the bunches collide, several individual proton-proton collisions can occur nearly at the same time. Usually, one is interested in the highest energetic proton-proton collision such that rare events can be observed. The remaining less energetic and uninteresting proton-proton collisions are called pile-up. The pile-up can be reduced by employing, for example, cuts on the objects with low p_T and high $|\eta|$. However, the pile-up may deteriorate the accuracy of the measurement of the missing transverse energy of the event that we are interested in.

Chapter 5

Top Quark

The top quark is the fundamental particle with the larger mass value in the SM, and due to this property, its phenomenology has a special role in the testing of the SM prediction and the studying of physics Beyond the Standard Model (BSM). Since it is heavier than the $W^{\pm}$ bosons, it is the only quark that decays into a real (on-shell) $W^{\pm}$ boson and a bottom quark and that possesses a lifetime shorter than its hadronization time. Moreover, its mass value makes the top quark the only fermion whose Yukawa coupling to the Higgs boson is of the order of unity, which suggests it may have a special role in the EW symmetry-breaking mechanism.

In hadron collisions, such as the ones at the LHC, top quarks are mainly produced in pairs ($t\bar{t}$) through the processes of $q\overline{q}$ annihilation ($q\overline{q} \rightarrow t\bar{t}$) and gluon-gluon fusion ($gg \rightarrow t\bar{t}$). In Figure 5.1 two LO subprocesses in the production of the $t\bar{t}$ final state at the LHC are illustrated as Feynman diagrams. From data in [9], considering proton-proton collisions with a center-of-mass energy ($\sqrt{s}$) of 13 TeV, 90% of $t\bar{t}$ production at the LHC is from gluon-gluon fusion and, assuming a top quark mass of 172.5 GeV, the resulting theoretical prediction of the $t\bar{t}$ production cross-section at next-to-next-to leading order (NNLO) in QCD including next-to-next-to-leading-log (NNLL) soft gluon resummation accuracy is $\sigma_{t\bar{t}} = 831.8^{+19.8+35.1}_{-29.2-35.1}$ pb, where the first uncertainty is from scale dependence and the second one from parton distribution functions. In Figure 5.2 the measured and predicted cross-sections for the $t\bar{t}$ production at the Tetravon and LHC are shown.

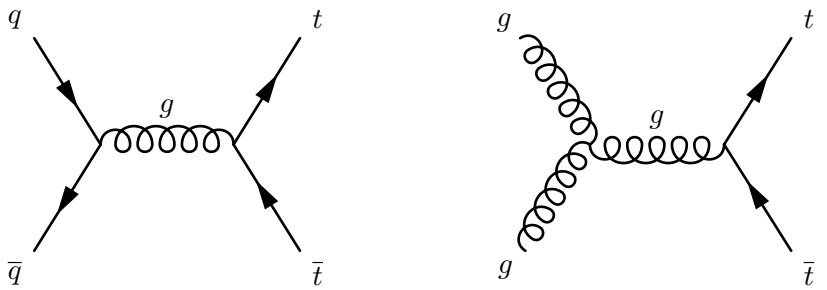

(a) $q\overline{q}$ annihilation subprocess (b) gluon-gluon fusion subprocess

Figure 5.1: Feynman diagrams of 2 of the main LO subprocesses in the production of the $t\bar{t}$ final state at the LHC. The Feynman diagram in 5.1a is a $q\overline{q}$ annihilation subprocess and the one in 5.1b is a gluon-gluon fusion subprocess.

Single t-quark production also occurs at the LHC, but with smaller cross-sections than the ones of the $t\bar{t}$ production. The relevant subprocesses for this process are the $\overline{q}'q \rightarrow t\bar{b}$ ($\overline{q}'q \rightarrow \bar{t}b$) and $qb \rightarrow q't$ ($\overline{q}\bar{b} \rightarrow \overline{q}'\bar{t}$), which are mediated by virtual s-channel and t-channel $W^{\pm}$ bosons respectively, and the Wt-associated production $bg \rightarrow W^{-}t$ ($\bar{b}g \rightarrow W^{+}\bar{t}$). At the LHC, the s- and t-channel cross-sections

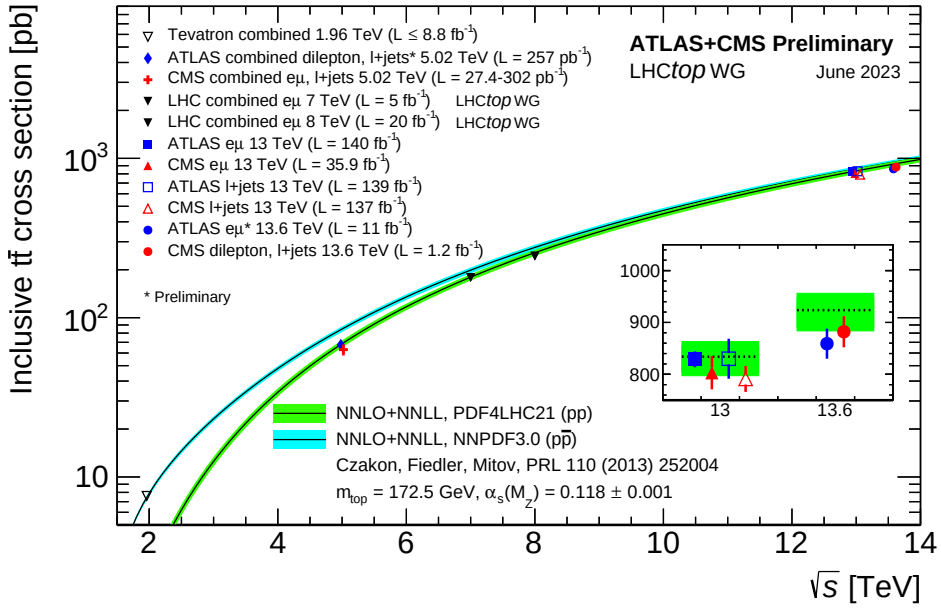

Figure 5.2: Measured and predicted cross-sections for the $t\bar{t}$ production at the Tetravon and at the LHC in function of the center-of-mass energy. Image from [47].

for the single t quark and the single $\bar{t}$ quark are not the same, due to the charge-asymmetric initial state of two protons, and so the cross-sections for the single top production here presented are the sum of the cross-sections of the single t-quark production and the single $\bar{t}$-quark, labeled as $\sigma_{t+\bar{t}}$. The calculated cross-sections of the channels of these subprocesses at the LHC at $\sqrt{s} = 13$ TeV for $m_t = 172.5$ GeV are [9]:

- ***s*-channel:** $\sigma_{t+\bar{t}} = 10.3^{+0.29+0.27}_{-0.24-0.27}$ pb, with 62% of the $\sigma_{t+\bar{t}}$ value coming from σ_t; calculated at NLO;
- ***t*-channel:** $\sigma_{t+\bar{t}} = 215^{+2.1}_{-1.3}$ pb with the uncertainties coming from scale variation only; calculated at NNLO;
- ***Wt*-associated production:** $\sigma_{t+\bar{t}} = 71.7^{+1.8+3.40}_{-1.8-3.40}$ pb, with $\sigma_t = \sigma_{\bar{t}}$; approximately calculated at NNLO.

In Figure 5.3 the measured and predicted cross-section for the single top production at the LHC is shown.

With cross-sections smaller than $t\bar{t}$ and single top quark production, final states with $t\bar{t}$ pairs associated with other particles can be produced at hadron colliders, such as $t\bar{t}V$, $t\bar{t}VV$ (with $V = \gamma, W^{\pm}, Z$), $t\bar{t}H$, $t\bar{t}$, $t\bar{t}b\bar{b}$ and $t\bar{t}t\bar{t}$.

The large mass of the top-quark being above the Wb threshold and $|V_{tb}| \gg |V_{tc}|, |V_{ts}|$ (see appendix B) leads to the decay of the top quark being dominated by the process $t \to Wb$. The top quark lifetime is around 0.5×10^{-24} s [9], while the QCD hadronization timescale is around 10^{-24} s and the top quark spin decorrelation[1] timescale is around 10^{-21}s [48], thus the top quark decays before its hadronization, and before it radiates a gluon, meaning that its spin information is preserved in the distribution of angular observables of its decay products [49]. The distribution of angular observables of some top decay products (the leptons in our case) will be used in this dissertation to discern the considered

[1]Spin decorrelation of a quark happens when it radiates a gluon, flipping its spin.

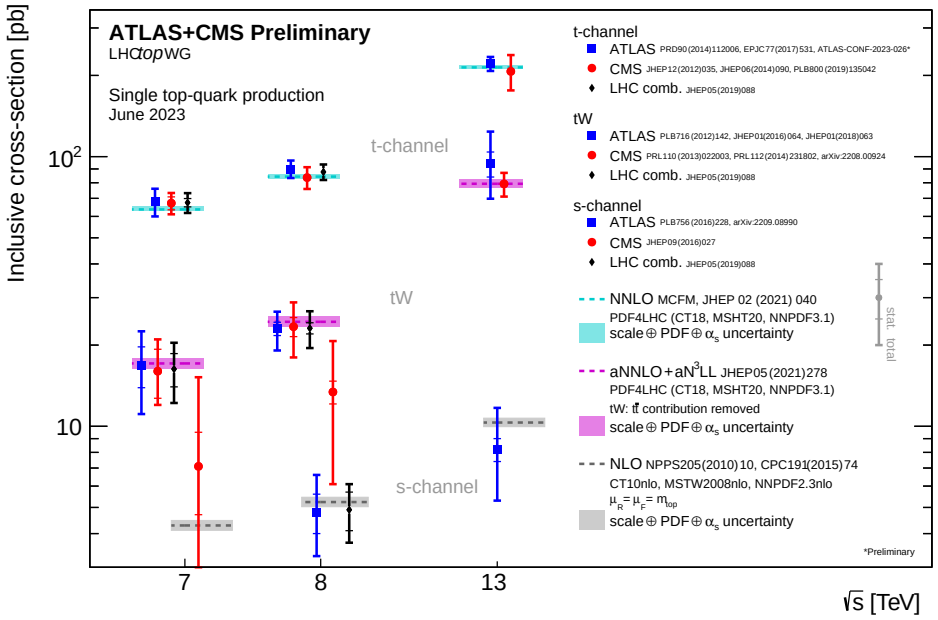

Figure 5.3: Measured and predicted cross-sections of the 3 channels of single top production at the LHC in function of the center-of-mass energy. Image from [47].

signal process, $t\bar{t}Y_{1^+}$, from the SM background, since we expect them to possess different shapes in specific angular distributions but very similar kinematics and final states. Moreover, the spins of the t and $\bar{t}$ quarks are correlated in the $t\bar{t}$ production from QCD processes at hadron collisions.

The $t\bar{t}$ production can have the following three main final states (the remaining ones are the same as the following ones but with the bottom quarks replaced by charm or strange quarks):

- **All-hadronic channel:** $t\bar{t} \rightarrow W^+bW^-\bar{b} \rightarrow q\bar{q}'bq''\bar{q}'''\bar{b}$;
- **Lepton+jets channel:** $t\bar{t} \rightarrow W^+bW^-\bar{b} \rightarrow q\bar{q}'bl^-\bar{\nu}_l\bar{b} + l^+\nu_l bq''\bar{q}'''\bar{b}$;
- **Dileptonic channel:** $t\bar{t} \rightarrow W^+bW^-\bar{b} \rightarrow l^+\nu_l bl'^-\bar{\nu}_{l'}\bar{b}$.

and their relative contributions, including hadronic corrections and assuming lepton universality[2], are 45.7 %, 43.8 % and 10.5 % [9], respectively. In Figures 5.4a and 5.4b, the $t\bar{t}$ pair decay channels and their branching fractions are illustrated, respectively. The coloured particles in these channels may radiate extra QCD radiation that leads to extra isolated jets in the final state. Even though the dileptonic channel is the one with the smallest relative contribution, it is the channel with lower levels of contamination from non top quark backgrounds at the LHC, when compared with the other channels. The reason for this is the number of jets present in the $t\bar{t}$ final states which, for the dileptonic decay, is the lowest (only 2 b-jets should be expected). Moreover, jets are objects that significantly complicate the event reconstruction thus, by keeping a lower number of expected jets, the event reconstruction does not get an unnecessarily harder task. Additionally, the charged leptons are more sensitive to the spin correlation measurements than the jets.

The t- and $\bar{t}$-quarks constitute a very low fraction of the nucleons, which makes them the partons with the lowest contribution to the DM-nucleon scattering, which by itself is a low energy interaction compared to the interactions that hadron colliders are capable of producing. Thus, from direct detection,

[2]Lepton universality of a specific interaction assumes that the interaction coupling values between leptons and the gauge bosons of that interaction are independent of the flavour of the charged leptons.

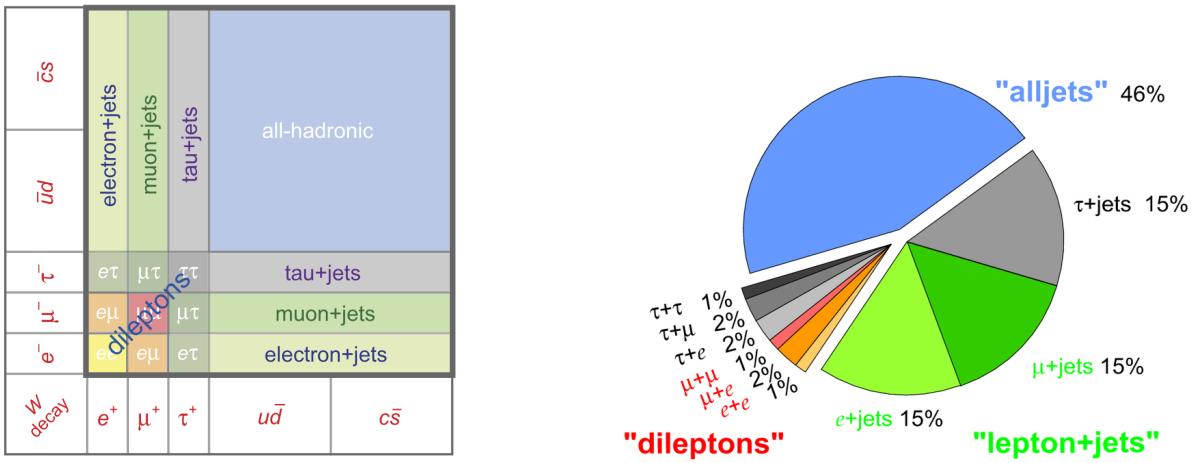

(a) $t\bar{t}$ pair decay channels

(b) $t\bar{t}$ pair branching fractions

Figure 5.4: $t\bar{t}$ pair decay channels 5.4a and their branching fractions 5.4b. In 5.4a the t ($\bar{t}$) quark decay channels are represented by the W^+ (W^-) boson (which originates from the t ($\bar{t}$) quark) decay channels in the horizontal (vertical) axis. The boxes with the label l^+ (l^-), where $l = e, \mu, \tau$ represent the leptonic decay channels of the W^+ (W^-) boson, thus it is implied that a neutrino (anti-neutrino) from the same generation as l^+ (l^-) is produced alongside this lepton. In 5.4b the labels "alljets" and "dileptons" refer to the all-hadronic and dileptonic channels of the $t\bar{t}$ pair decay, respectively. Image in 5.4a is from [50], and image in 5.4b is from [51].

it is difficult to set limits on the couplings of the top quarks with the DM mediators or effective couplings of the top quarks with the DM particles [52]. Therefore, we employ the currently high center-of-mass energy and luminosity at the LHC to produce the highest number of top quark events up until now, and thus, in our work, set stricter limits on the possible interaction between top quarks and a DM mediator than the ones from direct detection searches.

Chapter 6

Search for a light vector DM particle in the $t\bar{t}$ final state at the LHC

The main goal of the work of this dissertation is to study the sensitivity of chosen angular observables' distributions that we could possibly access at the LHC for a light DM vector mediator produced alongside a $t\bar{t}$ pair in the presence of the SM background, in order to set exclusion limits on the couplings of the DM mediator to the top quarks. By "light DM vector mediator" we mean a DM vector mediator with a mass value down to 0.1 GeV, generated using MADGRAPH5_AMC@NLO. We will also reconstruct the $t\bar{t}$ pair and calculate the exclusion limits on the coupling of the mediator to the top quarks for higher masses of the DM vector mediator: 1, 10, 100, and 125 GeV.

To probe the CP-nature of the couplings of the Higgs boson to the top quarks through the $t\bar{t}H$ channel, several observables were proposed in the literature [53–83]. In a previous work in our project group, [1], two of those observables were chosen to probe the CP-nature of the Yukawa coupling of the top quarks to a DM scalar mediator: the azimuthal angle difference of the charged leptons resulting from the decay of the top quarks, $\Delta\phi_{l^+l^-}$, and the b_4 variable evaluated in the laboratory frame (LAB), defined as: $b_4 = \frac{(p^z_t \cdot p^z_{\bar{t}})}{(|\vec{p}_t| \cdot |\vec{p}_{\bar{t}}|)}$. Here $\vec{p}_{t(\bar{t})}$ and $p^z_{t(\bar{t})}$ are the linear momentum vector and its z-component, of the top (anti-top) quark, respectively. b_4 can also be written as $b_4 = \cos\theta_t \times \cos\theta_{\bar{t}}$, where $\theta_{t(\bar{t})}$ is the polar angle of the top (anti-top) quark in the LAB coordinate system. Even though the DM mediator in this dissertation is not a scalar one, we will also employ these two angular observables to test their sensitivity to discriminate the $t\bar{t}Y_{1^+}$ signals from backgrounds at the LHC. To get the distributions of these angular observables we will have to reconstruct the kinematics of the $t\bar{t}$ system and decay products.

6.1 Event Generation

$t\bar{t}Y_{1^+}$ signal events produced from proton-proton collisions at the LHC were generated at $\sqrt{s} = 13$ TeV using the Monte Carlo (MC) event generator MADGRAPH5_AMC@NLO [84] (we used the 2.9.14 version) with the Spin-1 DMsimp model [38], described in 3.3.1, at Next-to-Leading Order (NLO) in QCD. The generated signal included only the dileptonic channel of the $t\bar{t}$ pair decay ($t\bar{t} \to W^+\bar{b}W^- \to bl^+\nu_l\bar{b}l^-\overline{\nu}_l$), considering only final states with electrons and muons. τ decays were not included in this analysis, due to the fact that their decay greatly complicates the event reconstruction. The generation of these events was performed for five different Y_{1^+} mass values: 0.1[1], 1, 10, 100 and

[1]Numerically, the cross-section value of the $t\bar{t}Y_{1^+}$ signal process diverges when the mediator Y_{1^+} is set to be massless. Thus, in this dissertation, the lowest considered mass value for the mediator Y_{1^+} was 0.1 GeV instead of 0 GeV.

125 GeV, and for each mass the same set of model parameter values for the event generation was chosen. This set is shown in Table 6.1.

Table 6.1: Chosen Spin-1 DMsimp model parameter values for the generation of $t\bar{t}Y_{1^+}$ signal events in MADGRAPH5_AMC@NLO. The signal events were generated for 5 different Y_{1^+} mass values with the same model parameter values.

$m_{Y_{1^+}}$	0.1, 1, 10, 100, 125 GeV
m_t	172.5 GeV
$m_f, f \neq t$	0 GeV
m_W	80.4 GeV
$\Gamma_{Y_{1^+}}$	0 GeV
g^V_{u33}	0.25
g^A_{u33}	0
$g^V_{u_{ij}}, ij \neq 33$	0
$g^A_{u_{ij}}, ij \neq 33$	0

All fermions were taken to be massless in the event generation, except the top quarks ($m_f = 0$ for $f \neq t$, where the f index represents a fermion). The decay of the mediator, $\Gamma_{Y_{1^+}}$, was set to 0 since we want it to be completely invisible with no decay products[2]. The vector coupling of the mediator to the top-quarks, g^V_{u33}, was set to $g_{SM} \equiv 0.25$, as suggested in [38, 85] as a benchmark for the spin-1 mediator scenario in order to reproduce the SM predictions for $pp \rightarrow Zj(j) \rightarrow \tau^+\tau^- j(j)$[3]. All the other couplings in the model were set to 0: ($g^A_{u33} = 0$ and $g^{V/A}_{u_{ij}} = 0$, for $i \neq 3$ and $j \neq 3$).

MADSPIN [86] was used in order to preserve the spin correlation effects during the decay of heavy particles. PYTHIA [87] was utilized for parton shower and hadronization. In the event generation, we chose the minimum jet p_T to be 10 GeV, the jet radius parameter for the jet clustering algorithm to be 0.4 and the jet clustering algorithm to be the anti-k_T [46], which was performed by FASTJET [88] [89]. The minimum photon p_T was set to be 20 GeV.

In Figure 6.1, Feynman Diagrams (calculated using MADGRAPH5_AMC@NLO) of 4 of the main contributing subprocesses to the cross-section of the $t\bar{t}Y_{1^+}$ signal are shown. By far, gluon fusion is the main subprocess in the production of the $t\bar{t}Y_{1^+}$ final state at $\sqrt{s} = 13$ TeV at the LHC. The branching ratio of gluon fusion is around 90% to 95% for the considered mass values of Y_{1^+}.

SM background processes were also generated with MADGRAPH5_AMC@NLO. These processes were chosen once they may originate final states with topologies similar to signal events. The SM background processes generated at Leading Order (LO) are:

- $t\bar{t}$ (plus up to 3 jets[4]);
- $t\bar{t}V$ (plus up to 1 jet);
- single top:

[2]Nevertheless, the decay products of Y_{1^+} with a mass bellow $m_{Y_{1^+}} = 125$ GeV would mainly be DM particles (or none if the DM particles are massive enough), X_D, since the mass of the top-quarks, m_t, is larger than $m_{Y_{1^+}} = 125$ GeV and so the Y_{1^+} decay to top-quarks would be largely suppressed and off-shell, meaning that this decay would not produce detectable SM particles, and given that we will not reconstruct the DM mediator, neither the analysis nor the results would change in any significant way.

[3]Note that value of this coupling is just a choice in order to get SM-like cross-sections from the MADGRAPH5_AMC@NLO; any other value for this coupling could have been chosen.

[4]Here, jets refer to gluons and quarks (anti-quarks) lighter than the b-quark that after hadronization may result in an actual jet.

  - s-channel;
  - t-channel;
  - Wt-channel:

- W (plus up to 4 jets);
- Z (plus up to 4 jets);
- $Wb\bar{b}$ (plus up to 2 jets);
- $Zb\bar{b}$ (plus up to 2 jets);
- WW, ZZ, WZ diboson processes (plus up to 3 jets);

where $V = Z, W^{\pm}$. Additional top quark backgrounds were also generated at NLO. These are:

- $t\bar{t}H$;
- $t\bar{t}b\bar{b}$.

The full list of backgrounds can lead to events with 2 isolated leptons of opposite charge and at least 2 jets.

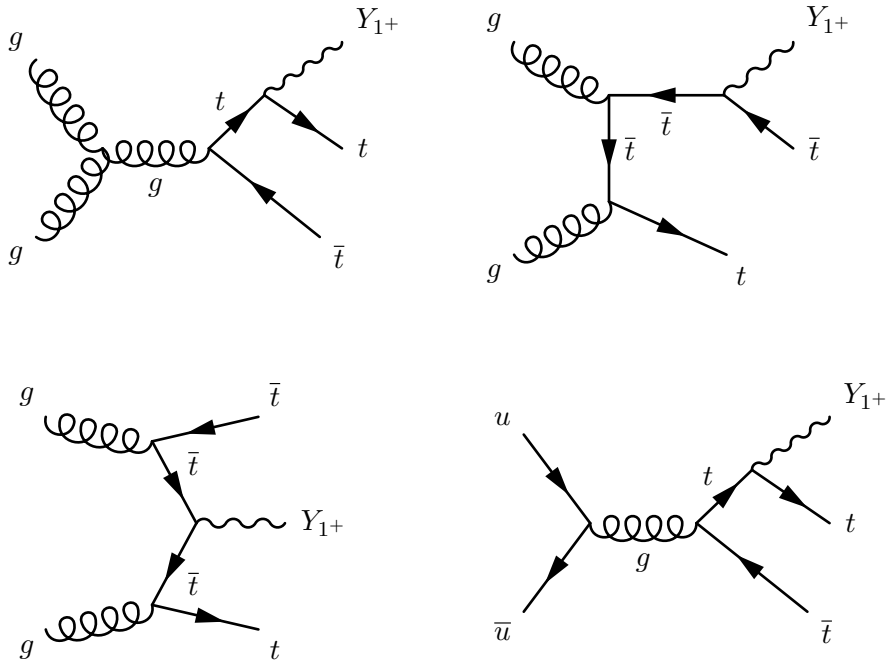

Figure 6.1: Feynman diagrams of 4 of the main subprocesses in the production of the $t\bar{t}Y_{1+}$ final state at $\sqrt{s} = 13$ TeV at the LHC. These and the remaining Feynman diagrams underlying the $t\bar{t}Y_{1+}$ production were calculated using MADGRAPH5_AMC@NLO.

The order in QCD at which the signal and background processes were generated with MADGRAPH5_AMC@NLO, their number of generated events and cross-section values are displayed in Table 6.2. The number of generated $t\bar{t}Y_{1+}$ signal events for $m_{Y_{1+}} > 0.1$ GeV is roughly half of that for $m_{Y_{1+}} = 0.1$ GeV once in our work we focus on the lowest DM mediator mass. The cross-section values of the signal events are calculated using MADGRAPH5_AMC@NLO. The same is not true for some background processes where higher order calculations are available, in particular when considering

top quark production. The cross-section for $t\bar{t}$ + 3 jets was computed at next-to-next-to-leading order (NNLO) in QCD in [90], and, for single top quark, was computed at NNLO in QCD [91, 92] for the t-channel, and NLO in QCD for both the Wt-channel [93] and s-channel [94, 95].

Table 6.2: $t\bar{t}Y_{1+}$ signal (dileptonic channel) and SM background processes generated with MADGRAPH5_AMC@NLO, and the order in QCD at which they were generated, their number of generated events and cross-sections values.

	Process	Order	Number of events	Cross-section (pb)
$t\bar{t}Y_{1+}$ signal (dileptonic channel)	$t\bar{t}Y_{1+}$ ($m_{Y_{1+}} = 0.1$ GeV)	NLO	999 862	0.6094
	$t\bar{t}Y_{1+}$ ($m_{Y_{1+}} = 1$ GeV)	NLO	499 926	0.3837
	$t\bar{t}Y_{1+}$ ($m_{Y_{1+}} = 10$ GeV)	NLO	499 921	0.1701
	$t\bar{t}Y_{1+}$ ($m_{Y_{1+}} = 100$ GeV)	NLO	499 889	0.0240
	$t\bar{t}Y_{1+}$ ($m_{Y_{1+}} = 125$ GeV)	NLO	499 901	0.01725
Background	$t\bar{t}H$	NLO	2 499 612	0.023
	$t\bar{t}b\bar{b}$	NLO	1 499 725	0.79
	$t\bar{t}$ + up to 3 jets	LO	3 593 628	37.89
	$t\bar{t}V$ + up to 1 jet	LO	120 194	0.062
	Single top (s-channel)	LO	500 000	2.19
	Single top (t-channel)	LO	500 000	46.86
	Single top (Wt-channel)	LO	500 000	15.18
	W + up to 4 jets	LO	167 519	34500.0
	Z + up to 4 jets	LO	160 456	3120.0
	$Wb\bar{b}$ + up to 2 jets	LO	155 511	289.0
	$Zb\bar{b}$ + up to 2 jets	LO	153 508	123.0
	WW + up to 3 jets	LO	119 409	84.2
	WZ + up to 3 jets	LO	41 849	37.9
	ZZ + up to 3 jets	LO	215 885	11.0

6.2 ATLAS detector simulation

The fast simulation of the ATLAS detector response was performed using the DELPHES package [96], applying the default ATLAS parameter card and without taking into account pile-up effects. It outputs observables related to the isolated charged leptons, photons, missing transverse energy, and jets. These observables are then used in the analysis. A summary of the parameters included in the default ATLAS parameter card are presented below.

6.2.1 DELPHES simulation parameters

The particle propagation is set to occur within a cylinder with radius $r = 1.15$ m and half-lenght $l = 3.51$ m where a magnetic field with amplitude of 2 T is applied, resembling the ATLAS inner detector.

The particle tracking efficiencies are set to be dependent on the $|\eta|$ and p_T values of the charged hadrons, electrons and muons. For $|\eta| > 2.5$ or $p_T \leqslant 0.1$ GeV, all charged particle tracking efficiencies are set to zero; for 0.1 GeV $< p_T \leqslant 1$ GeV and $1.5 < |\eta| \leqslant 2.5$ the tracking efficiencies are 60%, 50%

and 70% for the charged hadrons, electrons and muons, respectively; for $p_T > 1$ GeV, those efficiencies are set to be equal or higher than 85%, 83% and 98% for the aforementioned types of particles, respectively. Momentum resolution for charged particle tracks are functions of $|\eta|$ and p_T and it deteriorates for larger values of these variables.

The energy deposition fractions in ECAL (f_{ECAL}) and HCAL (f_{HCAL}) are set to distinct values depending on the particle type: for electrons, photons and π^0 mesons $f_{\text{ECAL}} = 1$ and $f_{\text{HCAL}} = 0$; for muons and neutrinos $f_{\text{ECAL}} = f_{\text{HCAL}} = 1$; for the K_S^0 kaon and Λ baryon $f_{\text{ECAL}} = 0.3$ and $f_{\text{HCAL}} = 0.7$; for any other long-lived particle $f_{\text{ECAL}} = 0$ and $f_{\text{HCAL}} = 1$.

The identification efficiencies of the photons, electrons and muons with $p_T > 10$ GeV are set to 95% for $|\eta| \leqslant 1.5$ and 85% for $1.5 < |\eta| \leqslant 2.5$[5]. For $p_T \leqslant 10$ GeV or $|\eta| > 2.5$[6] the identification efficiencies of those particles are set to 0%. The reconstruction of these three particle types requires an isolation criterion such that one can differentiate the particles that come from the primary interaction like, for example, the ones associated with jets. The detected particles (each one with index i) with $p_{T,\,i} > p_T^{min}$ and within a cone of $\Delta R_{ij} < R$ around a detected particle, j, of one of these 3 types are assessed to compute the isolation variable, I. I is defined as $\frac{\sum_i p_{T,\,i}}{p_{T,\,j}}$ and the particle j is labeled as isolated if $I < I_{min}$. In DELPHES, the input parameters to compute the isolation variable for those particle types are $p_T^{min} = 0.1$ GeV, $R = 0.5$, and $I_{min} = 0.12$[7].

For the jet reconstruction, the anti-k_T clustering algorithm [46] was once again employed, where the jet radius parameter was set to 0.6 and only jets with p_T values larger than 20 GeV were considered. Regarding flavour-tagging, the b-tagging efficiency increases with the p_T value of the considered jet. At the imposed minimum p_T value of 20 GeV for the jet reconstruction, the b-tagging efficiency is 53% for b-jets and 7% for c-jets mistagged as b-jets. At $p_T > 20$ GeV values the maximum b-tagging efficiency is 73% and 14.5% for b-jets and c-jets, respectively. For the remaining jets, this efficiency is set to 0.21% at the $p_T = 20$ GeV limit and it slowly increases for larger p_T values, to account for misidentification of jets other than the c-jets as b-jets.

6.3 Analysis

Following the event generation and detector simulation, an event analysis is applied to the generated signal and background events. We used MADANALYSIS5 (version 1.7.21) [97] in the expert mode [98] to perform the analysis.

At the LHC we only have access to the measured data of the detected objects and one of the main goals of the analysis is to infer information on the physics processes, from that measured data. The difference of data with respect to simulations is that in the simulations we have access to the parton level information. We need then to estimate how the simulated parton level data would translate in terms of measured data, as if we were measuring data at the LHC. For that, we simulated what would actually be detected at the LHC (using DELPHES, as stated before), and then proceeded to its analysis. This involves the reconstruction of objects and, whenever required, access to the corresponding partons at generator level, for matching studies. For the analysis of the signal and background events, selection cuts on the events had to be applied, detailed discussed in the next section, 6.3.1. In 6.3.2 we discuss how the matching and reconstruction of the events were done.

[5] $1.5 < |\eta| \leqslant 2.7$ for the muons.
[6] $|\eta| > 2.7$ for the muons.
[7] $I_{min} = 0.25$ for muons.

6.3.1 Event Selection

The event selection on the signal and background event samples has the main purpose of increasing the signal to background ratio. This includes discarding $t\bar{t}Y_{1^+}$ generated signal events whose $t\bar{t}$ pairs cannot be successfully reconstructed. We apply cuts on the number of objects and on the values of physical observables such as, among others, the p_T and η, of jets and charged leptons. The cuts on the number of objects are such that they agree with what we expect from the final state topology of our signal. We expect two b-tagged jets and two opposite charged leptons in these events. The cuts on the p_T and η values of the jets and leptons is motivated by the limitations of the detector, and by interesting signal properties. For example, the detector cannot detect particles with θ values near 0 and most of the interesting high-energy processes have events with objects with high p_T values and θ values far from 0.

In four distinct instances in our work, we applied selection cuts to the events. The first instance was in the generation of the signal events and in its detector simulation to avoid generating large phase space regions that will be removed by the analysis cuts (as presented in 6.1 and 6.2). The second selection cut is made right before the reconstruction of the events (so it is called pre-selection cut), and is applied to both signal and background events. The conditions of the second selection cut are:

- Jets and leptons reconstructed by DELPHES should have $|\eta| < 2.5$ and $p_T > 20$ GeV, to further reject events that would be harder to reconstruct given the low transverse momentum of their objects;
- We require at least two jets and two isolated leptons of opposite charge in the events. This decision was made since we are interested in the dileptonic channel of the decay of the $t\bar{t}$ pair;

The third selection cut is made during the reconstruction of the signal and background events:

- The event must contain a reconstructed $t\bar{t}$ pair, through a kinematic fit. If the analysis of the event has found no solution for the neutrino reconstruction, then the event is discarded.

The fourth and final selection cut to the signal and background events is made after the reconstruction and right before the evaluation of the exclusion limits:

- The invariant mass of the two-lepton system was required to fulfil $|m_{l^+l^-} - m_Z| > 10$ GeV. This requirement avoids contamination from the Z + jets background (as one can see from 6.2, it is one of largest backgrounds regarding its cross-section);
- The number of b-tagged jets must be equal to 2.

Even though it will increase the signal to background ratio, the event selection has two negative effects. The cuts on the physical observables may possibly remove detector objects which would match better to the parton level than the ones that "survive" the event selection cuts. This has an impact on the efficiency of how close the reconstructed events are to the generated ones. The cuts that reject events may be discarding a substantial amount of signal events and so increasing the statistical error of our analysis.

6.3.2 Matching and Kinematic Reconstruction

Before the actual reconstruction, we may perform the match of the objects at the detector level simulated by DELPHES with the generated objects at parton level. Both the matching and kinematic reconstruction are employed using MADANALYSIS5, which has access to three different levels of analysis for each generated event:

- **Parton/Generator level (GEN):** this level has all the information from the MADGRAPH5_AMC@NLO event generation; one has all the information about all the particles within the event, including the invisible particles such as the neutrinos and the Y_{1^+} mediator. At this level, it is possible to track the parent particle of each particle within a decay chain, and reconstruct the whole decay chain of any particle;

- **Reconstruction with Truth-Match level (REC):** at this level, one has access to the GEN level and the simulated data which are the jets and charged leptons reconstructed by DELPHES[8]. These reconstructed objects are matched to the GEN level particles they are most likely to be reconstructed from. So at this level, one can assess how good the reconstruction is, and change it in order to increase the percentage of simulated events correctly matched to GEN level. The Thruth-Matched (TM) reconstruction corresponds to the best reconstruction method that we can hope to achieve, given that MADANALYSIS has access to the GEN level information during the reconstruction.

- **Reconstruction without TM level (EXP):** this level has no access to the GEN level (as in a real experiment like ATLAS) once there is only information about the jets and leptons reconstructed by DELPHES.

In TM reconstruction, it is assumed that the possible right match between one GEN object and one detector object occurs when we find the REC jet or charged lepton with the least ΔR distance to the GEN quark and charged lepton, respectively, considering all possible combinations. The $\Delta R_{i,j}$ between those objects is defined as:

$$\Delta R_{i,j} = \sqrt{(\eta_i^{GEN} - \eta_j^{REC})^2 + (\phi_i^{GEN} - \phi_j^{REC})^2}, \tag{6.1}$$

being i and j the indexes of the GEN and REC objects, respectively. The possible right match will be finally accepted only if $\Delta R \leqslant 0.5$ for jets and $\Delta R \leqslant 0.1$ for charged leptons. An event is discarded if there is not a minimum of 2 truth-matched opposite charged leptons and 2 truth-matched jets.

Since we lost the GEN level information in the reconstruction without TM, there is now a much larger number of possible assignments between EXP jets and the b and $\bar{b}$ GEN quarks (which are products of the t-quark and $\bar{t}$-quark decay, respectively), and so the correct identification of these jets is even more difficult. In our analysis, we are taking into account a maximum of 10 EXP jets, and so we choose the 10 with the largest p_T values since we expect the b-jets to be one of the most energetic ones. We need then some criteria to help us reconstruct the events without TM: the 2 chosen EXP isolated charged leptons are the positive charged one with the largest p_T value and the negative charged one with the largest p_T value. They are assumed to result from the $W^{\pm}$ boson decays, which in turn are products of the decay of the top quarks (it is easy to determine the charge of these leptons, so it is almost always possible to determine if an EXP charged lepton comes from the top or the anti-top quark); 2 chosen EXP jets from the set of 10 with largest p_T values are assumed to originate from the b-quarks of the decays of the top-quarks and this choice relies on a multivariate data analysis method in order to discriminate between correct and wrong assignments of jets to the GEN bottom quarks. We used the Toolkit for Multivariate Data Analysis, TMVA [99], which employs GEN level information from the ΔR, $\Delta\phi$ and $\Delta\theta$ distributions between the l^+ (l^-) lepton and the $b(\bar{b})$-quark (labeled as $b_t(\bar{b}_{\bar{t}})$), both originating from the $t(\bar{t})$-quark decay, respectively. The invariant mass difference distribution between the pairs (b_t, l^+) and $(\bar{b}_{\bar{t}}, l^-)$ is also used. We build the distributions fed to TMVA, using GEN information. For the

[8]Do not confuse reconstructed objects from DELPHES with reconstructed objects in the analysis. The former ones are simply the objects simulated as in the ATLAS environment from the GEN level objects.

correct assignments we use the particles' information from the same and correct decay chains. Taking every wrong jet-assignment into account would be a very unpractical task and so we decided for the main and simpler wrong jet-assignment: wrongly assign an EXP jet to a b_t-quark ($\bar{b}_{\bar{t}}$-quark) while it originates from the $\bar{b}_{\bar{t}}$-quark (b-quark), i.e, jets from the wrong decays are used.

In Figure 6.2, the normalized GEN angular distributions for the pairs (l^+, b_t) and $(l^+, \bar{b}_{\bar{t}})$ and the normalized GEN distribution of the invariant mass difference between the pairs (l^+, b_t) and $(l^-, \bar{b}_{\bar{t}})$ are shown, from the $t\bar{t}Y_{1^+}$ generated signal events with $m_{1^+} = 0.1$ GeV. The distributions of the sample labeled as "signal" and coloured as blue are the ones corresponding to the correct assignments. The distributions of the sample labeled as "background"[9] and coloured as red are the ones of the wrong assignments. To optimize finding the correct two jet-assignments, the equivalent angular distributions for the l^- lepton were also used. From the observation of these distributions, we conclude that the GEN level kinematic distributions of the correct and wrong assignments do not overlap that much, and actually, the peak of one distribution roughly coincides with the valley of the other distribution. This is useful, since the less these distributions overlap the better the multivariate data analysis methods employed by TMVA will be at simultaneously accepting the correct assignments and rejecting the wrong assignments. The correlation matrices of the aforementioned variables for both the signal and back-

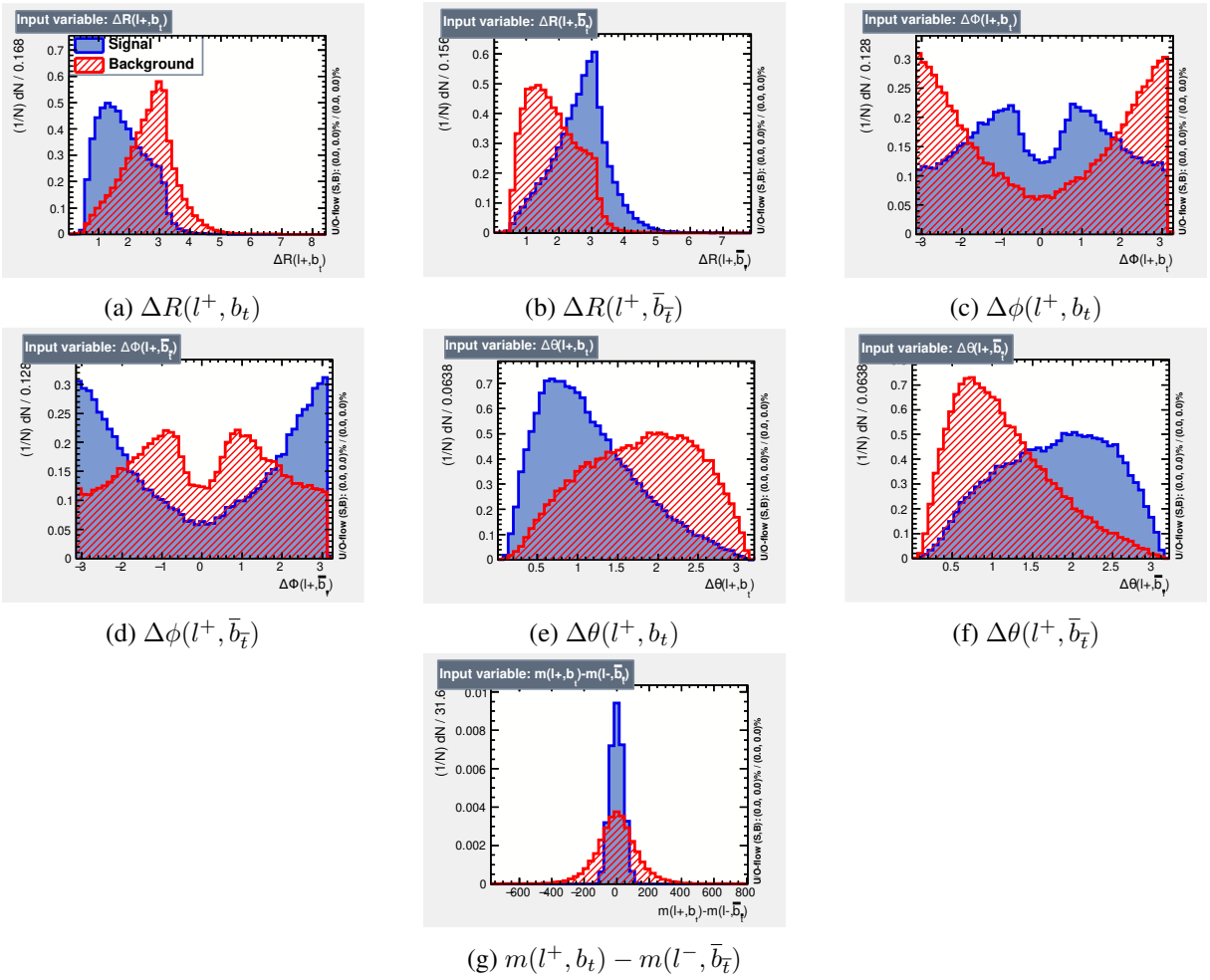

(a) $\Delta R(l^+, b_t)$ (b) $\Delta R(l^+, \bar{b}_{\bar{t}})$ (c) $\Delta\phi(l^+, b_t)$

(d) $\Delta\phi(l^+, \bar{b}_{\bar{t}})$ (e) $\Delta\theta(l^+, b_t)$ (f) $\Delta\theta(l^+, \bar{b}_{\bar{t}})$

(g) $m(l^+, b_t) - m(l^-, \bar{b}_{\bar{t}})$

Figure 6.2: Normalized distributions of the TMVA input variables for the signal (blue) and background (red) samples, from the $t\bar{t}Y_{1^+}$ signal events with $m_{Y_{1^+}} = 0.1$ GeV. The input variables, ΔR, $\Delta\phi$, $\Delta\theta$ and the invariant mass difference, are computed at GEN level.

[9] Do not confuse with the SM background.

ground samples are presented in Figure 6.3. Afterwards, several multivariate statistical methods (BDTG,

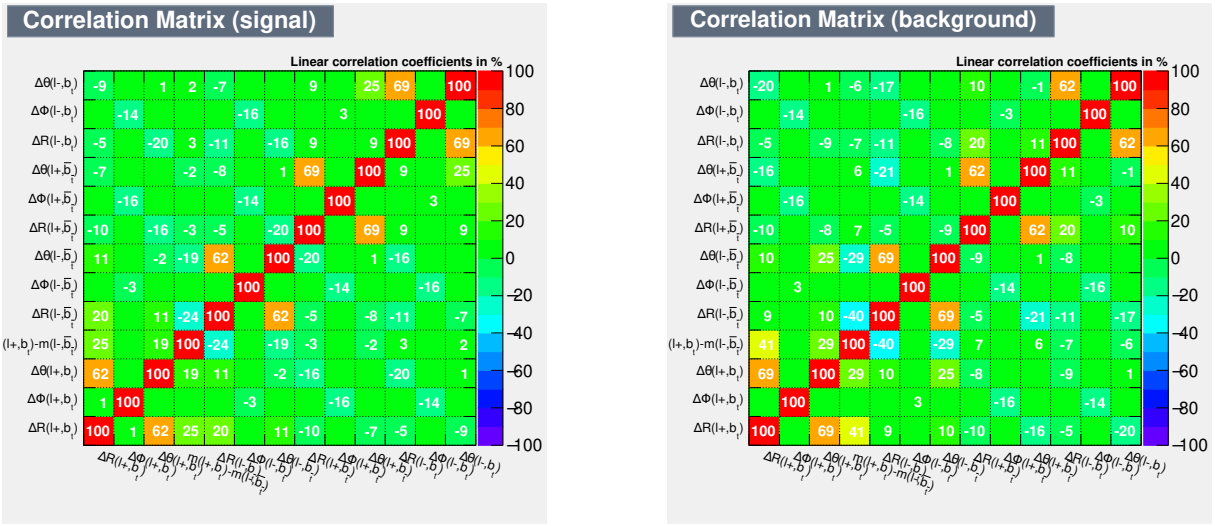

(a) (b)

Figure 6.3: Matrix correlations between all the TMVA input variables for the signal sample (6.3a), and for the background sample (6.3b), from the $t\bar{t}Y_{1+}$ signal events with $m_{Y_{1+}} = 0.1$ GeV.

BDT, BDTD, BDTMitFisher, Likelihood, BoostedFisher, Fisher, BDTB) were trained by TMVA, using the distributions in Figure 6.2 for training and testing. All the individual distributions were combined into a single discriminant classifier for each one of the methods. This resulted in the Recieving Operating Characterictic (ROC) curve shown in Figure 6.4a. According to this curve, the multivariate statistical method that has the largest acceptance of correct combinations while also having the largest rejection of incorrect combinations was the Boosted Decision Tree with Gradient boost (BDTG) [100], whose discriminant distributions are shown in Figure 6.4b.

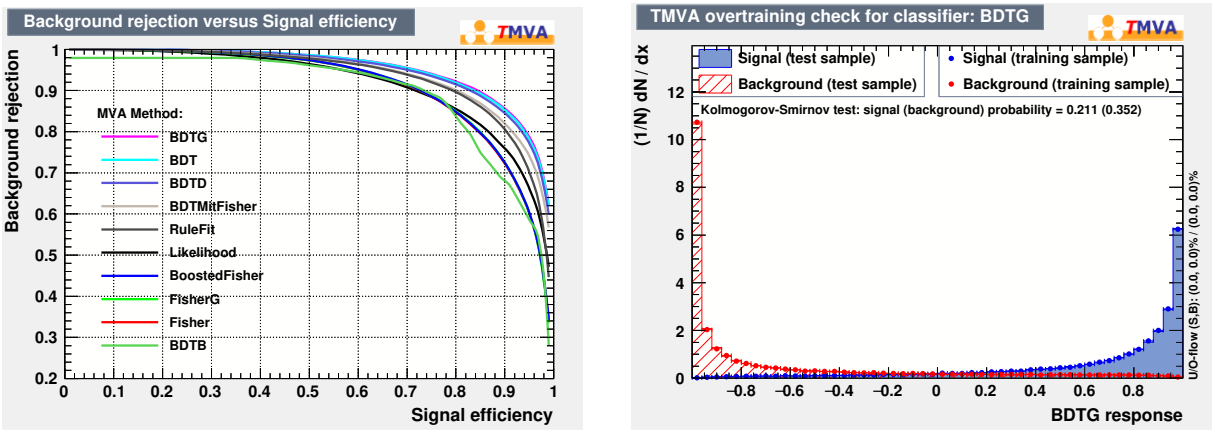

(a) (b)

Figure 6.4: 6.4a: Wrong combination rejection VS correct combination acceptance (ROC curve) of different multi-variate methods; 6.4b: Distribution of the BDTG discriminant for the signal and background in training and test samples. Both figures apply to $t\bar{t}Y_{1+}$ signal events with $m_{Y_{1+}} = 0.1$ GeV.

The TMVA outputs the weights computed by every multi-variate method and we use the ones from the BDTG method in our reconstruction without TM. These weights were computed from the signal event sample with $m_{Y_{1+}} = 0.1$ GeV, and the reconstruction without TM of all the signal and background events made use of these weights in order to get the most probably correct assignment of 2 jets from the

available 10 EXP jets to the GEN b- and $\bar{b}$-quarks from the decay of the $t\bar{t}$ pair, and so, to get the most probably correct pairing between those 2 EXP jets and the EXP l^+ and l^-, such that the pair formed by 1 EXP jet and 1 EXP $l^\pm$ comes from the same top quark in the $t\bar{t}$ pair decay. The reconstruction of the signal events with $m_{Y_{1^+}} \neq 0.1$ GeV would have been more efficient if we had computed and made use of the correspondent weights, however the reconstruction would not be that significantly better and so we are stuck only with the chosen weights. The $t\bar{t}Y_{1^+}$ signal event sample with $m_{Y_{1^+}} = 0.1$ GeV was the chosen one because it is the signal event sample with the lowest mediator mass, which is the case we are interested in, the most. At this point, we have matched 2 EXP opposite charged leptons and 2 EXP jets to the 2 GEN opposite charged leptons and the 2 GEN bottom quarks from the $t\bar{t}$ pair decay, respectively. Furthermore, the events whose invariant masses of the EXP pairs (b_t,l^+) and ($\bar{b}_{\bar{t}}$,l^-) are larger than 150 GeV, are discarded. We end up assigning the four-momentum of the 2 chosen EXP jets to the four-momentum of the b and $\bar{b}$ quarks of the $t\bar{t}$ pair decay.

After the matching, whether with or without the TM, we proceeded to the kinematic reconstruction of the t and $\bar{t}$ quarks from their respective decay products. In the dileptonic channel final state, the neutrinos are the only decay products that are not detectable by the detector. Therefore, for the kinematic reconstruction of the neutrinos we made use of the following set of equations:

$$\begin{aligned}
(p_{l^+} + p_\nu)^2 &= m_{W^+}^2; \\
(p_{l^-} + p_{\overline{\nu}})^2 &= m_{W^-}^2; \\
(p_{W^+} + p_{b_t})^2 &= m_t^2; \\
(p_{W^-} + p_{\bar{b}_{\bar{t}}})^2 &= m_{\bar{t}}^2; \\
p_\nu^x + p_{\overline{\nu}}^x &= \not{E}_T^x; \\
p_\nu^y + p_{\overline{\nu}}^y &= \not{E}_T^y,
\end{aligned} \tag{6.2}$$

being p_i the four-momentum of the particle i, p_i^μ is the μ-component of this four-momentum, m_i the on-shell mass of the i particle and $\not{E}_T^{x/y}$ the x/y component of the missing transverse energy. The first four equations are the relativistic on-shell energy–momentum relations for the decays of the $W^\pm$ bosons and of the top quarks, while the last two are the transverse momentum conservation for each one of the x and y components of the transverse momentum assuming that only the neutrinos contribute to it. The last two conditions are actually an approximation. We are not counting on the Y_{1^+} missing energy, by assuming that the missing transverse energy from the Y_{1^+} mediator is negligible comparing to the neutrinos contribution. Since the neutrinos are assumed to be massless, the 0 component of the neutrinos four-momenta is determined from their linear momenta, $E_{\nu/\overline{\nu}}^2 = |\vec{p}_{\nu/\overline{\nu}}|^2$, thus we have six unknown quantities - the components of the linear momenta of the ν and $\overline{\nu}$ - before trying to find a solution that agrees with the set of equations in 6.2. The first four equations in 6.2 are quadratic equations, thus there may be several solutions for the momenta of ν and $\overline{\nu}$ that also agree with the two last equations in 6.2. Therefore we have to rely on a non-analytical method to attempt to find the best solution for the momenta of the neutrinos. The procedure to find the best solution for the four-momenta of the neutrinos is the following:

1. The input masses of the t and $\bar{t}$ quarks for the 3$^{\text{th}}$ and 4$^{\text{th}}$ equations in 6.2 are randomly sampled from 2-Dimensional Probability Density Functions (2D PDF's), $P(m_t, m_{\bar{t}})$, constructed from GEN level information of the $t\bar{t}Y_{1^+}$ generated signal with $m_{Y^+} = 0.1$ GeV;

2. The input masses of the W^+ and W^- bosons for the 1$^{\text{st}}$ and 2$^{\text{nd}}$ equations in 6.2 are randomly

sampled from 2D PDF's constructed from GEN level information of the $t\bar{t}Y_{1^+}$ generated signal events with $m_{Y^+} = 0.1$ GeV. However, since the $W^{\pm}$ bosons are decay products of the t and $\bar{t}$ quarks, the allowed mass distribution of the former ones depend on the masses of the latter ones. Thus the masses of the $W^{\pm}$ are randomly sample from the 2D PDF's $P(m_{W^+}, m_t)$ and $P(m_{W^-}, m_{\bar{t}})$ considering only the slice of bins containing the previously randomly sampled m_t and $m_{\bar{t}}$ values;

3. After randomly sampling the 4 mass values, a fine random variation of the initial sampled mass values is performed, within the resolution of the $P(m_{W^+}, m_t)$ and $P(m_{W^-}, m_{\bar{t}})$ 2D PDF's, which is 1 GeV $\times$ 1 GeV. We get two sets of mass values for the top quarks and the $W^{\pm}$ bosons: the initial one and the fine fitted one;

4. For each set of sampled t, $\bar{t}$ and $W^{\pm}$ mass values, the solutions of the system of equations in 6.2 are attempted to be found. If no solution is found for any set of sampled mass values, the random sampling of mass values t, $\bar{t}$ and $W^{\pm}$ and their fine variation (steps 1, 2 and 3) are repeated until at least one solution of the system of equations in 6.2 is found. If no solution is found after 500 of these attempts, the event is discarded;

5. If one finds solutions for the system of equations in 6.2, the solution chosen to reconstruct the event is the one which gives the best kinematic fit, defined as the one that maximizes the following likelihood:

$$L \propto \frac{1}{p_{T_\nu} p_{T_{\overline{\nu}}}} P(p_{T_\nu}) P(p_{T_{\overline{\nu}}}) P(p_{T_t}) P(p_{T_{\bar{t}}}) P(p_{T_{t\bar{t}}}), \tag{6.3}$$

where $P(p_{T_{\overline{\nu}}}), P(p_{T_t}), P(p_{T_{\bar{t}}})$ and $P(p_{T_{t\bar{t}}})$ are the smoothed version of the PDF's from the GEN level transverse momenta of the ν, $\overline{\nu}$, t, $\bar{t}$ and $t\bar{t}$ system, respectively, from the $t\bar{t}Y_{1^+}$ generated signal events with $m_{Y^+} = 0.1$ GeV. The purpose of the PDF's is such that the p_T of the distributions of the reconstructed objets resemble the ones at GEN level. The signal events were generated at NLO in QCD which allows a gluon to be radiated by any coloured particle in the event. If energetic enough, the gluon may originate a new jet. On the other hand, the kinematic fit follows a LO approach, and uses reconstructed b and $\overline{b}$ jets that are less energetic than the original b- and $\overline{b}$-quark partons (note that we chose 2 jets from a larger number of jets that detector simulation reconstructed). This leads to solutions where the ν and $\overline{\nu}$ are too energetic. To compensate for this effect, the factor $\frac{1}{p_{T_\nu} p_{T_{\overline{\nu}}}}$ was introduced in 6.3 by giving less weight to the solutions whose p_T of the neutrinos have extreme values. This factor also compensates for detector effects that may result in overestimating the ν and $\overline{\nu}$ p_T values after reconstruction, since we do not take those effects into account by assuming that all the missing transverse energy comes from the neutrinos.

In Figure 6.5 we show 2D plots with the correlations between the p_T of the reconstructed without TM (EXP level) neutrinos, top quarks, W^+ bosons sand $t\bar{t}$ systems and their corresponding GEN level (at NLO with shower effects) p_T, in order to evaluate the quality of the reconstruction without TM for the $m_{Y_{1^+}} = 0.1$ GeV. In the kinematic fit, we expect the EXP level distributions to resemble the GEN level ones. We do not expect, however, to recover the GEN level kinematics of each event, since the leptons, jets and $\not{E}_T$ used for the kinematic fit are already affected by detector effects, limitations of the employed algorithms, etc. Thus, the higher the correlation values per bin are concentrated along the $x = y$ axis, the closer are the EXP kinematics to the GEN kinematics of each event, resulting in a better quality of the analysis method employed to reconstruct without TM. The 2D plots p_T correlations between EXP and GEN levels for the $\bar{t}$-quark, $\overline{\nu}$ and W^- boson are very similar to the ones of the t-quark, ν and W^+ boson

and so, the former ones are not shown in Figure 6.5. The higher correlation values per bin in the 2D plot of the p_T of the neutrinos in Figure 6.5 are more spread out than for the other objects, meaning that, out of these objects, the neutrinos are the ones whose EXP p_T values deviate the most from their GEN level counterparts. This is due to the reconstructed neutrinos having to compensate for all the energy losses, resolution effects in the event, and depending on the reconstructed leptons and bottom quarks, which make them to be kinematically a bit different from the GEN level neutrinos. As we move backwards in the decay chain, the correlation between the EXP p_T and the GEN p_T gets slightly better. Nonetheless, from observing these plots we can see that there is a clear high correlation between the GEN level p_T and the ones from the EXP level for all these objects, including the t- and $\bar{t}$-quarks and $t\bar{t}$ system, which makes it possible to reconstruct the $t\bar{t}$ system despite not attempting to reconstruct the Y_{1+} mediator produced alongside the $t\bar{t}$ pair. This gives us confidence on the strategy of the analysis method employed in our work.

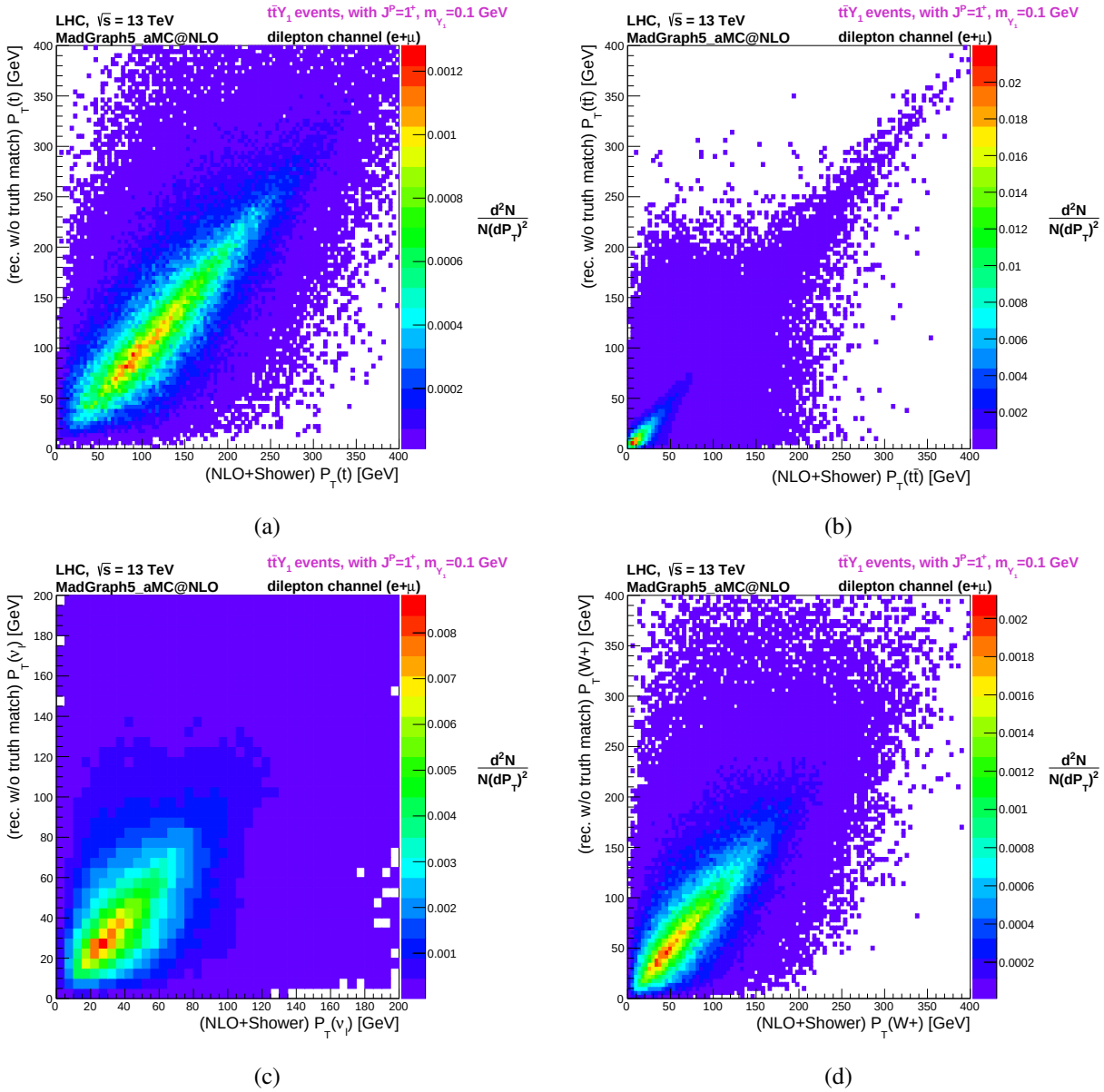

Figure 6.5: Two-Dimensional distributions of the transverse momentum of the reconstructed without TM (vertical axes, "rec. w/o truth match") top-quark (6.5a), $t\bar{t}$ system (6.5b), neutrino 6.5c and W^+ boson 6.5d versus the corresponding GEN level transverse momentum distributions (horizontal axes, "NLO+Shower") for $t\bar{t}Y_{1+}$ events with $m_{Y_{1+}} = 0.1$ GeV.

In Figures 6.6, 6.7, 6.8 and 6.9 we show similar plots to the ones in Figure 6.5 but for the cases where $m_{Y_{1+}} = 1$, 10, 100 and 125 GeV, respectively. We observe a loss of correlation between the EXP level and GEN level p_T values of the reconstructed objects with the increase of the mass of the vector DM mediator, revealing a loss of quality in the event reconstruction. The fit is affected by the mass value of the vector DM mediator, which clearly violate the approximation that the $\not{E}_T$ is only due to the undetected neutrinos (this approximation was set by imposing the last two equations of 6.2 in the kinematic fit), as the mediator mass increases.

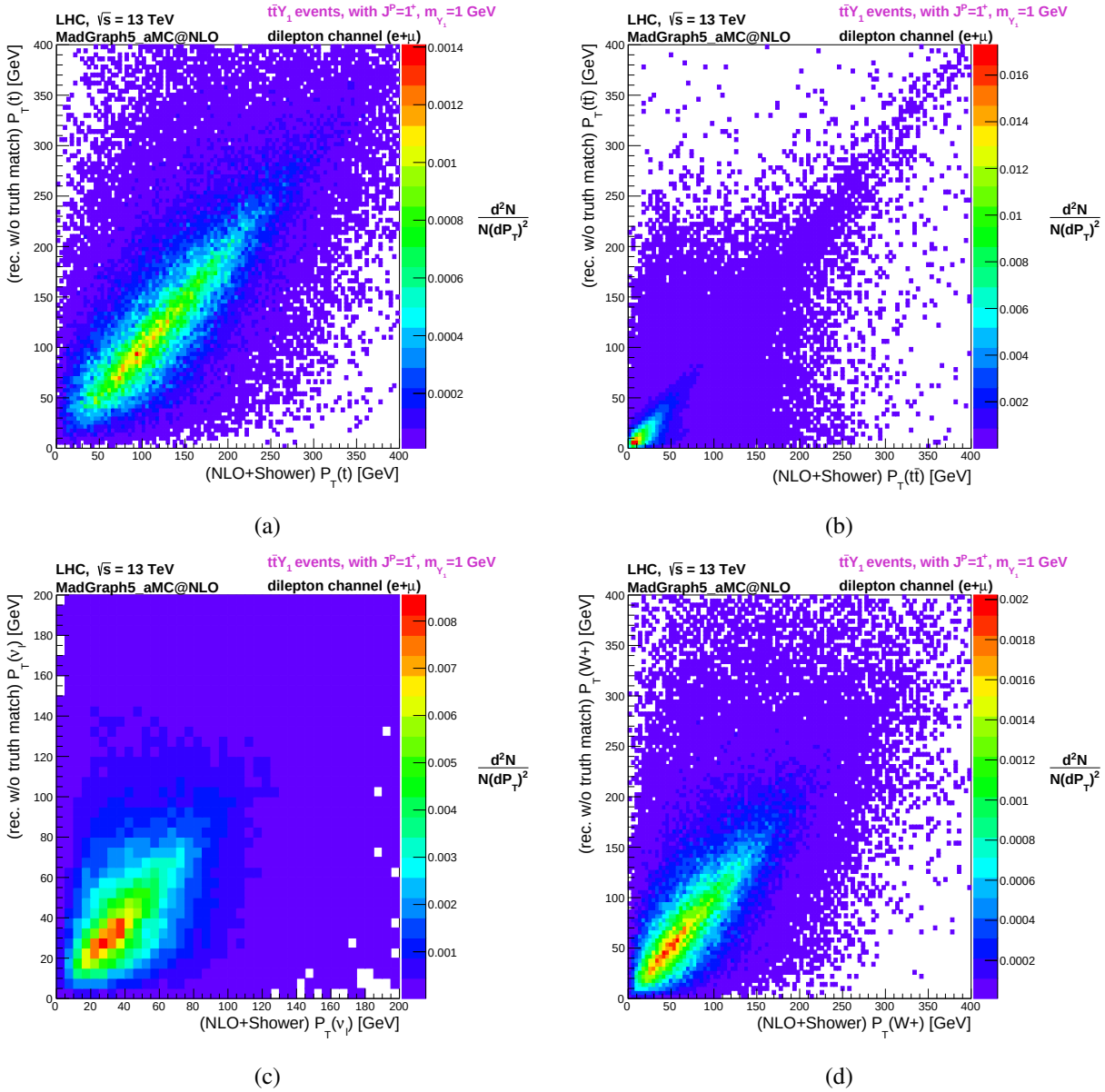

Figure 6.6: Two-Dimensional distributions of the transverse momentum of the reconstructed without TM (vertical axes, "rec. w/o truth match") top-quark (6.6a), $t\bar{t}$ system (6.6b), neutrino 6.6c and W^+ boson 6.6d versus the corresponding GEN level transverse momentum distributions (horizontal axes, "NLO+Shower") for $t\bar{t}Y_{1+}$ events with $m_{Y_{1+}} = 1$ GeV.

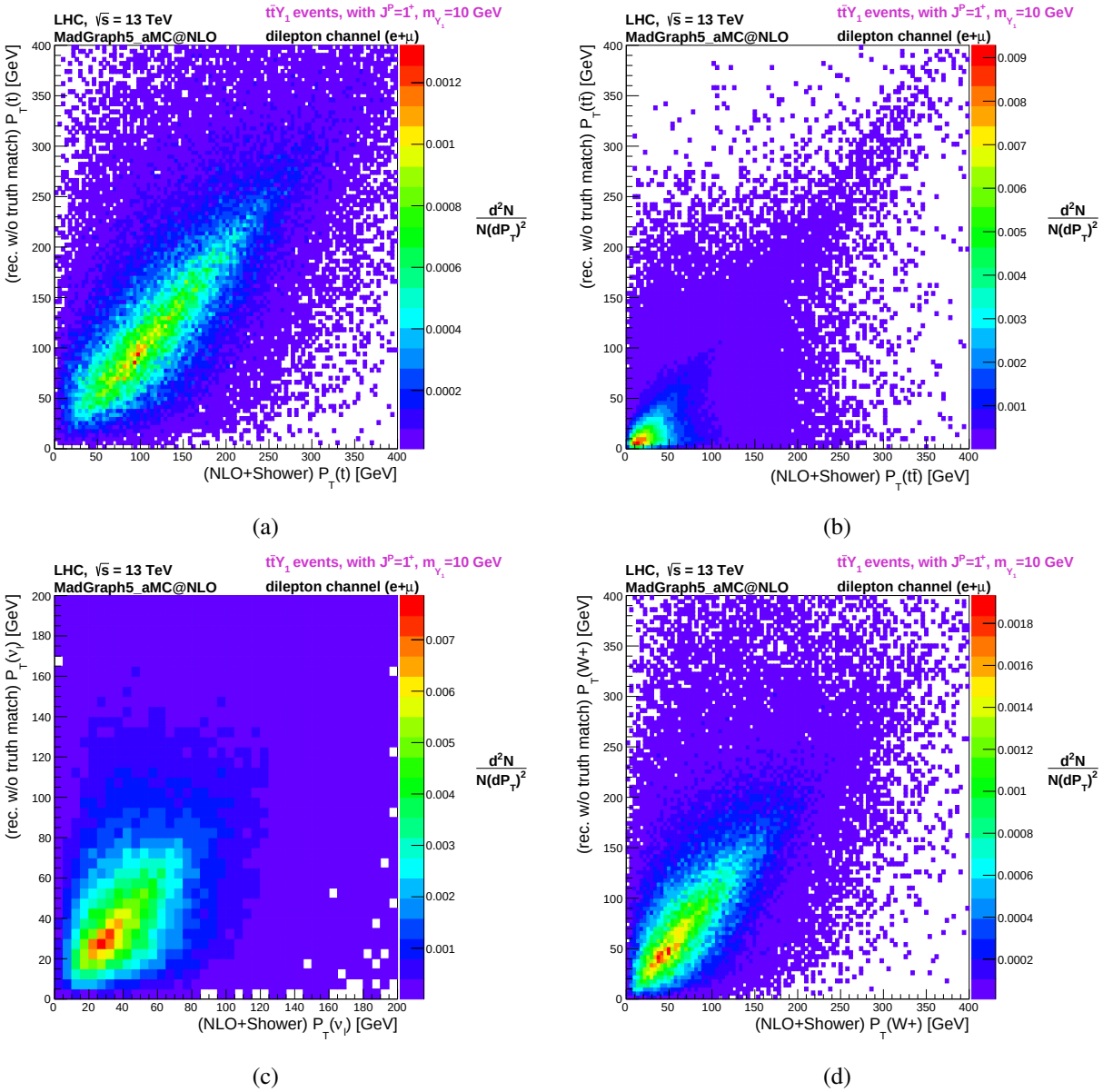

Figure 6.7: Two-Dimensional distributions of the transverse momentum of the reconstructed without TM (vertical axes, "rec. w/o truth match") top-quark (6.7a), $t\bar{t}$ system (6.7b), neutrino 6.7c and W^+ boson 6.7d versus the corresponding GEN level transverse momentum distributions (horizontal axes, "NLO+Shower") for $t\bar{t}Y_{1+}$ events with $m_{Y_{1+}} = 10$ GeV.

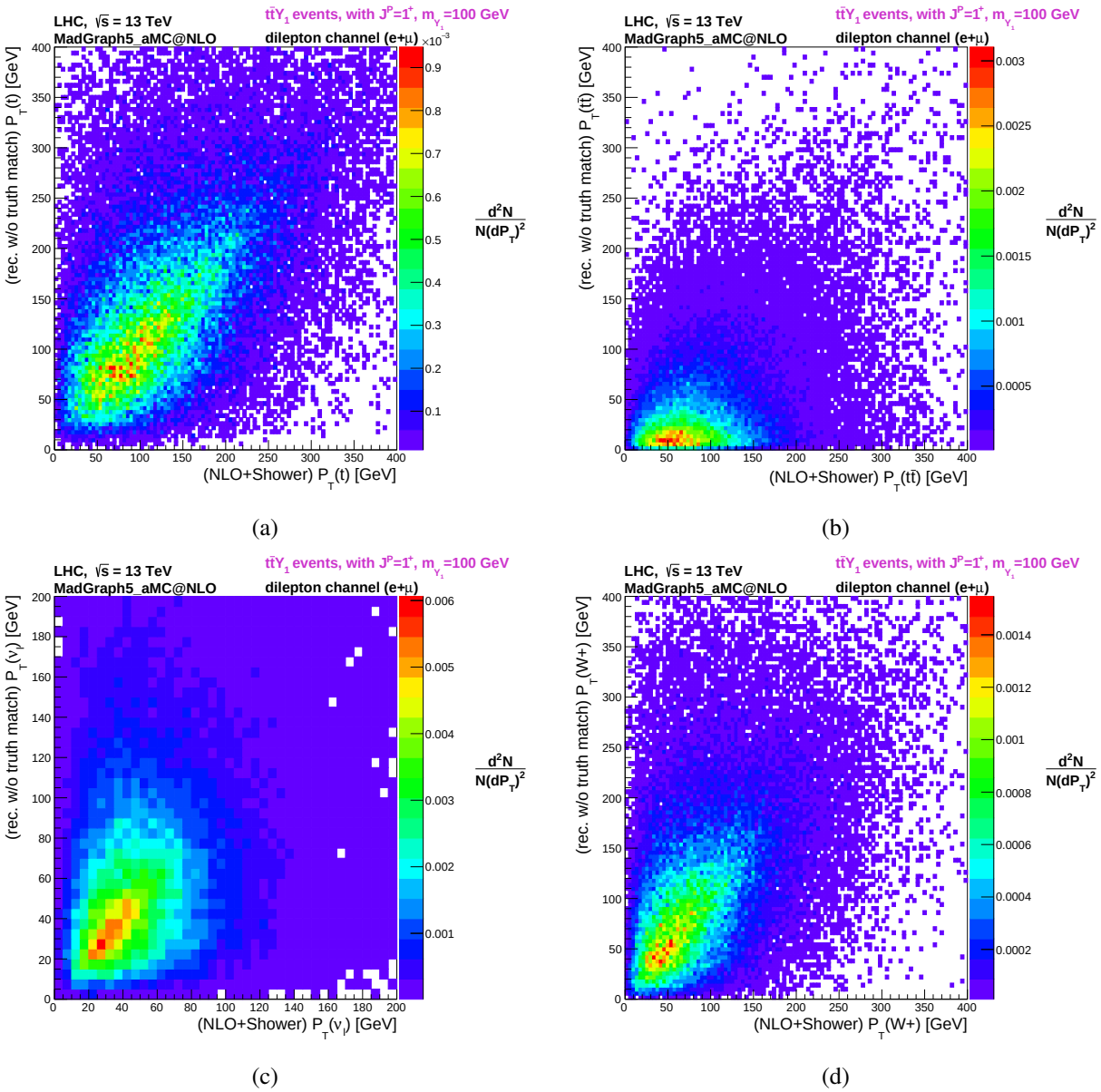

Figure 6.8: Two-Dimensional distributions of the transverse momentum of the reconstructed without TM (vertical axes, "rec. w/o truth match") top-quark (6.8a), $t\bar{t}$ system (6.8b), neutrino 6.8c and W^+ boson 6.8d versus the corresponding GEN level transverse momentum distributions (horizontal axes, "NLO+Shower") for $t\bar{t}Y_{1+}$ events with $m_{Y_{1+}} = 100$ GeV.

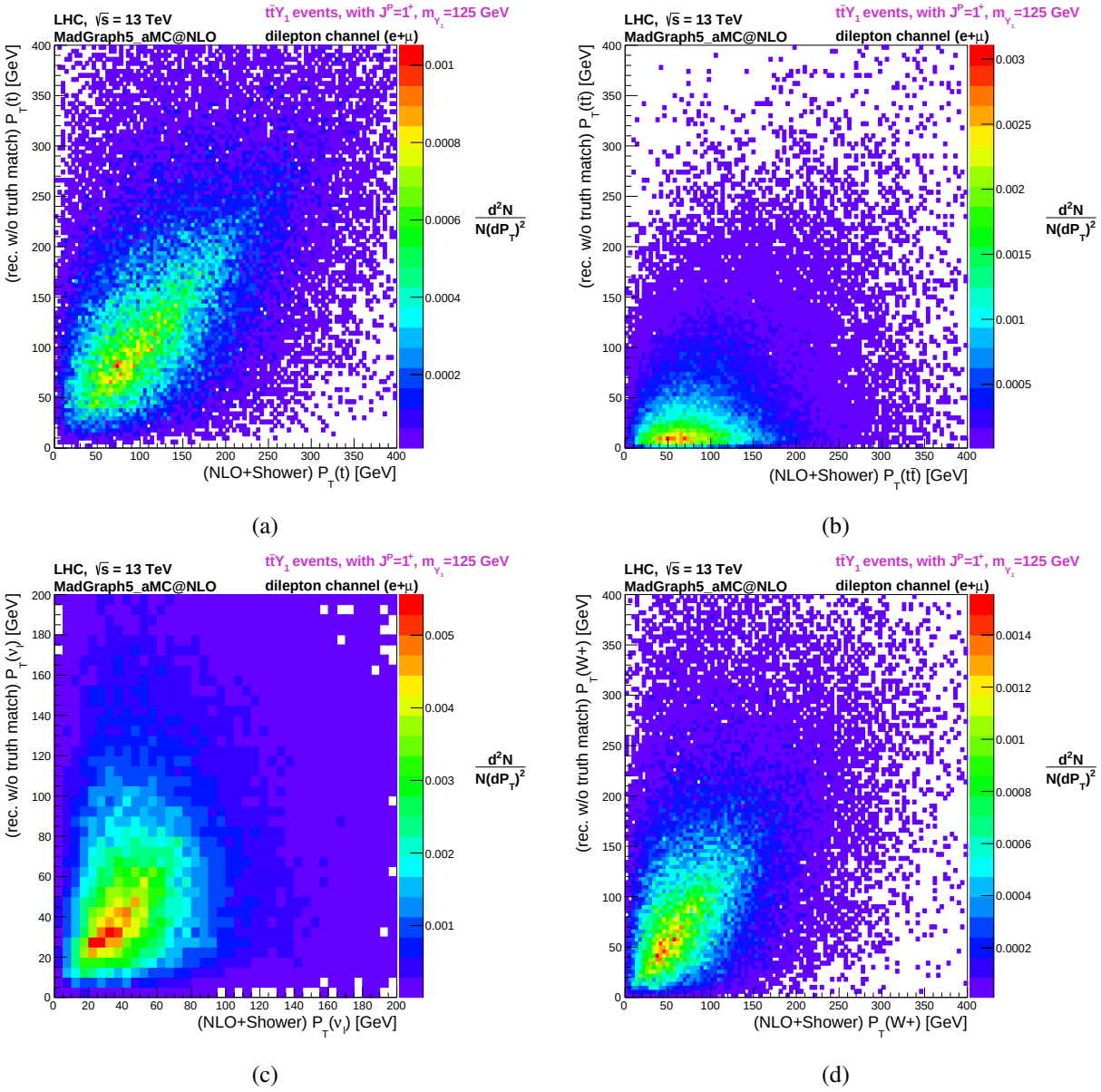

Figure 6.9: Two-Dimensional distributions of the transverse momentum of the reconstructed without TM (vertical axes, "rec. w/o truth match") top-quark (6.9a), $t\bar{t}$ system (6.9b), neutrino 6.9c and W^+ boson 6.9d versus the corresponding GEN level transverse momentum distributions (horizontal axes, "NLO+Shower") for $t\bar{t}Y_{1+}$ events with $m_{Y_{1+}} = 125$ GeV.

6.3.3 Efficiencies

In Table 6.3 we present the efficiencies in percentage of the signal events that survived the several analysis cuts, for different mediator masses. There the pre-selection cut represented by the line "$N_{\text{jets}} \geqslant 2$ and $N_{\text{lep}} \geqslant 2$" includes selected jets and leptons with $|\eta| < 2.5$ and $p_T > 20$ GeV and the respective shown efficiency is the number of events that survive such selection cuts divided by the number of generated events, in percentage. The following 3 lines represent efficiencies related to the matching and reconstruction with and without TM. Those efficiencies are normalized to the percentage of events that survive the selection cuts represented by "$N_{\text{jets}} \geqslant 2$ and $N_{\text{lep}} \geqslant 2$". In the next line, the percentage of events that were successfully reconstructed[10] without TM (EXP) and have the 2 charged leptons and the 2 assigned jets with the same match as when those events were successfully reconstructed with TM (REC)

[10]By successfully reconstructed events we mean events whose reconstruction enabled to find kinematic fit solutions.

are shown. Finally the last line shows the percentage of successfully reconstructed EXP events that survived the final selection cuts ($|m_{l^+l^-} - m_Z| > 10$ GeV and $N_{b\text{-jets}} = 2$).

Table 6.3: Efficiencies (in %), rounded to two decimal places, of the selection cuts and of the reconstruction methods performed in the analysis of the $t\bar{t}Y_{1^+}$ signal events as function of the mass of Y_{1^+}. "$N_{\text{jets}} \geqslant 2$ and $N_{\text{lep}} \geqslant 2$" already includes selected jets and leptons with $|\eta| < 2.5$ and $p_T > 20$ GeV.

	Efficiency (%)				
$m_{Y_{1^+}}$ (GeV)	0.1	1	10	100	125
$N_{jets} \geqslant 2$ and $N_{lep} \geqslant 2$	28.15	28.10	28.33	28.88	28.88
Matching with TM	78.22	78.42	77.78	76.17	75.69
Reconstruction with TM (after matching)	56.85	55.67	50.66	33.60	31.08
Reconstruction without TM (TMVA matching included)	61.22	60.07	55.72	39.43	36.99
Percentage of EXP events that have REC = EXP Match	62.70	62.35	59.82	51.60	50.10
$\|m_{l^+l^-} - m_Z\| > 10$ GeV and $N_{b\text{-jets}} = 2$	36.73	36.64	36.24	34.73	34.72

These are good reconstruction efficiency values compared to the typical values for any SM $t\bar{t}$ system kinematic reconstruction, supporting our trust in the performed analysis for the $t\bar{t}Y_{1^+}$ signal events.

6.4 Results and Discussion

After the successful reconstruction of the $t\bar{t}$ system in the $t\bar{t}Y_{1^+}$ signal events for a set of masses of the vector DM mediator Y_{1^+}, we studied the angular distributions of some signal variables of interest in order to use them and finally compute Confidence Level limits on the exclusion of the SM plus a vector DM mediator Y_{1^+} that couples to the top quarks against the SM for different masses, at the LHC.

6.4.1 Angular distributions

From an older project in our group, [1], a very similar signal was studied. There, the DM mediator was a pure scalar or pseudo-scalar instead of a pure vector particle. In that project, two angular distributions to probe both the CP-nature of the scalar mediator and to discern the signal from the SM background were chosen from the literature: the b_4 and the $\Delta\phi_{l^+l^-}$ distributions. In this work we also used these two distributions. In Figure 6.10 the expected number of events that survived all cuts and were successfully reconstructed without TM for the different SM backgrounds and for our signal with $m_{Y_{1^+}} = 0.1$ GeV is shown for an integrated luminosity of 100 fb^{-1}, for three different observables: b_4, $\Delta\phi_{l^+l^-}$ and missing transverse energy. There, the label "Diboson" refers to the WW+3 jets, WZ+3 jets and ZZ+3 jets backgrounds, "Z+jets" refers to the Z+4 jets and $Zb\bar{b}$+2 jets background , "W+jets" refers to the W+4 jets and $Wb\bar{b}$+2 jets backgrounds, and "$t\bar{t}c\bar{c}, t\bar{t}$+light jets" refers to the $t\bar{t}$+3 jets background. We can see that, by far, the $t\bar{t}$+3 jets is the process which contributes the most for the SM background. The reason for this is that this background process has the most similar topology to the $t\bar{t}Y_{1^+}$ final state.

In Figure 6.10a we observe that the EXP b_4 distribution of the $t\bar{t}Y_{1^+}$ signal events tends to populate more the negative values of this observable while the EXP b_4 distribution of the background events tends to populate more the positive values. In Figure 6.10b we observe that the EXP $\Delta\phi_{l^+l^-}$ distribution of the $t\bar{t}Y_{1^+}$ signal events tends to populate more the extreme values of this observable than the EXP $\Delta\phi_{l^+l^-}$ distribution of the background events. We included the missing transverse energy distributions in this figure once this is a typical distribution used in searches for DM. However, for this case, we see that the shape of the $\not{E}_T$ distributions of the signal and of the background, Figure 6.10c, have very similar shapes,

meaning that it would not be a good observable for the aforementioned purpose. For easy reading, we have scaled the signal for illustration purposes.

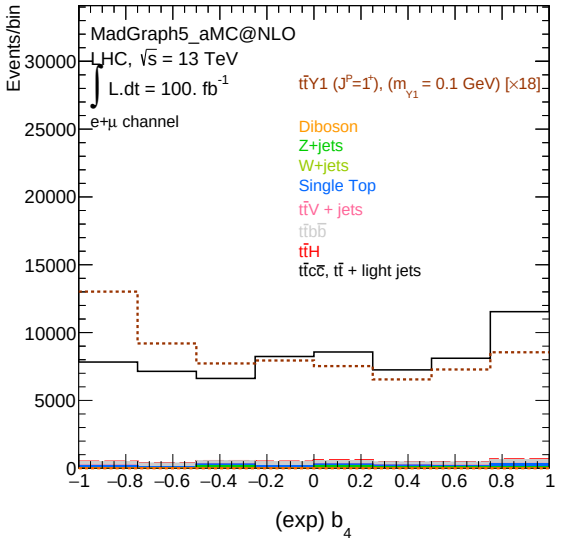

(a)

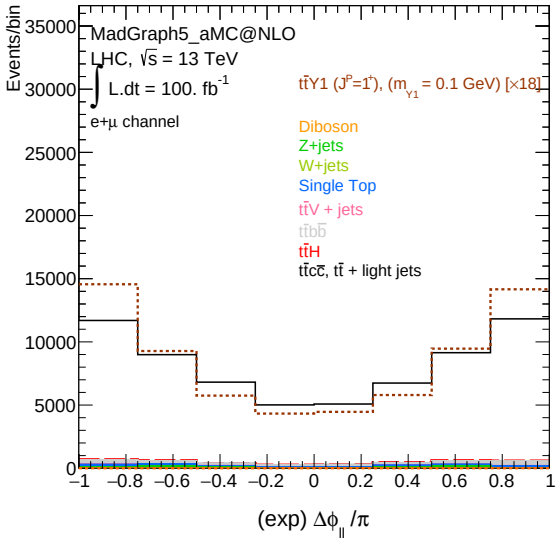

(b)

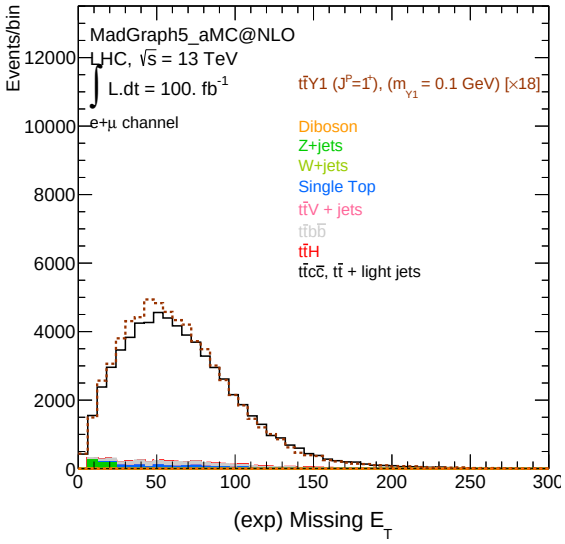

(c)

Figure 6.10: Expected number of background and $t\bar{t}Y_{1+}$ signal events successfully reconstructed without TM considering the final selection cuts for an integrated luminosity of 100 fb^{-1}, for different distributions: b_4 (6.10a), $\Delta\phi_{l^+l^-}$ (6.10b) and missing transverse energy (6.10c). The signal events have $m_{Y_{1+}} = 0.1$ GeV and its distribution was scaled by $\times 18$ for a better comparison with the background distributions.

The number of $t\bar{t}Y_{1+}$ signal and SM background events, normalized to an integrated luminosity of 100 fb^{-1} are shown in Table 6.4. In this table, the calculated cross-section from the aforementioned number of events normalized to $L = 100$ fb^{-1}, σ_{EXP}, are displayed, as well as the ratio between that cross-section and the cross-section in 6.2, $\frac{\sigma_{\text{EXP}}}{\sigma_{\text{GEN}}}$, for each one of the $t\bar{t}Y_{1+}$ signal and SM background considered processes. σ_{EXP} would be the expected cross-section for each one of the considered processes at the LHC after applying the analysis described in 6.3.The ratio $\frac{\sigma_{\text{EXP}}}{\sigma_{\text{GEN}}}$ is roughly the expected fraction of events that pass through the analysis for each one of the considered produced processes at

the LHC. From the $\frac{\sigma_{\text{EXP}}}{\sigma_{\text{GEN}}}$ column, we observe that the performed reconstruction without the SM and the selection cuts indeed increased the signal to background ratio. More specifically, we observe how the $|m_{l^+l^-} - m_Z| > 10$ GeV final cut reduced the Z + up to 4 jets and $Zb\bar{b}$ + up to 2 jets background processes.

Table 6.4: $t\bar{t}Y_{1^+}$ signal (dileptonic channel) and SM background processes considered in 6.2 and the respective number of events that were successfully reconstructed without TM and that survived the final selection cuts normalized for an integrated luminosity value of 100 fb^{-1} (N_{EXP}), the respective cross-section from the latter number of events (σ_{EXP}), and the respective ratio between that cross-section value and the cross-section value presented in 6.2 $\left(\frac{\sigma_{\text{EXP}}}{\sigma_{\text{GEN}}}\right)$ in percentage.

	Process	N_{EXP}	σ_{EXP} (pb)	$\frac{\sigma_{\text{EXP}}}{\sigma_{\text{GEN}}}$ (%)
$t\bar{t}Y_{1^+}$ signal (dileptonic channel)	$t\bar{t}Y_{1^+}$ ($m_{Y_{1^+}} = 0.1$ GeV)	3766.19	0.0376619	6.180
	$t\bar{t}Y_{1^+}$ ($m_{Y_{1^+}} = 1$ GeV)	2345.67	0.0234567	6.113
	$t\bar{t}Y_{1^+}$ ($m_{Y_{1^+}} = 10$ GeV)	960.95	0.0096095	5.649
	$t\bar{t}Y_{1^+}$ ($m_{Y_{1^+}} = 100$ GeV)	95.29	0.0009529	3.970
	$t\bar{t}Y_{1^+}$ ($m_{Y_{1^+}} = 125$ GeV)	63.87	0.0006387	3.7028
Background	$t\bar{t}H$	68.93	0.0006893	2.997
	$t\bar{t}b\bar{b}$	2002.36	0.020026	2.535
	$t\bar{t}$ + up to 3 jets	61445.30	0.6144530	1.622
	$t\bar{t}V$ + up to 1 jet	96.56	0.0009656	1.557
	Single top (s-channel)	0	0	0
	Single top (t-channel)	0	0	0
	Single top (Wt-channel)	1114.41	0.0111441	0.07341
	W + up to 4 jets	0	0	0
	Z + up to 4 jets	0	0	0
	$Wb\bar{b}$ + up to 2 jets	0	0	0
	$Zb\bar{b}$ + up to 2 jets	560.88	0.0056088	0.004560
	WW + up to 3 jets	0	0	0
	WZ + up to 3 jets	0	0	0
	ZZ + up to 3 jets	10.19	0.0001019	0.0009264

6.4.2 Exclusion Confidence Level Limits

Confidence Level (CL) limits associated with the $t\bar{t}Y_{1^+}$ signal were then calculated for three different scenarios, following the prescription described in [101] and [102], after successful reconstruction of signal and background events, and picking sensitive observables at the LHC that could discriminate the signal from the background.

We shortly explain bellow how these CL's were calculated for each considered scenario.

When dealing with search results, one can make a hypothesis test in order to assess how much does the considered data sample support or exclude a particular hypothesis from the set of hypotheses that one may take into account. The hypothesis test has usually two hypothesis: the null hypothesis (H_0) and the alternative or signal hypothesis (H_1). Commonly, in High Energy Particle Physics, H_0 is the

background and H_1 is the background+signal, when one wants to compare new physics distributions with the expected ones from the SM background. In our work, we will use the calculated CL values as degrees of confidence for the exclusion of H_1 under the assumption that H_0 is true, for three different scenarios (each scenario has a distinct pair of considered hypotheses (H_0,H_1)). We consider the b_4 and the $\Delta\phi_{l^+l^-}$ distributions for the calculation of the CL's. We define a test-statistic for the CL's computation. The test-statistic is a quantity calculated from the data samples from both hypotheses that indicates which hypothesis is more compatible with the expected observations. The chosen test-statistic for our work was the likelihood-ratio test, Q, which is the ratio of the probability densities of H_1 and H_0 ($L(H_1)$ and $L(H_0)$, respectively[11]). Since the expected number of signal and background events is small enough in our work, the probability density of each hypothesis can be described by Poisson distributions. Moreover, we are dealing with N_{chan} independent search channels. We use distributions similar to the ones in Figures 6.10a and 6.10b, which have 8 bins (thus $N_{\text{chan}} = 8$ in the calculation of the CL's in our work) in the b_4 and $\Delta\phi_{l^+l^-}$ distributions. Q is then defined by:

$$Q = \frac{L(H_1)}{L(H_0)} = \prod_{i=1}^{N_{\text{chan}}} \frac{L_i(H_1)}{L_i(H_0)} = \prod_{i=1}^{N_{\text{chan}}} \frac{\left(\frac{e^{-\lambda_{1i}}\lambda_{1i}^{n_i}}{n_i!}\right)}{\left(\frac{e^{-\lambda_{0i}}\lambda_{0i}^{n_i}}{n_i!}\right)} = e^{-(\lambda_{1tot}-\lambda_{0tot})} \prod_{i=1}^{N_{\text{chan}}} \left(\frac{\lambda_{1i}}{\lambda_{0i}}\right)^{n_i}, \tag{6.4}$$

where n_i is the number of expected events in each channel assuming a certain hypothesis (so Q assuming H_1 is different from Q assuming H_0), and $\lambda_{a\,i}$ and $\lambda_{a\,tot} = \sum_{i=1}^{N_{\text{chan}}} \lambda_{a\,i}$ are the number of predicted events per channel and the total number of events, respectively, for the $H_{a\in\{0,1\}}$ hypothesis. The expected number of events in each channel are the ones that would be seen in an actual experiment. In our work, we "simulated" them by randomly generating 1000000 pseudo-experiments (we call each random number value generation a pseudo-experiment) for both H_0 and H_1 hypotheses. In each pseudo-experiment, the number of expected events for each channel, n_i, is randomly generated according to a Poisson distribution for that channel, where the mean value of the Poisson distribution is the predicted number of events of that channel, $\lambda_{a\,i}$, according to the considered hypothesis, H_a.

The CL for the exclusion of the alternative hypothesis is defined as a function of the test-statistic:

$$1 - CL = P(Q \geqslant Q_{\text{exp}}|H) = \int_{Q_{\text{exp}}}^{\infty} \frac{dP(Q|H)}{dQ}\, dQ, \tag{6.5}$$

where Q_{exp} is the value expected for the test-statistic assuming a given hypothesis (H). $\ln Q$ is computed and used to construct both $\frac{dP(Q|H_1)}{dQ}$ and $\frac{dP(Q|H_0)}{dQ}$, which are built from the simulated pseudo-experiments assuming the H_1 and the H_0 hypothesis, respectively. $\ln Q_{\text{exp}}$ is set to the median of $\frac{dP(Q|H_0)}{dQ}$.

If $1 - CL \leqslant \alpha$, with α defined as the significance level of the test, we can claim that, assuming a given null hypothesis, the alternative hypothesis is excluded with a Confidence Level of $CL \times 100\%$.

6.4.2.1 Scenario 1

The first and the main scenario of our work is:

- **Scenario 1:** Exclusion of the SM plus a new pure vector DM mediator (Y_{1^+}), assuming the SM. H_0 is the SM-only hypothesis, consisting of background events, and H_1 is the SM plus a new pure

[11] Do not confuse the probability densities of the hypotheses H_1 and H_0 described in this section with the likelihood in 6.3 which was used to determine the best kinematic fit.

vector DM mediator signal hypothesis, consisting of the $t\bar{t}Y_{1+}$ signal plus background events. In this scenario, λ_{1i} is equal to the sum of λ_{0i} and the number of $t\bar{t}Y_{1+}$ signal events of that channel.

In Scenario 1, the exclusion CL limits were computed on $\kappa = \frac{g^V_{u33}}{g_{SM}}$, a multiplicative factor of the coupling constant between the top quarks and the Y_{1+} mediator $g_{SM} = 0.25$ fixed on the generation of the $t\bar{t}Y_{1+}$ signal. From now on, $g^V_{u33} = \kappa g_{SM}$ is the coupling constant between the top quarks and Y_{1+} of the $t\bar{t}Y_{1+}$ signal. This procedure was done for each one of the generated masses of Y_{1+}, and for the two observables used in the analysis, the b_4 and $\Delta\phi_{l^+l^-}$.

The expected exclusion limits on $\frac{g^V_{u33}}{g_{SM}}$ for Scenario 1 at $m_{Y_{1+}} = 0.1$ GeV for the b_4 and $\Delta\phi_{l^+l^-}$ distributions are shown in Figures 6.11 and 6.12, for an integrated luminosity of 200 fb^{-1} and 3000 fb^{-1}, respectively. The CL limits are illustrated as contour plots in the 2D $\left(\frac{g^V_{u33}}{g_{SM}}, \frac{g^A_{u33}}{g_{SM}}\right)$ plane[12]. The 200 fb^{-1} integrated luminosity value corresponds roughly to the RUN 2 integrated luminosity plus the contribution from the first year of RUN 3, while the 3000 fb^{-1} value is the maximum expected integrated luminosity value at the end of the High-Luminosity LHC phase [103].

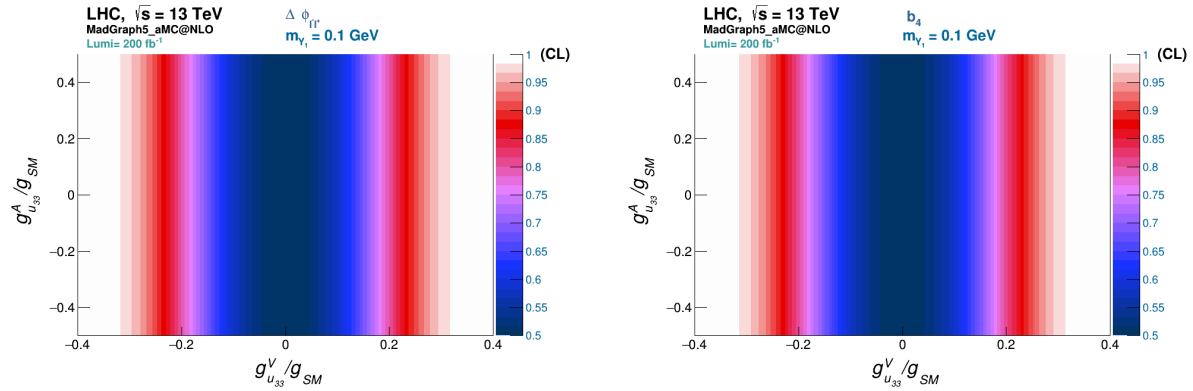

Figure 6.11: Contour plots of the expected exclusion CL limits on the multiplicative factor of the coupling constant between the top quarks and the Y_{1+} mediator for the exclusion of the SM plus a vector DM mediator, Y_{1+}, with $m_{Y_{1+}} = 0.1$ GeV and vector couplings with the top quarks, against the SM as null hypothesis, from the $\Delta\phi_{l^+l^-}$ (left) and b_4 (right) distributions. The exclusion CL limits are shown for an integrated luminosity of $L = 200$ fb^{-1}.

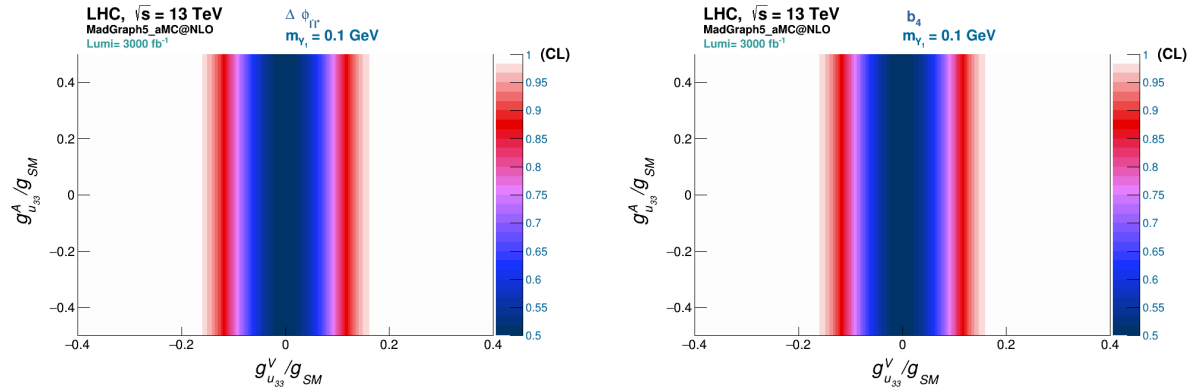

Figure 6.12: Contour plots of the expected exclusion CL limits on the multiplicative factor of the coupling constant between the top quarks and the Y_{1+} mediator for the exclusion of the SM plus a vector DM mediator, Y_{1+}, with $m_{Y_{1+}} = 0.1$ GeV and vector couplings with the top quarks, against the SM as null hypothesis, from the $\Delta\phi_{l^+l^-}$ (left) and b_4 (right) distributions. The exclusion CL limits are shown for an integrated luminosity of $L = 3000$ fb^{-1}.

[12]Note that since g^A_{u33} and $\frac{g^A_{u33}}{g_{SM}}$ are null in our work, these contour plots are vertical, and no information is obtained from the $\frac{g^A_{u33}}{g_{SM}}$ axis. We chose to display the CL limits in a 2D plane for better visualization of the data.

In Figure 6.13 the expected 68% and 95% exclusion CL limits on $\frac{g^V_{u33}}{g_{SM}}$ as a function of $m_{Y_{1+}}$ for the $\Delta\phi_{l^+l^-}$ and b_4 distributions are plotted for the integrated luminosity values 200 fb^{-1} and 3000 fb^{-1}. In Tables 6.5 and 6.6 we explicitly show the values of the calculated 68% and 95% exclusion CL limits on $\frac{g^V_{u33}}{g_{SM}}$ from the $\Delta\phi_{l^+l^-}$ and b_4, respectively.

Table 6.5: Expected exclusion CL limits on $\frac{g^V_{u33}}{g_{SM}}$ for the exclusion of the SM plus Y_{1+} assuming the SM as null hypothesis, at 68% (blue) and 95% (red) Confidence Levels as function of the mass of Y_{1+}, $m_{Y_{1+}}$, for the fixed integrated luminosity values of $L = 200$ fb^{-1} and $L = 3000$ fb^{-1} from the $\Delta\phi_{l^+l^-}$ distributions.

		Exclusion CL limits from $\Delta\phi_{l^+l^-}$ on $\frac{g^V_{u33}}{g_{SM}}$			
		$L = 200$ fb^{-1}		$L = 3000$ fb^{-1}	
		68% CL	95% CL	68% CL	95% CL
$m_{Y_{1+}}$ (GeV)	0.1	$-0.15, 0.1484$	$-0.2804, 0.2796$	$-0.0756, 0.0756$	$-0.142, 0.142$
	1	$-0.1865, 0.1875$	$-0.3545, 0.3545$	$-0.0965, 0.0955$	$-0.1795, 0.1805$
	10	$-0.2952, 0.292$	$-0.5528, 0.5544$	$-0.1496, 0.1496$	$-0.2808, 0.2808$
	100	$-0.93125, 0.93125$	$-1.75625, 1.75625$	$-0.4775, 0.4725$	$-0.8875, 0.8925$
	125	$-1.137, 1.125$	$-2.139, 2.127$	$-0.579, 0.579$	$-1.077, 1.083$

Table 6.6: Expected exclusion CL limits on $\frac{g^V_{u33}}{g_{SM}}$ for the exclusion of the SM plus Y_{1+} assuming the SM as null hypothesis, at 68% (blue) and 95% (red) Confidence Levels as function of the mass of Y_{1+}, $m_{Y_{1+}}$, for the fixed integrated luminosity values of $L = 200$ fb^{-1} and $L = 3000$ fb^{-1} from the b_4 distributions.

		Exclusion CL limits from b_4 on $\frac{g^V_{u33}}{g_{SM}}$			
		$L = 200$ fb^{-1}		$L = 3000$ fb^{-1}	
		68% CL	95% CL	68% CL	95% CL
$m_{Y_{1+}}$ (GeV)	0.1	$-0.1452, 0.146$	$-0.2772, 0.2764$	$-0.0756, 0.0748$	$-0.1404, 0.1396$
	1	$-0.1855, 0.1845$	$-0.3495, 0.3485$	$-0.0955, 0.0945$	$-0.1765, 0.1775$
	10	$-0.2888, 0.2904$	$-0.5448, 0.5432$	$-0.148, 0.148$	$-0.2776, 0.2776$
	100	$-0.91875, 0.91875$	$-1.71875, 1.71875$	$-0.4725, 0.4675$	$-0.8775, 0.8775$
	125	$-1.119, 1.137$	$-2.115, 2.115$	$-0.579, 0.573$	$-1.071, 1.071$

Similar plots to these ones but with the calculated 68% and 95% exclusion CL limits on the cross-section of the dileptonic channel[13] of the $t\bar{t}Y_{1+}$ signal process are shown in Figure 6.14. Given that in our event generation the force mediated by Y_{1+} is only computed at LO, the cross-section of the $t\bar{t}Y_{1+}$ signal process is proportional to the square of the coupling constant of the top-quarks with the mediator, $\sigma \propto (g^V_{u33})^2$. In our event generation we fixed $g^V_{u33} = g_{SM} = 0.25$, and so, we also got a fixed generated cross-section for the dileptonic channel of the $t\bar{t}Y_{1+}$ signal process for each considered $m_{Y_{1+}}$ value. In the computation of the CL limits on the cross-section, we assess different values of the cross-section of the signal process for g^V_{u33} values other than 0.25 by simply multiplying the generated cross-section by $\left(\frac{g^V_{u33}}{g_{SM}}\right)^2$.

[13]From now on, we will simply omit "dileptonic channel" and so, when we refer to the cross-section of a signal process, we are only taking into account the dileptonic channel of the signal process.

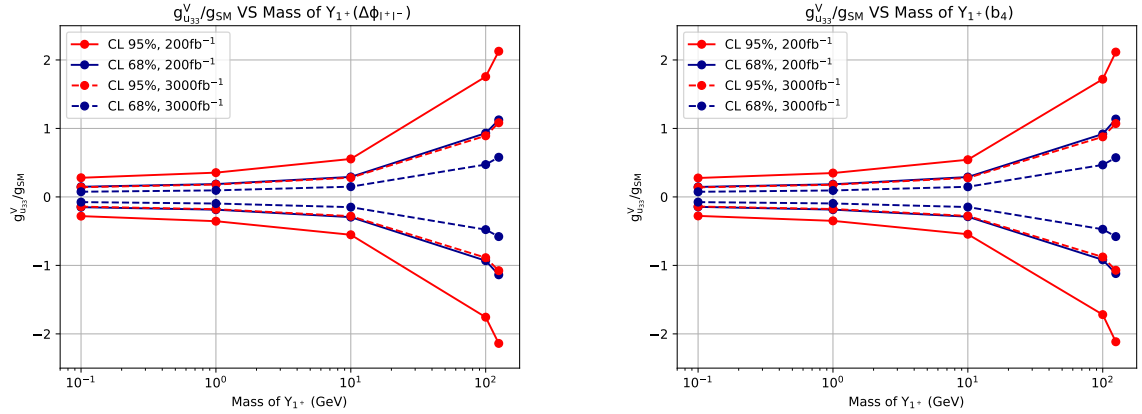

Figure 6.13: Expected exclusion CL limits on $\frac{g^V_{u33}}{g_{SM}}$ for the exclusion of the SM plus Y_{1+} assuming the SM as null hypothesis, at 68% (blue) and 95% (red) Confidence Levels as function of the mass of Y_{1+}, $m_{Y_{1+}}$, for the fixed integrated luminosity values of $L = 200$ fb^{-1} (solid line) and $L = 3000$ fb^{-1} (dashed line), from the $\Delta\phi_{l^+l^-}$ (left) and b_4 (right) distributions. The assessed $m_{Y_{1+}}$ values are $m_{Y_{1+}} = 0.1, 1, 10, 100$ and 125 GeV.

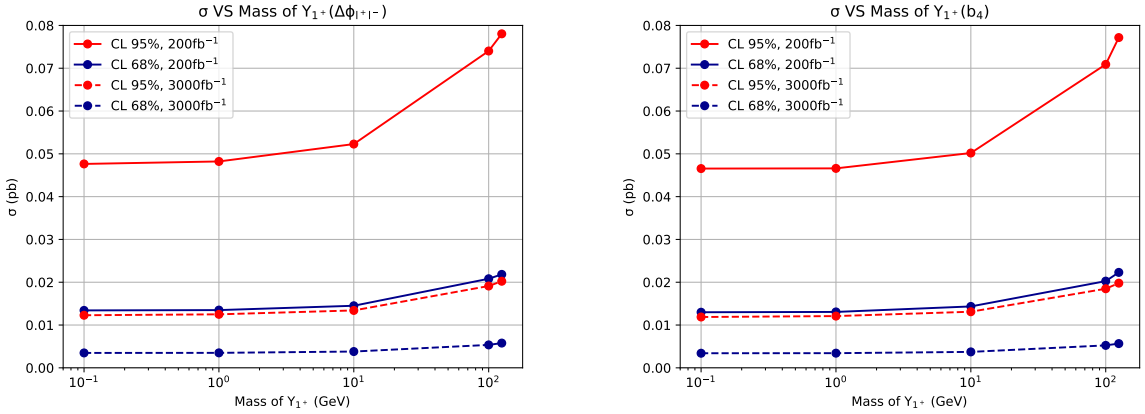

Figure 6.14: Expected exclusion CL limits on the cross-section of the $t\bar{t}Y_{1+}$ signal process for the exclusion of the SM plus Y_{1+} assuming the SM as null hypothesis, at the 68% (blue) and 95% (red) Confidence Levels as function of the mass of Y_{1+}, $m_{Y_{1+}}$, for the fixed integrated luminosity values of $L = 200$ fb^{-1} (solid line) and $L = 3000$ fb^{-1} (dashed line), from the $\Delta\phi_{l^+l^-}$ (left) and b_4 (right) distributions. The assessed $m_{Y_{1+}}$ values are $m_{Y_{1+}} = 0.1, 1, 10, 100$ and 125 GeV.

In order to have a better understanding on how the exclusion 68% and 95% CL limits depend on the integrated luminosity value, we chose two masses of Y_{1+} ($m_{Y_{1+}} = 1$ and 10 GeV) and plotted the expected exclusion 68% and 95% CL limits on $\frac{g^V_{u33}}{g_{SM}}$ (see Figure 6.15) and on the cross-section of the $t\bar{t}Y_{1+}$ signal process (see Figure 6.16) as a function of the integrated luminosity, from the $\Delta\phi_{l^+l^-}$ and b_4 distributions.

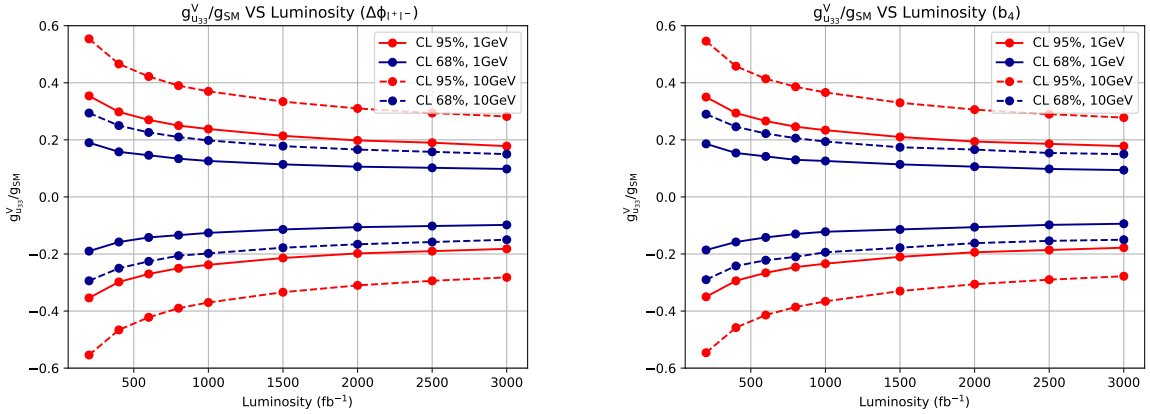

Figure 6.15: Expected exclusion CL limits on $\frac{g^V_{u33}}{g_{SM}}$ for the exclusion of the SM plus Y_{1+} assuming the SM as null hypothesis, at the 68% (blue) and 95% (red) Confidence Levels as function of the integrated luminosity for the fixed $m_{Y_{1+}}$ values of 1 (solid line) and 10 GeV (dashed line), from the $\Delta\phi_{l^+l^-}$ (left) and b_4 (right) distributions. The assessed integrated luminosity values are $L = 200$, 400, 600, 800, 1000, 1500, 2000, 2500 and 3000 fb^{-1}.

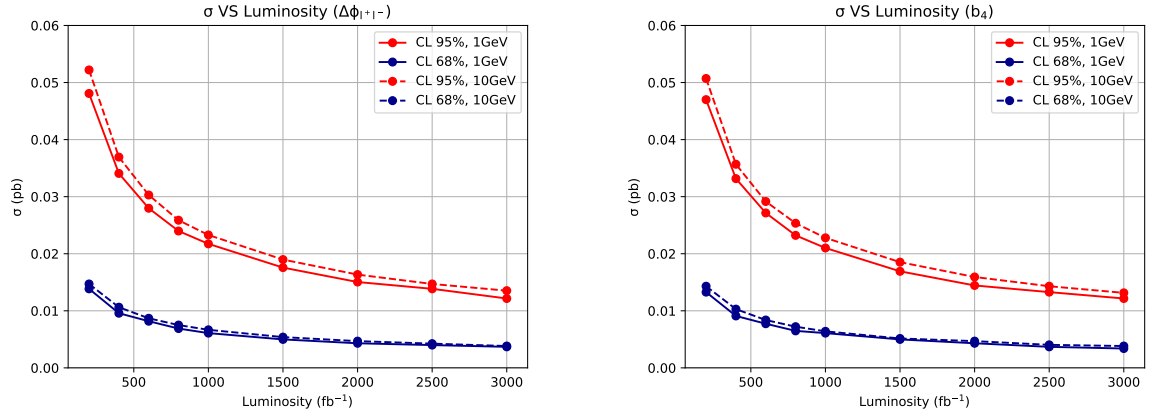

Figure 6.16: Expected Exclusion CL limits on the cross-section of the $t\bar{t}Y_{1+}$ signal process for the exclusion of the SM plus Y_{1+} assuming the SM as null hypothesis, at the 68% (blue) and 95% (red) Confidence Levels as function of the integrated luminosity for the fixed $m_{Y_{1+}}$ values of 1 and 10 GeV, from the $\Delta\phi_{l^+l^-}$ (left) and b_4 (right) distributions. The assessed integrated luminosity values are $L = 200$, 400, 600, 800, 1000, 1500, 2000, 2500 and 3000 fb^{-1}.

In Figures 6.13 and 6.15, the hypothesis SM plus Y_{1+} is expected to be excluded with a Confidence Level $> 95\%$ when its $\left|\frac{g^V_{u33}}{g_{SM}}\right|$ value is larger than the one set by the red line for the considered $m_{Y_{1+}}$ and integrated luminosity values, and angular distribution used to set the exclusion limits on each one of these Figures, when assuming the SM as the null hypothesis.

Similarly, in Figures 6.14 and 6.16, the hypothesis SM plus Y_{1+} is expected to be excluded with a Confidence Level $> 95\%$ when the cross-section of the $t\bar{t}Y_{1+}$ signal is larger than the one set by the red line for the considered $m_{Y_{1+}}$ and integrated luminosity values, and angular distribution used to set the exclusion limits on each one of these Figures, when assuming the SM as the null hypothesis.

From Figures 6.11, 6.12, 6.13, 6.14, 6.15 and 6.16, and Tables 6.5 and 6.6, we observe that a larger integrated luminosity imposes stricter exclusion limits as one would expect since a larger integrated luminosity means that we have a larger number of background and signal events and so it is easier to distinguish the signal distribution from the background distribution by taking the statistical deviations from the predicted number of background and signal events into account. On the other hand, since a

larger $m_{Y_{1^+}}$ value decreases the cross-section of the $t\bar{t}Y_{1^+}$ signal process, as we saw in 6.2, we get less signal events when comparing to the number of background events for larger masses of Y_{1^+}, making it harder to discern the $t\bar{t}Y_{1^+}$ signal plus SM background from the SM background alone, thus the exclusion CL limits get looser. It is worthy to note again that the analysis performed in this work is optimized for $m_{Y_{1^+}} = 0.1$ GeV, and so the larger the mass of Y_{1^+} the further we are from an optimal reconstruction and correct exclusion CL limits on the $t\bar{t}Y_{1^+}$ signal with a mass of Y_{1^+} different from 0.1 GeV. Moreover, we observed that the exclusion CL limits from the b_4 distribution are slightly stricter than the ones from the $\Delta\phi_{l^+l^-}$ distribution, which means that the b_4 is slightly better at discerning the $t\bar{t}Y_{1^+}$ signal plus SM background from the SM background.

6.4.2.2 Scenarios 2 and 3

In our project group, a very similar work, [1], to the one presented in this dissertation was done but for $t\bar{t}Y$ signal events where the DM mediator Y is a pure scalar, Y_{0^+}, a pure pseudo-scalar, Y_{0^-}, or a mix of both states with couplings to the top quarks. With this in mind, one may calculate what are the exclusion CL limits on the spin of the mediator Y being 0 if one accepts the SM plus a pure vector DM mediator as being the null hypothesis. In other words: if the Y_{1^+} mediator is actually discovered and the SM is extended to include this particle, can we be sure that the mediator Y does not actually have spin 0? Making use of the generated events for the $t\bar{t}Y_{0^+}$ and $t\bar{t}Y_{0^-}$ signal processes from [1], and reconstructing those events with our analysis, we considered two more scenarios in which the null hypothesis is the SM plus a Y_{1^+} mediator with couplings to the top quarks:

- **Scenario 2:** Exclusion of the SM plus a new pure scalar DM mediator (Y_{0^+}), assuming the SM plus a vector DM mediator (Y_{1^+}). H_0 is the SM plus a vector DM mediator hypothesis, consisting of the $t\bar{t}Y_{1^+}$ signal plus background events, and H_1 is the SM plus a new pure scalar DM mediator hypothesis, consisting of the $t\bar{t}Y_{0^+}$ signal plus background events;

- **Scenario 3:** Exclusion of the SM plus a new pure pseudo-scalar DM mediator (Y_{0^-}), assuming the SM plus a vector DM mediator (Y_{1^+}). H_0 is the SM plus a vector DM mediator hypothesis, consisting of the $t\bar{t}Y_{1^+}$ signal plus background events, and H_1 is the SM plus a new pure scalar DM mediator hypothesis, consisting of the $t\bar{t}Y_{0^-}$ signal plus background events.

In these two scenarios the coupling constant of the Y_{1^+} with the top-quarks was fixed to 0.25. The lowest mass value of the DM mediator in both the present work and in the work in [1] is $m_Y = 1$ GeV, and so we only used that value for the masses of Y_{1^+}, Y_{0^+} and Y_{0^-} on the evaluation of the exclusion CL limits in Scenarios 2 and 3. The cross-section, the order in QCD at which the event generation was computed and the number of generated events for the $t\bar{t}Y_{0^+}$ and $t\bar{t}Y_{0^-}$ signals for a mass of the DM mediator Y equal to 1 GeV [1], are presented in Table 6.7. The scalar and pseudo-scalar couplings of the Y_0 mediator with the top quarks were set to $g_{SM} = 1$ for the event generation of the $t\bar{t}Y_{0^+}$ and $t\bar{t}Y_{0^-}$ signals, respectively [1].

Table 6.7: $t\bar{t}Y_{0^+}$ and $t\bar{t}Y_{0^-}$ signal processes generated with MADGRAPH5_AMC@NLO, and the order in QCD at which they were generated, their number of generated events and cross-section values.

Process	Order	Number of events	Cross-section (pb)
$t\bar{t}Y_{0^+}$ (1 GeV)	LO	500.000	2.914
$t\bar{t}Y_{0^-}$ (1 GeV)	LO	500.000	0.023

We performed the same analysis described in 6.3, which is an analysis optimized for the $t\bar{t}Y_{1+}$ with $m_{Y_{1+}} = 0.1$ GeV. In Table 6.8 we present the efficiencies in percentage of the selection cuts and of the reconstruction methods performed in the analysis of the $t\bar{t}Y_{0+}$ and $t\bar{t}Y_{0-}$ signal events for $m_{Y_0} = 1$ GeV. Note that the efficiencies values here presented must be interpreted as described in 6.3.3 for Table 6.3.

Table 6.8: Efficiencies (in %), rounded to two decimal places, of the selection cuts and of the reconstruction methods performed in the analysis of the $t\bar{t}Y_{0+}$ and $t\bar{t}Y_{0-}$ signal events for a mass of Y_0 value equal to 1 GeV. The analysis performed on these spin 0 DM mediator signal events is the same one described in 6.3. "$N_{\text{jets}} \geqslant 2$ and $N_{\text{lep}} \geqslant 2$" already includes selected jets and leptons with $|\eta| < 2.5$ and $p_T > 20$ GeV.

	Efficiency (%)	
m_{Y_0} (GeV)	Y_{0+} signal; $m_{Y_{0+}} = 1$ GeV	Y_{0-} signal; $m_{Y_{0-}} = 1$ GeV
$N_{jets} \geqslant 2$ and $N_{lep} \geqslant 2$	27.94	30.07
Matching with TM	75.49	70.33
Reconstruction with TM (after matching)	55.80	50.09
Reconstruction without TM (TMVA matching included)	57.81	53.96
Percentage of EXP events that have REC = EXP Match	41.23	30.77
$\lvert m_{l^+l^-} - m_Z \rvert > 10$ GeV and $N_{b\text{-jets}} = 2$	31.30	30.10

As we did for Scenario 1, in these two last scenarios we used the b_4 and $\Delta\phi_{l^+l^-}$ distributions. In Figures 6.17 and 6.18 the b_4 and $\Delta\phi_{l^+l^-}$ distributions used in Scenario 2 and Scenario 3 are shown, respectively.

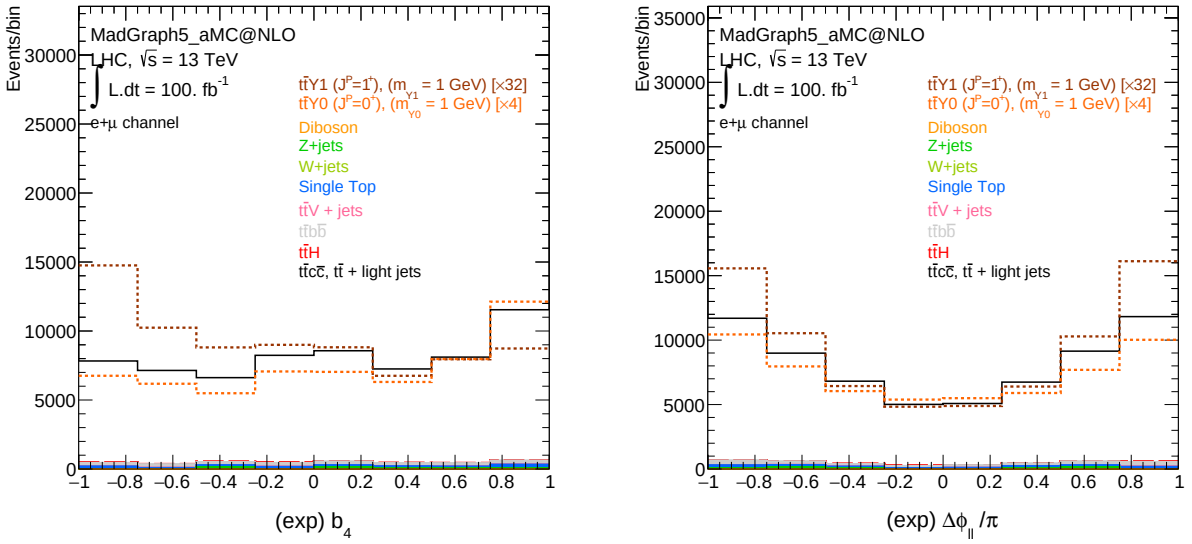

(a) (b)

Figure 6.17: Expected number of background, $t\bar{t}Y_{1+}$ and $t\bar{t}Y_{0+}$ signal events reconstructed without TM for an integrated luminosity of 100 fb^{-1}, for different distributions: b_4 (6.17a) and $\Delta\phi_{l^+l^-}$ (6.17b). The signal events have $m_Y = 1$ GeV and the $t\bar{t}Y_{1+}$ and $t\bar{t}Y_{0+}$ signal distributions were scaled by $\times 32$ and $\times 4$ for a better comparison with the background distributions.

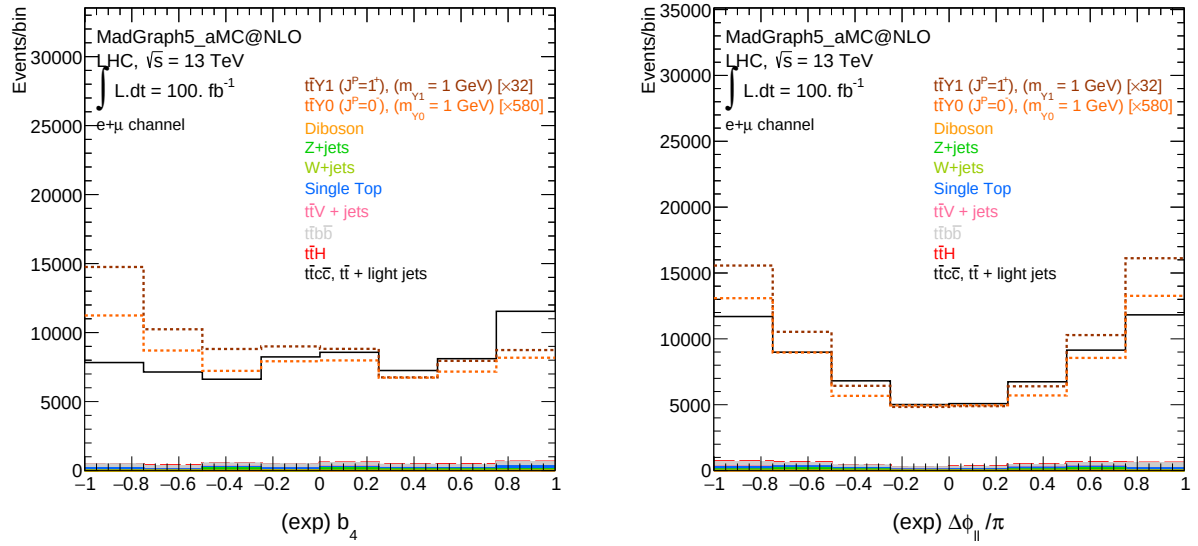

(a) (b)

Figure 6.18: Expected number of background, $t\bar{t}Y_{1+}$ and $t\bar{t}Y_{0-}$ signal events reconstructed without TM for an integrated luminosity of 100 fb^{-1}, for different distributions: b_4 (6.17a) and $\Delta\phi_{l^+l^-}$ (6.17b). The signal events have $m_Y = 1$ GeV and the $t\bar{t}Y_{1+}$ and $t\bar{t}Y_{0-}$ signal distributions were scaled by $\times 32$ and $\times 580$ for a better comparison with the background distributions.

In Table 6.9 we display the same type of data displayed in Table 6.4 but for the $t\bar{t}Y_{0+}$ and $t\bar{t}Y_{0-}$ signal events for $m_{Y_0} = 1$ GeV.

Table 6.9: $t\bar{t}Y_{0+}$ and $t\bar{t}Y_{0-}$ signal (dileptonic channel) processes considered in 6.7 and the respective number of events that were successfully reconstructed without TM and that survived the final selection cuts normalized for an integrated luminosity value of 100 fb^{-1} (N_{EXP}), the respective cross-section from the latter number of events (σ_{EXP}), and the respective ratio between that cross-section value and the cross-section value presented in 6.7 ($\frac{\sigma_{\text{EXP}}}{\sigma_{\text{GEN}}}$) in percentage.

	Process	N_{EXP}	σ_{EXP} (pb)	$\frac{\sigma_{\text{EXP}}}{\sigma_{\text{GEN}}}$ (%)
$t\bar{t}Y_0$ signal (dileptonic channel)	$t\bar{t}Y_{0+}$ ($m_{Y_{0+}} = 1$ GeV)	14733.77	0.1473377	5.056
	$t\bar{t}Y_{0-}$ ($m_{Y_{0-}} = 1$ GeV)	112.33	0.0011233	4.884

In Scenario 2 we remarkably observed that the SM plus Y_{1+} hypothesis excludes the SM plus Y_{0+} hypothesis at approximately 100% CL for any $\frac{g^S_{u33}}{g_{SM}}$ value using the $\Delta\phi_{l^+l^-}$ and b_4 distributions for $L = 200$ and 3000 fb^{-1}. For this scenario, the lowest confidence level at which exclusion CL limits on $\frac{g^S_{u33}}{g_{SM}}$ were evaluated out of both distributions was 99.425% for $\frac{g^S_{u33}}{g_{SM}} = 0.395834$ using the $\Delta\phi_{l^+l^-}$ distribution, for $L = 200$ fb^{-1}.

For Scenario 3, the SM plus Y_{1+} hypothesis does not exclude the SM plus Y_{0-} hypothesis as good as it did in Scenario 2. In Figure 6.19 the exclusion CL limits on $\frac{g^P_{u33}}{g_{SM}}$ for Scenario 3 from the b_4 and $\Delta\phi_{l^+l^-}$ distributions are shown for an integrated luminosity equal to 200 fb^{-1}, for $m_Y = 1$ GeV. The exclusion CL limits are illustrated as contour plots in the 2D plane $\left(\frac{g^V_{u33}}{g_{SM}}, \frac{g^P_{u33}}{g_{SM}}\right)$[14]. Still regarding Scenario 3, we expect that for an integrated luminosity equal to 3000 fb^{-1} the SM plus Y_{1+} hypothesis excludes the SM plus Y_{0-} hypothesis at approximately 100% CL for any $\frac{g^P_{u33}}{g_{SM}}$ value using the $\Delta\phi_{l^+l^-}$ and b_4 distributions.

[14]Note that $\frac{g^V_{u33}}{g_{SM}} = 1$ since g^V_{u33} is fixed to $g_{SM} = 0.25$ in this scenario, thus these contour plots are horizontal, and no information is obtained from the $\frac{g^V_{u33}}{g_{SM}}$ axis. We chose to display the CL limits in a 2D plane for better visualization of the data.

For this scenario, at $L = 3000$ fb^{-1}, the lowest confidence level at which exclusion CL limits on $\frac{g^P_{u33}}{g_{SM}}$ were evaluated out of both distributions was 99.943% at $\frac{g^P_{u33}}{g_{SM}} = 4.54931$ and $\frac{g^P_{u33}}{g_{SM}} = 4.57481$ using the $\Delta\phi_{l^+l^-}$ distribution.

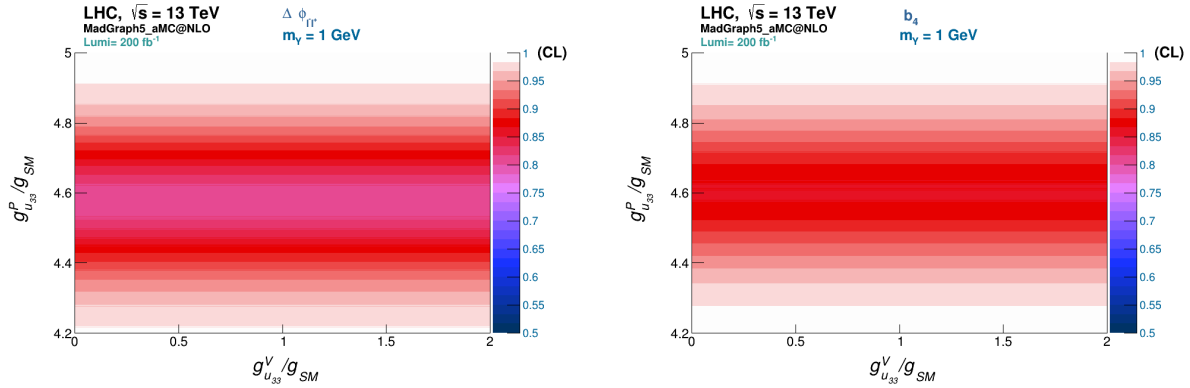

Figure 6.19: Contour plots of the expected CL limits on the multiplicative factor of the coupling constant between the top quarks and the Y_{0^-} mediator for the exclusion of the SM plus a pseudo-scalar DM mediator, Y_{0^-}, with $m_{Y_{0^-}} = 1$ GeV and pseudo-scalar couplings with the top quarks, against the SM plus a vector DM mediator, Y_{1^+}, with $m_{Y_{1^+}} = 1$ GeV and vector couplings with the top quarks as null hypothesis, from the $\Delta\phi_{l^+l^-}$ (left) and b_4 (right) distribution. The exclusion CL limits are shown for an integrated luminosity of $L = 200$ fb^{-1}.

The observation that, for $L = 200$ fb^{-1}, the SM plus a pseudo-scalar DM mediator hypothesis in Scenario 3 is not so easily excluded as the SM plus a scalar DM mediator hypothesis in Scenario 2 against the SM plus a vector DM mediator null hypothesis is due to the shapes of the signal b_4 and $\Delta\phi_{l^+l^-}$ distributions in Figures 6.17 and 6.18. In Figure 6.17 the shape of the $t\bar{t}Y_{1^+}$ signal distributions of those two observables are more different in shape relative to the $t\bar{t}Y_{0^+}$ signal ones than to the $t\bar{t}Y_{0^-}$ signal, thus it is harder to get a $\frac{g^S_{u33}}{g_{SM}}$ value such that the background + $t\bar{t}Y_{0^+}$ signal distributions are similar in shape to the background + $t\bar{t}Y_{1^+}$ signal ones than it is to get a $\frac{g^P_{u33}}{g_{SM}}$ value such that the background + $t\bar{t}Y_{0^-}$ signal distributions are similar to the background + $t\bar{t}Y_{1^+}$ ones.

In Scenario 3 at $L = 200$ fb^{-1}, the minimum confidence level at which exclusion CL limits on $\frac{g^P_{u33}}{g_{SM}}$ were computed was 80.300% at $\frac{g^P_{u33}}{g_{SM}} = 4.578$ and 86.111% at $\frac{g^P_{u33}}{g_{SM}} = 4.618$, using the $\Delta\phi_{l^+l^-}$ and b_4 distributions, respectively. On the other hand, the minimum confidence level achieved for Scenario 3 at $L = 3000$ fb^{-1} and for the Scenario 2 at $L = 200$ and 3000 fb^{-1} was around 100%, so we can state that the SM plus a vector DM mediator null hypothesis excludes at a good level the SM plus a scalar or a pseudo-scalar DM mediator hypotheses, under these integrated luminosity values for these scenarios.

Chapter 7

Conclusions

In this work we made use of the on-going analysis of a $t\bar{t}$ final state at the LHC to probe the existence of DM that couples to a mediator that in turn would couple to the SM. With this goal in mind, we present an approach to fully reconstruct the kinematics of the $t\bar{t}$ system present in $t\bar{t}Y_{1^+}$ events produced at the LHC. The signal is generated using a simplified DM model called DMsimp. In order to simplify this kinematic reconstruction, we assumed the missing transverse energy to be fully accounted by the invisible particles in the SM - the neutrinos - and we did not attempt to reconstruct the DM mediator. This approximation was valid for the lowest mass of the DM mediator considered in our work ($m_{Y_{1^+}} = 0.1$ GeV) according to the correlations observed between the GEN level and EXP level kinematics of the final state particles of the $t\bar{t}Y_{1^+}$ process, shown in Figure 6.5. These correlations are also shown in Figures 6.6, 6.7, 6.8 and 6.9 for $m_{Y_{1^+}} = 1$, 10, 100 and 125 GeV, respectively, and from their observation one can conclude that the quality of the analysis deteriorates with the increase of the mass of the vector DM mediator, which tell us that our approximation loses its validity for higher vector DM mediator masses. Furthermore, in order to have another check for the validation of the analysis performed in this work, we observed that we achieved a relatively high percentage of correct parings of b-jets and charged leptons from the same parent top using multivariate statistical methods from TMVA.

We chose two angular observables, $\Delta\phi_{l^+l^-}$ and b_4, that were sensitive to the presence of a vector DM mediator with different mass scales in a SM background, to illustrate our findings. The signal and background distributions of these observables were then used to set exclusion limits in the scenario that assumes the SM as the null hypothesis and the SM plus a vector DM mediator with couplings to the top quarks as alternative hypothesis, for luminosities between 200 fb^{-1} and 3000 fb^{-1}, corresponding to the expected full luminosity of the High-Luminosity Phase of the LHC (HL-LHC). We concluded that these two angular observables are indeed good observables to set exclusion limits on the existence of a vector DM mediator assuming the SM as the null hypothesis. We observed that these exclusion limits get less strict - and so worse - with the increase of the mass of the mediator as one would expect as the cross-sections of the $t\bar{t}Y_{1^+}$ signal processes get smaller for larger mass values of the vector DM mediator. We also observed that the b_4 distributions gives slightly stricter - and so better - exclusion limits than the $\Delta\phi_{l^+l^-}$ distributions for this scenario. In this scenario, our analysis and the chosen angular observable distributions were capable of setting exclusion limits at 95% CL, for L between 200 and 3000 fb^{-1}, on $g^V_{u_{33}}$ values smaller than the $g_{SM} = 0.25$ value for the coupling constant of the top quarks with Y_{1^+} when $m_{Y_{1^+}} = 0.1$, 1 and 10 GeV.

Motivated by a previous work in our group, we considered two other scenarios where the SM plus a vector DM mediator with couplings to the top quarks is the null hypothesis and the SM plus a scalar or a pseudo-scalar DM mediator with couplings with the top quarks are the alternative hypotheses. The

mass of the mediator in these 3 hypotheses was only studied for the 1 GeV value. Besides the scenario with the SM plus pseudo-scalar DM mediator as the alternative hypothesis for a luminosity of 200 fb^{-1} (where we got around 80% CL and 85% CL as the lowest achieved CL values using the $\Delta\phi_{l^+l^-}$ and b_4 distributions, respectively), the SM plus a vector DM mediator hypothesis 100% excludes the SM plus a scalar DM mediator hypothesis for luminosity values of 200 and 3000 fb^{-1} and the SM plus a pseudo-scalar DM mediator hypothesis for a luminosity value of 3000 fb^{-1}. We then conclude that the $\Delta\phi_{l^+l^-}$ and b_4 observables are also good to discern the spin of the DM mediator (at least to distinguish between spin 0 and spin 1 when the DM mediator has well-defined CP quantum numbers) and that, if a signal very similar to the $t\bar{t}Y_{1^+}$ is discovered in the future at LHC, then, using these angular observables, we can almost exclude the hypothesis of the DM mediator being a pure scalar or a pure pseudo-scalar assuming it is a pure vector signal.

Bibliography

[1] Duarte Azevedo et al. "Search for an invisible scalar in $t\bar{t}$ final states at the LHC". In: *JHEP* 11 (2023), p. 125. DOI: 10.1007/JHEP11(2023)125. arXiv: 2308.00819 [hep-ph].

[2] Sergio González Fernández. "Search for new phenomena in mono-X final states using pp collision data collected in Run-2 by the ATLAS experiment at the LHC". In: *PoS* ICHEP2020 (2021), p. 658. DOI: 10.22323/1.390.0658.

[3] Deepak Kumar. "Search for Dark Matter with mono-X Signatures in CMS". In: *PoS* ICHEP2022 (Nov. 2022), p. 260. DOI: 10.22323/1.414.0260.

[4] Georges Aad et al. "Combination of searches for invisible decays of the Higgs boson using 139 fb^{-1} of proton-proton collision data at $\sqrt{s}$ =13 TeV collected with the ATLAS experiment". In: *Phys. Lett. B* 842 (2023), p. 137963. DOI: 10.1016/j.physletb.2023.137963. arXiv: 2301.10731 [hep-ex].

[5] Ulrich Haisch, Priscilla Pani, and Giacomo Polesello. "Determining the CP nature of spin-0 mediators in associated production of dark matter and $t\bar{t}$ pairs". In: *Journal of High Energy Physics* 2017.2 (Feb. 2017). ISSN: 1029-8479. DOI: 10.1007/jhep02(2017)131. URL: http://dx.doi.org/10.1007/JHEP02(2017)131.

[6] Ulrich Haisch and Giacomo Polesello. "Searching for dark matter in final states with two jets and missing transverse energy". In: *Journal of High Energy Physics* 2019.2 (Feb. 2019). ISSN: 1029-8479. DOI: 10.1007/jhep02(2019)128. URL: http://dx.doi.org/10.1007/JHEP02(2019)128.

[7] J. Hermann and M. Worek. "The impact of top-quark modelling on the exclusion limits in $t\bar{t}$+DM searches at the LHC". In: *The European Physical Journal C* 81.11 (Nov. 2021). ISSN: 1434-6052. DOI: 10.1140/epjc/s10052-021-09831-0. URL: http://dx.doi.org/10.1140/epjc/s10052-021-09831-0.

[8] Ulrich Haisch, Giacomo Polesello, and Stefan Schulte. "Searching for pseudo Nambu-Goldstone boson dark matter production in association with top quarks". In: *Journal of High Energy Physics* 2021.9 (Sept. 2021). ISSN: 1029-8479. DOI: 10.1007/jhep09(2021)206. URL: http://dx.doi.org/10.1007/JHEP09(2021)206.

[9] R. L. Workman and Others. "Review of Particle Physics". In: *PTEP* 2022 (2022), p. 083C01. DOI: 10.1093/ptep/ptac097.

[10] Herbi K. Dreiner, Howard E. Haber, and Stephen P. Martin. *From Spinors to Supersymmetry*. Cambridge, UK: Cambridge University Press, July 2023. ISBN: 978-1-139-04974-0. DOI: 10.1017/9781139049740.

[11] C. S. Wu et al. "Experimental Test of Parity Conservation in β Decay". In: *Phys. Rev.* 105 (1957), pp. 1413–1414. DOI: 10.1103/PhysRev.105.1413.

[12] Marco Drewes. "The Phenomenology of Right Handed Neutrinos". In: *Int. J. Mod. Phys. E* 22 (2013), p. 1330019. DOI: 10.1142/S0218301313300191. arXiv: 1303.6912 [hep-ph].

[13] Peter W. Higgs. "Spontaneous Symmetry Breakdown without Massless Bosons". In: *Phys. Rev.* 145 (4 1966), pp. 1156–1163. DOI: 10.1103/PhysRev.145.1156. URL: https://link.aps.org/doi/10.1103/PhysRev.145.1156.

[14] John F. Gunion et al. *The Higgs Hunter's Guide*. Vol. 80. 2000. ISBN: 978-0-429-49644-8. DOI: 10.1201/9780429496448.

[15] Hanno Bertle. Goldstone Boson and Higgs Mechanism. https://fenix.tecnico.ulisboa.pt/downloadFile/1689468335641966/21_Bertle.pdf. 2018.

[16] J. Goldstone. "Field Theories with Superconductor Solutions". In: *Nuovo Cim.* 19 (1961), pp. 154–164. DOI: 10.1007/BF02812722.

[17] Jeffrey Goldstone, Abdus Salam, and Steven Weinberg. "Broken Symmetries". In: *Phys. Rev.* 127 (1962), pp. 965–970. DOI: 10.1103/PhysRev.127.965.

[18] S. F. Novaes. Standard Model: An Introduction. 2000. arXiv: hep-ph/0001283 [hep-ph]. URL: https://arxiv.org/abs/hep-ph/0001283.

[19] J. H. Christenson et al. "Evidence for the 2π Decay of the K_2^0 Meson". In: *Phys. Rev. Lett.* 13 (4 1964), pp. 138–140. DOI: 10.1103/PhysRevLett.13.138. URL: https://link.aps.org/doi/10.1103/PhysRevLett.13.138.

[20] Makoto Kobayashi and Toshihide Maskawa. "CP-Violation in the Renormalizable Theory of Weak Interaction". In: *Progress of Theoretical Physics* 49.2 (Feb. 1973), pp. 652–657. ISSN: 0033-068X. DOI: 10.1143/PTP.49.652. eprint: https://academic.oup.com/ptp/article-pdf/49/2/652/5257692/49-2-652.pdf. URL: https://doi.org/10.1143/PTP.49.652.

[21] Gustavo C. Branco, Luis Lavoura, and Joao P. Silva. *CP Violation*. Vol. 103. 1999.

[22] Marco Cirelli, Alessandro Strumia, and Jure Zupan. Dark Matter. 2024. arXiv: 2406.01705 [hep-ph]. URL: https://arxiv.org/abs/2406.01705.

[23] F. Zwicky. "Die Rotverschiebung von extragalaktischen Nebeln". In: *Helv. Phys. Acta* 6 (1933), pp. 110–127. DOI: 10.1007/s10714-008-0707-4.

[24] Sinclair Smith. "The Mass of the Virgo Cluster". In: *Astrophys. J.* 83 (Jan. 1936), p. 23. DOI: 10.1086/143697.

[25] Gianfranco Bertone and Dan Hooper. "History of dark matter". In: *Reviews of Modern Physics* 90.4 (Oct. 2018). ISSN: 1539-0756. DOI: 10.1103/revmodphys.90.045002. URL: http://dx.doi.org/10.1103/RevModPhys.90.045002.

[26] K. C. Freeman. "On the Disks of Spiral and S0 Galaxies". In: *Astrophys. J.* 160 (June 1970), p. 811. DOI: 10.1086/150474.

[27] Douglas Clowe et al. "A Direct Empirical Proof of the Existence of Dark Matter". In: *The Astrophysical Journal* 648.2 (Aug. 2006), L109–L113. ISSN: 1538-4357. DOI: 10.1086/508162. URL: http://dx.doi.org/10.1086/508162.

[28] Tommaso L. Treu, Philip J. Marshall, and Douglas Clowe. "Gravitational Lensing". In: *Physics to a Degree* (2018). URL: https://api.semanticscholar.org/CorpusID:264969518.

[29] A LEWIS and A CHALLINOR. "Weak gravitational lensing of the CMB". In: *Physics Reports* 429.1 (June 2006), 1–65. ISSN: 0370-1573. DOI: 10.1016/j.physrep.2006.03.002. URL: http://dx.doi.org/10.1016/j.physrep.2006.03.002.

[30] M. Ryleigh Davis et al. "A survey of galaxy redshifts. II. The large scale space distribution." In: *The Astrophysical Journal* 253 (1982), pp. 423–445. URL: https://api.semanticscholar.org/CorpusID:123051823.

[31] R. D. Peccei and Helen R. Quinn. "Constraints imposed by CP conservation in the presence of pseudoparticles". In: *Phys. Rev. D* 16 (6 1977), pp. 1791–1797. DOI: 10.1103/PhysRevD.16.1791. URL: https://link.aps.org/doi/10.1103/PhysRevD.16.1791.

[32] R. D. Peccei and Helen R. Quinn. "CP Conservation in the Presence of Pseudoparticles". In: *Phys. Rev. Lett.* 38 (25 1977), pp. 1440–1443. DOI: 10.1103/PhysRevLett.38.1440. URL: https://link.aps.org/doi/10.1103/PhysRevLett.38.1440.

[33] Steven Weinberg. "A New Light Boson?" In: *Phys. Rev. Lett.* 40 (4 1978), pp. 223–226. DOI: 10.1103/PhysRevLett.40.223. URL: https://link.aps.org/doi/10.1103/PhysRevLett.40.223.

[34] Antonio Boveia and Caterina Doglioni. "Dark Matter Searches at Colliders". In: *Annual Review of Nuclear and Particle Science* 68.1 (Oct. 2018), 429–459. ISSN: 1545-4134. DOI: 10.1146/annurev-nucl-101917-021008. URL: http://dx.doi.org/10.1146/annurev-nucl-101917-021008.

[35] Jalal Abdallah et al. "Simplified models for dark matter searches at the LHC". In: *Physics of the Dark Universe* 9–10 (Sept. 2015), 8–23. ISSN: 2212-6864. DOI: 10.1016/j.dark.2015.08.001. URL: http://dx.doi.org/10.1016/j.dark.2015.08.001.

[36] CSABA CSÁKI. "THE MINIMAL SUPERSYMMETRIC STANDARD MODEL". In: *Modern Physics Letters A* 11.08 (Mar. 1996), 599–613. ISSN: 1793-6632. DOI: 10.1142/s021773239600062x. URL: http://dx.doi.org/10.1142/S021773239600062X.

[37] Gerard Jungman, Marc Kamionkowski, and Kim Griest. "Supersymmetric dark matter". In: *Physics Reports* 267.5–6 (Mar. 1996), 195–373. ISSN: 0370-1573. DOI: 10.1016/0370-1573(95)00058-5. URL: http://dx.doi.org/10.1016/0370-1573(95)00058-5.

[38] Mihailo Backović et al. Higher-order QCD predictions for dark matter production at the LHC in simplified models with s-channel mediators. 2015. arXiv: 1508.05327 [hep-ph]. URL: https://arxiv.org/abs/1508.05327.

[39] G. Aad et al. "The ATLAS Experiment at the CERN Large Hadron Collider". In: *JINST* 3 (2008), S08003. DOI: 10.1088/1748-0221/3/08/S08003.

[40] S. Chatrchyan et al. "The CMS Experiment at the CERN LHC". In: *JINST* 3 (2008), S08004. DOI: 10.1088/1748-0221/3/08/S08004.

[41] CERN. CERN Webpage. URL: https://home.cern.

[42] Georges Aad et al. "The ATLAS experiment at the CERN Large Hadron Collider: a description of the detector configuration for Run 3". In: *JINST* 19.05 (2024), P05063. DOI: 10.1088/1748-0221/19/05/P05063. arXiv: 2305.16623 [physics.ins-det].

[43] CERN. ATLAS Open Data Webpage. URL: https://opendata.atlas.cern.

[44] Florian Bechtel. The underlying event in proton-proton collisions. 2009. DOI: 10.3204/DESY-THESIS-2009-015.

[45] Valeria Tano. The Underlying Event in Hadron-Hadron Collisions. 2002. arXiv: hep-ex/0205023 [hep-ex]. URL: https://arxiv.org/abs/hep-ex/0205023.

[46] Matteo Cacciari, Gavin P Salam, and Gregory Soyez. "The anti-ktjet clustering algorithm". In: *Journal of High Energy Physics* 2008.04 (Apr. 2008), 063–063. ISSN: 1029-8479. DOI: 10.1088/1126-6708/2008/04/063. URL: http://dx.doi.org/10.1088/1126-6708/2008/04/063.

[47] S. Navas et al. "Review of particle physics". In: *Phys. Rev. D* 110.3 (2024), p. 030001. DOI: 10.1103/PhysRevD.110.030001.

[48] Gregory Mahlon and Stephen J. Parke. "Spin correlation effects in top quark pair production at the LHC". In: *Physical Review D* 81.7 (Apr. 2010). ISSN: 1550-2368. DOI: 10.1103/physrevd.81.074024. URL: http://dx.doi.org/10.1103/PhysRevD.81.074024.

[49] A. Sirunyan et al. "Measurement of the top quark polarization and tt spin correlations using dilepton final states in proton-proton collisions at $\sqrt{s}$ =13 TeV". In: *Physical Review D* 100 (Oct. 2019).

[50] Kevin Lannon, Fabrizio Margaroli, and Chris Neu. "Measurements of the production, decay and properties of the top quark: a review". In: *The European Physical Journal C* 72.8 (Aug. 2012). ISSN: 1434-6052. DOI: 10.1140/epjc/s10052-012-2120-0. URL: http://dx.doi.org/10.1140/epjc/s10052-012-2120-0.

[51] Caterina Monini. "Single-top s channel cross-section measurement with the ATLAS detector". PhD thesis. Sept. 2014. DOI: 10.13140/RG.2.2.20009.75364.

[52] Kingman Cheung et al. "The top window for dark matter". In: *Journal of High Energy Physics* 2010.10 (Oct. 2010). ISSN: 1029-8479. DOI: 10.1007/jhep10(2010)081. URL: http://dx.doi.org/10.1007/JHEP10(2010)081.

[53] Werner Bernreuther and Arnd Brandenburg. "Tracing CP violation in the production of top quark pairs by multiple TeV proton-proton collisions". In: *Phys. Rev. D* 49 (9 May 1994), pp. 4481–4492. DOI: 10.1103/PhysRevD.49.4481. URL: https://link.aps.org/doi/10.1103/PhysRevD.49.4481.

[54] John F. Gunion and Xiao-Gang He. "Determining theCPNature of a Neutral Higgs Boson at the CERN Large Hadron Collider". In: *Physical Review Letters* 76.24 (June 1996), 4468–4471. ISSN: 1079-7114. DOI: 10.1103/physrevlett.76.4468. URL: http://dx.doi.org/10.1103/PhysRevLett.76.4468.

[55] P. S. Bhupal Dev et al. "Determining the CP properties of the Higgs boson". In: *Phys. Rev. Lett.* 100 (2008), p. 051801. DOI: 10.1103/PhysRevLett.100.051801. arXiv: 0707.2878 [hep-ph].

[56] R. Frederix et al. "Scalar and pseudoscalar Higgs production in association with a top–antitop pair". In: *Physics Letters B* 701.4 (2011), pp. 427–433. ISSN: 0370-2693. DOI: https://doi.org/10.1016/j.physletb.2011.06.012. URL: https://www.sciencedirect.com/science/article/pii/S0370269311006332.

[57] John Ellis et al. "Disentangling Higgs-top couplings in associated production". In: *Journal of High Energy Physics* 2014.4 (Apr. 2014). ISSN: 1029-8479. DOI: 10.1007/jhep04(2014)004. URL: http://dx.doi.org/10.1007/JHEP04(2014)004.

[58] Sara Khatibi and Mojtaba Mohammadi Najafabadi. "Exploring the anomalous Higgs-top couplings". In: *Phys. Rev. D* 90 (7 Oct. 2014), p. 074014. DOI: 10.1103/PhysRevD.90.074014. URL: https://link.aps.org/doi/10.1103/PhysRevD.90.074014.

[59] Federico Demartin et al. "Higgs characterisation at NLO in QCD: CP properties of the top-quark Yukawa interaction". In: *The European Physical Journal C* 74.9 (Sept. 2014). ISSN: 1434-6052. DOI: 10.1140/epjc/s10052-014-3065-2. URL: http://dx.doi.org/10.1140/epjc/s10052-014-3065-2.

[60] Archil Kobakhidze, Lei Wu, and Jason Yue. "Anomalous top-Higgs couplings and top polarisation in single top and Higgs associated production at the LHC". In: *Journal of High Energy Physics* 2014.10 (Oct. 2014). ISSN: 1029-8479. DOI: 10.1007/jhep10(2014)100. URL: http://dx.doi.org/10.1007/JHEP10(2014)100.

[61] Joseph Bramante, Antonio Delgado, and Adam Martin. "Cornering a hyper Higgs boson: Angular kinematics for boosted Higgs bosons with top pairs". In: *Phys. Rev. D* 89 (9 May 2014), p. 093006. DOI: 10.1103/PhysRevD.89.093006. URL: https://link.aps.org/doi/10.1103/PhysRevD.89.093006.

[62] Fawzi Boudjema et al. "Laboratory-frame observables for probing the top-Higgs boson interaction". In: *Phys. Rev. D* 92 (1 July 2015), p. 015019. DOI: 10.1103/PhysRevD.92.015019. URL: https://link.aps.org/doi/10.1103/PhysRevD.92.015019.

[63] Xiao-Gang He, Guan-Nan Li, and Ya-Juan Zheng. "Probing Higgs boson CP properties with $t\bar{t}H$ at the LHC and the 100 TeV pp collider". In: *International Journal of Modern Physics A* 30.25 (2015), p. 1550156. DOI: 10.1142/S0217751X15501560. eprint: https://doi.org/10.1142/S0217751X15501560. URL: https://doi.org/10.1142/S0217751X15501560.

[64] S. P. Amor dos Santos et al. "Angular distributions in $t\bar{t}H(H \to b\bar{b})$ reconstructed events at the LHC". In: *Phys. Rev. D* 92.3 (2015), p. 034021. DOI: 10.1103/PhysRevD.92.034021. arXiv: 1503.07787 [hep-ph].

[65] Andrei V. Gritsan et al. "Constraining anomalous Higgs boson couplings to the heavy-flavor fermions using matrix element techniques". In: *Phys. Rev. D* 94 (5 Sept. 2016), p. 055023. DOI: 10.1103/PhysRevD.94.055023. URL: https://link.aps.org/doi/10.1103/PhysRevD.94.055023.

[66] Matthew J. Dolan et al. "Determining the quantum numbers of simplified models in $t\bar{t}X$ production at the LHC". In: *Phys. Rev. D* 94 (1 July 2016), p. 015025. DOI: 10.1103/PhysRevD.94.015025. URL: https://link.aps.org/doi/10.1103/PhysRevD.94.015025.

[67] Dorival Gonçalves and David López-Val. "Pseudoscalar searches with dileptonic tops and jet substructure". In: *Phys. Rev. D* 94 (9 Nov. 2016), p. 095005. DOI: 10.1103/PhysRevD.94.095005. URL: https://link.aps.org/doi/10.1103/PhysRevD.94.095005.

[68] Matthew R. Buckley and Dorival Goncalves. "Constraining the Strength and CP Structure of Dark Production at the LHC: the Associated Top-Pair Channel". In: *Phys. Rev. D* 93.3 (2016), p. 034003. DOI: 10.1103/PhysRevD.93.034003. arXiv: 1511.06451 [hep-ph].

[69] Nicolas Mileo et al. "Pseudoscalar top-Higgs coupling: exploration of CP-odd observables to resolve the sign ambiguity". In: *Journal of High Energy Physics* 2016.7 (July 2016). ISSN: 1029-8479. DOI: 10.1007/jhep07(2016)056. URL: http://dx.doi.org/10.1007/JHEP07(2016)056.

[70] Matthew R. Buckley and Dorival Gonçalves. "Boosting the Direct CP Measurement of the Higgs-Top Coupling". In: *Physical Review Letters* 116.9 (Mar. 2016). ISSN: 1079-7114. DOI: 10.1103/physrevlett.116.091801. URL: http://dx.doi.org/10.1103/PhysRevLett.116.091801.

[71] S. Amor Dos Santos et al. "Probing the CP nature of the Higgs coupling in $t\bar{t}h$ events at the LHC". In: *Phys. Rev. D* 96.1 (2017), p. 013004. DOI: 10.1103/PhysRevD.96.013004. arXiv: 1704.03565 [hep-ph].

[72] Dorival Gonçalves, Jeong Han Kim, and Kyoungchul Kong. "Probing the top-Higgs Yukawa CP structure in dileptonic $t\bar{t}h$ with M2-assisted reconstruction". In: *Journal of High Energy Physics* 2018.6 (June 2018). ISSN: 1029-8479. DOI: 10.1007/jhep06(2018)079. URL: http://dx.doi.org/10.1007/JHEP06(2018)079.

[73] D. Azevedo et al. "CP tests of Higgs couplings in $t\bar{t}h$ semileptonic events at the LHC". In: *Phys. Rev. D* 98 (3 Aug. 2018), p. 033004. DOI: 10.1103/PhysRevD.98.033004. URL: https://link.aps.org/doi/10.1103/PhysRevD.98.033004.

[74] Jinmian Li et al. "Central-edge asymmetry as a probe of Higgs-top coupling in $t\bar{t}h$ production at the LHC". In: *Phys. Lett. B* 779 (2018), pp. 72–76. DOI: 10.1016/j.physletb.2018.02.009. arXiv: 1701.00224 [hep-ph].

[75] Andrea Ferroglia et al. "Role of the $t\bar{t}h$ rest frame in direct top-quark Yukawa coupling measurements". In: *Phys. Rev. D* 100.7 (2019), p. 075034. DOI: 10.1103/PhysRevD.100.075034. arXiv: 1909.00490 [hep-ph].

[76] Darius A. Faroughy et al. "Probing the CP nature of the top quark Yukawa at hadron colliders". In: *Journal of High Energy Physics* 2020.2 (Feb. 2020). ISSN: 1029-8479. DOI: 10.1007/jhep02(2020)085. URL: http://dx.doi.org/10.1007/JHEP02(2020)085.

[77] Duarte Azevedo et al. "Scalar mass dependence of angular variables in $t\bar{t}\phi$ production". In: *Journal of High Energy Physics* 2020.6 (June 2020). ISSN: 1029-8479. DOI: 10.1007/jhep06(2020)155. URL: http://dx.doi.org/10.1007/JHEP06(2020)155.

[78] Duarte Azevedo et al. "Light Higgs searches in $t\bar{t}\phi$ production at the LHC". In: *Journal of High Energy Physics* 2021.4 (Apr. 2021). ISSN: 1029-8479. DOI: 10.1007/jhep04(2021)077. URL: http://dx.doi.org/10.1007/JHEP04(2021)077.

[79] Blaž Bortolato et al. "Optimized probes of CP-odd effects in the $t\bar{t}h$ process at hadron colliders". In: *Nuclear Physics B* 964 (2021), p. 115328. ISSN: 0550-3213. DOI: https://doi.org/10.1016/j.nuclphysb.2021.115328. URL: https://www.sciencedirect.com/science/article/pii/S0550321321000250.

[80] Qing-Hong Cao et al. A New Observable for Measuring CP Property of Top-Higgs Interaction. 2020. arXiv: 2008.13442 [hep-ph]. URL: https://arxiv.org/abs/2008.13442.

[81] Dorival Gonçalves et al. "Direct Higgs-top CP-phase measurement with $t\bar{t}h$ at the 14 TeV LHC and 100 TeV FCC". In: *Journal of High Energy Physics* 2022.1 (Jan. 2022). ISSN: 1029-8479. DOI: 10.1007/jhep01(2022)158. URL: http://dx.doi.org/10.1007/JHEP01(2022)158.

[82] Rahool Kumar Barman, Dorival Gonçalves, and Felix Kling. "Machine learning the Higgs boson-top quark CP phase". In: *Phys. Rev. D* 105 (3 Feb. 2022), p. 035023. DOI: 10.1103/PhysRevD.105.035023. URL: https://link.aps.org/doi/10.1103/PhysRevD.105.035023.

[83] Duarte Azevedo et al. "CP-violation, asymmetries and interferences in $t\bar{t}\phi$". In: *Journal of High Energy Physics* 2022.9 (Sept. 2022). ISSN: 1029-8479. DOI: 10.1007/jhep09(2022)246. URL: http://dx.doi.org/10.1007/JHEP09(2022)246.

[84] Johan Alwall et al. "MadGraph 5: going beyond". In: *Journal of High Energy Physics* 2011.6 (June 2011). ISSN: 1029-8479. DOI: 10.1007/jhep06(2011)128. URL: http://dx.doi.org/10.1007/JHEP06(2011)128.

[85] Antonio Boveia et al. Recommendations on presenting LHC searches for missing transverse energy signals using simplified s-channel models of dark matter. 2016. arXiv: 1603.04156 [hep-ex]. URL: https://arxiv.org/abs/1603.04156.

[86] Pierre Artoisenet et al. "Automatic spin-entangled decays of heavy resonances in Monte Carlo simulations". In: *Journal of High Energy Physics* 2013.3 (Mar. 2013). ISSN: 1029-8479. DOI: 10.1007/jhep03(2013)015. URL: http://dx.doi.org/10.1007/JHEP03(2013)015.

[87] Torbjörn Sjöstrand, Stephen Mrenna, and Peter Skands. "PYTHIA 6.4 physics and manual". In: *Journal of High Energy Physics* 2006.05 (May 2006), 026–026. ISSN: 1029-8479. DOI: 10.1088/1126-6708/2006/05/026. URL: http://dx.doi.org/10.1088/1126-6708/2006/05/026.

[88] Matteo Cacciari, Gavin P. Salam, and Gregory Soyez. "FastJet user manual: (for version 3.0.2)". In: *The European Physical Journal C* 72.3 (Mar. 2012). ISSN: 1434-6052. DOI: 10.1140/epjc/s10052-012-1896-2. URL: http://dx.doi.org/10.1140/epjc/s10052-012-1896-2.

[89] Matteo Cacciari and Gavin P. Salam. "Dispelling the N3 myth for the kt jet-finder". In: *Physics Letters B* 641.1 (2006), pp. 57–61. ISSN: 0370-2693. DOI: https://doi.org/10.1016/j.physletb.2006.08.037. URL: https://www.sciencedirect.com/science/article/pii/S0370269306010094.

[90] Michał Czakon and Alexander Mitov. "Top++: A program for the calculation of the top-pair cross-section at hadron colliders". In: *Computer Physics Communications* 185.11 (Nov. 2014), 2930–2938. ISSN: 0010-4655. DOI: 10.1016/j.cpc.2014.06.021. URL: http://dx.doi.org/10.1016/j.cpc.2014.06.021.

[91] John Campbell, Tobias Neumann, and Zack Sullivan. "Single-top-quark production in the t-channel at NNLO". In: *Journal of High Energy Physics* 2021.2 (Feb. 2021). ISSN: 1029-8479. DOI: 10.1007/jhep02(2021)040. URL: http://dx.doi.org/10.1007/JHEP02(2021)040.

[92] Richard D Ball et al. "The PDF4LHC21 combination of global PDF fits for the LHC Run III*". In: *Journal of Physics G: Nuclear and Particle Physics* 49.8 (July 2022), p. 080501. ISSN: 1361-6471. DOI: 10.1088/1361-6471/ac7216. URL: http://dx.doi.org/10.1088/1361-6471/ac7216.

[93] Nikolaos Kidonakis and Nodoka Yamanaka. "Higher-order corrections for tW production at high-energy hadron colliders". In: *Journal of High Energy Physics* 2021.5 (May 2021). ISSN: 1029-8479. DOI: 10.1007/jhep05(2021)278. URL: http://dx.doi.org/10.1007/JHEP05(2021)278.

[94] P. Kant et al. "HatHor for single top-quark production: Updated predictions and uncertainty estimates for single top-quark production in hadronic collisions". In: *Computer Physics Communications* 191 (June 2015), 74–89. ISSN: 0010-4655. DOI: 10.1016/j.cpc.2015.02.001. URL: http://dx.doi.org/10.1016/j.cpc.2015.02.001.

[95] M. Aliev et al. "HATHOR – HAdronic Top and Heavy quarks crOss section calculatoR". In: *Computer Physics Communications* 182.4 (Apr. 2011), 1034–1046. ISSN: 0010-4655. DOI: 10.1016/j.cpc.2010.12.040. URL: http://dx.doi.org/10.1016/j.cpc.2010.12.040.

[96] J. de Favereau et al. "DELPHES 3: a modular framework for fast simulation of a generic collider experiment". In: *Journal of High Energy Physics* 2014.2 (Feb. 2014). ISSN: 1029-8479. DOI: 10.1007/jhep02(2014)057. URL: http://dx.doi.org/10.1007/JHEP02(2014)057.

[97] Eric Conte, Benjamin Fuks, and Guillaume Serret. "MadAnalysis 5, a user-friendly framework for collider phenomenology". In: *Computer Physics Communications* 184.1 (Jan. 2013), 222–256. ISSN: 0010-4655. DOI: 10.1016/j.cpc.2012.09.009. URL: http://dx.doi.org/10.1016/j.cpc.2012.09.009.

[98] Eric Conte et al. "Designing and recasting LHC analyses with MadAnalysis 5". In: *The European Physical Journal C* 74.10 (Oct. 2014). ISSN: 1434-6052. DOI: 10.1140/epjc/s10052-014-3103-0. URL: http://dx.doi.org/10.1140/epjc/s10052-014-3103-0.

[99] A. Hoecker et al. TMVA - Toolkit for Multivariate Data Analysis. 2009. arXiv: physics/0703039 [physics.data-an]. URL: https://arxiv.org/abs/physics/0703039.

[100] Yann Coadou. "Boosted Decision Trees". In: *Artificial Intelligence for High Energy Physics*. WORLD SCIENTIFIC, Feb. 2022, 9–58. ISBN: 9789811234033. DOI: 10.1142/9789811234033_0002. URL: http://dx.doi.org/10.1142/9789811234033_0002.

[101] Alexander L. Read. "Presentation of search results: The CL_s technique". In: *J. Phys. G* 28 (2002). Ed. by M. R. Whalley and L. Lyons, pp. 2693–2704. DOI: 10.1088/0954-3899/28/10/313.

[102] Thomas Junk. "Confidence level computation for combining searches with small statistics". In: *Nuclear Instruments and Methods in Physics Research Section A: Accelerators, Spectrometers, Detectors and Associated Equipment* 434.2–3 (Sept. 1999), 435–443. ISSN: 0168-9002. DOI: 10.1016/s0168-9002(99)00498-2. URL: http://dx.doi.org/10.1016/S0168-9002(99)00498-2.

[103] G Apollinari et al. High Luminosity Large Hadron Collider HL-LHC. en. 2015. DOI: 10.5170/CERN-2015-005.1. URL: https://cds.cern.ch/record/2120673.

[104] Nicola Cabibbo. "Unitary Symmetry and Leptonic Decays". In: *Phys. Rev. Lett.* 10 (12 June 1963), pp. 531–533. DOI: 10.1103/PhysRevLett.10.531. URL: https://link.aps.org/doi/10.1103/PhysRevLett.10.531.

[105] G. BUCHALLA. "KAON AND CHARM PHYSICS: THEORY". In: *Flavor Physics for the Millennium*. WORLD SCIENTIFIC, Sept. 2001, 143–205. DOI: 10.1142/9789812811509_0004. URL: http://dx.doi.org/10.1142/9789812811509_0004.

[106] Gerhard Buchalla. CP Violation and Rare Kaon Decays. 1999. arXiv: hep-ph/9912369 [hep-ph]. URL: https://arxiv.org/abs/hep-ph/9912369.

Appendix A

Group Theory and Lie groups

A group G is a set of elements $\{g_i\}$ with a law for the ordered product of two elements, $g_i g_j$, such that the following four conditions are fulfilled:

1. For every $g_i, g_j \in G$, the product $g_i g_j \in G$;
2. The product law is associative: $(g_i g_j)g_k = g_i(g_j g_k)$;
3. There must be a unique identity element, e, in G, such that $eg_i = g_i e = g_i$ for all $g_i \in G$;
4. For all $g_i \in G$, there must be a unique inverse element, g_i^{-1}, such that $g_i g_i^{-1} = g_i^{-1} = e$.

A group can have a finite or infinite number of elements. If the product law is commutative ($g_i g_j = g_j g_i$) the group is called an Abelian group; otherwise, the group is a non-Abelian group. A representation of G is a mapping, D, of the elements of G onto a set of linear operators that operate on a specific vector space. A representation of G has the following properties:

- $D(e) = \mathbb{1}$, with $\mathbb{1}$ being the identity operator in the vector space where the linear operators of the representation D operate on;
- $D(g_i)D(g_j) = D(g_i g_j)$.

If the representation is finite-dimensional, the g_i elements of G are embedded into matrices that act on a specific vector space.

Continuous groups are groups whose elements are labeled by some continuously variable real parameters $\theta^i = \theta^1, \theta^2, ..., \theta^r$: $g(\theta^1, \theta^2, ..., \theta^r) \equiv g(\vec{\theta})$. The first condition, 1, for a set of elements $\{g_i\}$ to be a group G, takes the form $g(\vec{\theta})g(\vec{\Theta}) = g(\vec{\gamma}(\vec{\theta}, \vec{\Theta}))$ for a continuous group, where the parameters $\vec{\gamma}$ are continuous functions of the parameters $\vec{\theta}$ and $\vec{\Theta}$. If $\vec{\gamma}$ is an analytic function[1] of $\vec{\theta}$ and $\vec{\Theta}$, the group is called a Lie group. The product law being defined by an analytical function makes it possible to transform an element of the Lie Group $g(\vec{\theta})$ into a nearby element, and so into any other element of the Lie group through successive products under the product law determined by the analytical function $\vec{\gamma}$, given that every Lie group element is continuously connected to the original element $g(\vec{\theta})$. For simplicity, one can use the identity element, $e = g(\vec{0})$, to reach any element of the Lie group continuously connected to e. From the elements in the neighborhood of e, one determines the properties of any element continuously connected to e.

[1] An analytic function is a function that is locally given by a convergent power series.

The linear operators of a representation of a Lie group can also be parameterized by $\vec{\theta}: D(g(\vec{\theta})) = D(\vec{\theta})$. Taylor expanding $D(d\vec{\theta})$ (also called an infinitesimal group element) for the group element $g(d\vec{\theta})$ in the neighborhood of e and ignoring second or higher order terms, we get:

$$D(d\vec{\theta}) = \mathbb{1} - id\theta^a T^a, \tag{A.1}$$

where T^a is the group generator of index a[2] and it is defined as:

$$T^a \equiv i\frac{\partial D(\vec{\theta})}{\partial \theta^a}\bigg|_{\vec{\theta}=\vec{0}}. \tag{A.2}$$

In QFT, the operators act on the Fock space, thus the group elements and the group representation are usually parameterized in such a way that the product law for the representation operators in the Fock space looks appropriate. Usually, the exponential parametrization is the chosen one: by raising an infinitesimal group element, A.1, to some power we get another group element. With the infinitesimal parameters defined as $d\vec{\theta} = \lim_{n\to\infty} \frac{\vec{\theta}}{n}$, where $\vec{\theta}$ are finite parameters, we can define the linear operators of the representation of the Lie group element for finite $\vec{\theta}$ as:

$$D(\vec{\theta}) = \lim_{n\to\infty}\left(\mathbb{1} - i\frac{\theta^a}{n}T^a\right)^n = e^{-i\theta^a T^a}. \tag{A.3}$$

Thus we get the representation of the finite group element $g(\vec{\theta})$ as an exponential of $-i\theta^a T^a$[3]. The generators of a Lie group G form the vector basis of an algebra: the Lie algebra of G. A Lie algebra is defined by the following commutation relation:

$$[T^a, T^b] = if^{abc}T^c, \tag{A.4}$$

where the f^{abc} are the structure constants. The Lie groups are classified as Abelian if $f^{abc} = 0$ for any a, b, and c index values, and as non-Abelian if the structure constants are not all null. A representation of a Lie algebra embeds the Lie algebra generators into matrices. The two most important representations of a Lie algebra in physics are the fundamental representation and the adjoint representation. The fundamental representation is the smallest non-trivial representation of an algebra, while the adjoint representation is the one in which the generators are represented by the structure constants and its dimension is equal to the number of independent generators of the Lie algebra.

The U(N) and SU(N) Lie groups are two important classes of groups that the Standard Model employs in its gauge theories.

U(N) is the group of all $N \times N$ (in the fundamental representation) unitary matrices.

SU(N) is the group of all $N \times N$ (in the fundamental representation) unitary matrices with determinant equal to 1 which leads to its generators being hermitian and traceless in the exponential parametrization. It has $N^2 - 1$ independent generators. The simplest SU(N) group is SU(2) and so their elements are 2×2 unitary matrices U with $\det(U) = 1$. It has 3 generators and in the fundamental representation they are the Pauli matrices, τ^a, conventionally divided by 2:

$$T^a = \frac{\tau^a}{2}, \tag{A.5}$$

[2]This index can appear as a superscript or a subscript since it makes no difference. In this dissertation it sometimes appears as a subscript to not confuse the a index with an exponent.

[3]In 2 θ is written as $g_a\alpha^a$ to explicitly show the coupling constant g_a associated with the T^a generator of the group employed in the considered gauge theory.

where:

$$\tau^1 = \begin{bmatrix} 0 & 1 \\ 1 & 0 \end{bmatrix},\ \tau^2 = \begin{bmatrix} 0 & -i \\ i & 0 \end{bmatrix},\ \tau^3 = \begin{bmatrix} 1 & 0 \\ 0 & -1 \end{bmatrix}, \tag{A.6}$$

and the structure constants are:

$$f^{abc} = \epsilon^{abc}, \tag{A.7}$$

where ϵ^{abc} is the Levi-Civita antisymmetric tensor.

The SU(3) group has 8 generators which are the Gell-Mann matrices, λ^a, divided by two in the fundamental representation:

$$T^a = \frac{\lambda^a}{2}. \tag{A.8}$$

These matrices are:

$$\begin{aligned}
\lambda_1 &= \begin{bmatrix} 0 & 1 & 0 \\ 1 & 0 & 0 \\ 0 & 0 & 0 \end{bmatrix},\ \lambda_2 = \begin{bmatrix} 0 & -i & 0 \\ i & 0 & 0 \\ 0 & 0 & 0 \end{bmatrix},\ \lambda_3 = \begin{bmatrix} 1 & 0 & 0 \\ 0 & -1 & 0 \\ 0 & 0 & 0 \end{bmatrix}, \\
\lambda_4 &= \begin{bmatrix} 0 & 0 & 1 \\ 0 & 0 & 0 \\ 1 & 0 & 0 \end{bmatrix},\ \lambda_5 = \begin{bmatrix} 0 & 0 & -i \\ 0 & 0 & 0 \\ i & 0 & 0 \end{bmatrix}, \\
\lambda_6 &= \begin{bmatrix} 0 & 0 & 0 \\ 0 & 0 & 1 \\ 0 & 1 & 0 \end{bmatrix},\ \lambda_7 = \begin{bmatrix} 0 & 0 & 0 \\ 0 & 0 & -i \\ 0 & i & 0 \end{bmatrix},\ \lambda_8 = \frac{1}{\sqrt{3}} \begin{bmatrix} 1 & 0 & 0 \\ 0 & 1 & 0 \\ 0 & 0 & -2 \end{bmatrix}.
\end{aligned} \tag{A.9}$$

and the structure constants are:

$$\begin{aligned}
&f_{123} = 1 \\
&f_{147} = f_{165} = f_{246} = f_{257} = f_{345} = f_{376} = \frac{1}{2} \\
&f_{458} = f_{678} = \frac{\sqrt{3}}{2}.
\end{aligned} \tag{A.10}$$

To get the remaining non-zero structure constants, one just has to permute the indices of the structure constants above and consider that the structure constants are totally antisymmetric. All the other structure constants not related to these ones under index permutation are equal to zero.

Appendix B

CKM Matrix

The Cabibbo-Kobayashi-Maskawa (CKM) matrix, V_{CKM}, [20, 104] is a unitary matrix, which in general is a complex matrix, that arises from the mismatch between weak eigenstates and physical eigenstates in the quark sector.

A unitary square matrix of dimension n has n^2 real degrees of freedom. The standard parametrization of a $n \times n$ square unitary matrix is through $\frac{n(n-1)}{2}$ rotation angles and $\frac{n(n+1)}{2}$ phases. The CKM matrix has the property that its physical significance remains the same when one transforms the matrix element $V_{CKM,ij}$ as $V_{CKM,ij} \rightarrow V_{CKM,ij}e^{i(\theta_j-\theta_i)}$ with arbitrary phases θ_i and θ_j, where the index i labels the up-type quarks and the index j labels the down-type quarks. This is possible because one has the freedom to rephase the physical quark fields as $\hat{u}_i \rightarrow e^{i\theta_i}\hat{u}_i$ and $\hat{d}_j \rightarrow e^{i\theta_j}\hat{d}_j$. Only the differences $\theta_i - \theta_j$ appear in the transformation of the CKM matrix element $V_{CKM,ij}$, and so one may add a common value to all the three θ_i phases and all the three θ_j phases without altering the transformation, which leads to the transformation only involving $2n-1$ independent phases. This conclusion means that we can eliminate $2n-1$ phases from the CKM matrix through this transformation, meaning that these phases are physically irrelevant. The number of phases that cannot be removed is $\frac{(n-1)(n-2)}{2}$ [21].

If we had 2 generations of quarks, we would get a 2×2 CKM matrix, and its parameterization would involve 1 angle and 3 phases. All of these phases could be removed from the 2×2 CKM matrix and we could get a real CKM matrix and no source of CP-violation in the quark sector and therefore in the SM. However, we have 3 generations of quarks in the SM, thus we parameterize the CKM matrix with 3 angles (also called Euler angles, since it is a 3×3 matrix) and 6 phases, of which 5 are physically irrelevant. There remains a single phase that cannot be removed from the CKM matrix which is the source of CP-violation in the SM[1].

We saw that we have some freedom to rephase the CKM matrix elements, and so we need quantities related to the CKM matrix elements that are experimentally accessible. Since the transformation $V_{CKM,ij} \rightarrow V_{CKM,ij}e^{i(\theta_j-\theta_i)}$ leaves the moduli of the CKM matrix elements, $|V_{CKM,ij}|$, invariant, these moduli are experimentally the most accessible quantities of the CKM. Some cross-sections of processes that involve couplings with the CKM matrix are functions of $|V_{CKM,ij}|^2$, meaning that $|V_{CKM,ij}|$ could be experimentally determined. $|V_{CKM,ij}|$ has to be smaller than unity due to the unitary property of the CKM matrix which implies that the square of the moduli, $|V_{CKM,ij}|^2$, must add up to one along

[1] Actually we need a minimum of 3 generations of quarks to get CP violation in the quark sector as it is experimentally observed to exist [105, 106].

each row and each column of V_{CKM}:

$$\begin{aligned}
|V_{ud}|^2 + |V_{us}|^2 + |V_{ub}|^2 &= 1, \\
|V_{cd}|^2 + |V_{cs}|^2 + |V_{cb}|^2 &= 1, \\
|V_{td}|^2 + |V_{ts}|^2 + |V_{tb}|^2 &= 1, \\
|V_{ud}|^2 + |V_{cd}|^2 + |V_{td}|^2 &= 1, \\
|V_{us}|^2 + |V_{cs}|^2 + |V_{ts}|^2 &= 1, \\
|V_{ub}|^2 + |V_{cb}|^2 + |V_{tb}|^2 &= 1.
\end{aligned} \tag{B.1}$$

The experimental values from [9] of the moduli of the CKM matrix elements are listed below:

$$\begin{bmatrix} |V_{ud}| & |V_{us}| & |V_{ub}| \\ |V_{cd}| & |V_{cs}| & |V_{cb}| \\ |V_{td}| & |V_{ts}| & |V_{tb}| \end{bmatrix} = \begin{bmatrix} 0.97373 \pm 0.00031 & 0.2243 \pm 0.0008 & 0.00382 \pm 0.00020 \\ 0.221 \pm 0.004 & 0.975 \pm 0.006 & 0.0408 \pm 0.0014 \\ 0.0086 \pm 0.0002 & 0.0415 \pm 0.0009 & 1.014 \pm 0.029 \end{bmatrix}. \tag{B.2}$$

From these experimental values we can conclude that the transition amplitude of the decay of a quark into a $W^{\pm}$ boson and another quark is the strongest when the transition is within the same generation, less strong when it is between the 1st and 2nd generations, even less strong between the 2nd and 3rd generations and the weakest when it is between the 1st and 3rd generations.